An experimental and computational study of CO_2 absorption in aqueous solutions of tetraethylenepentamine.

By Rebecca Dowling

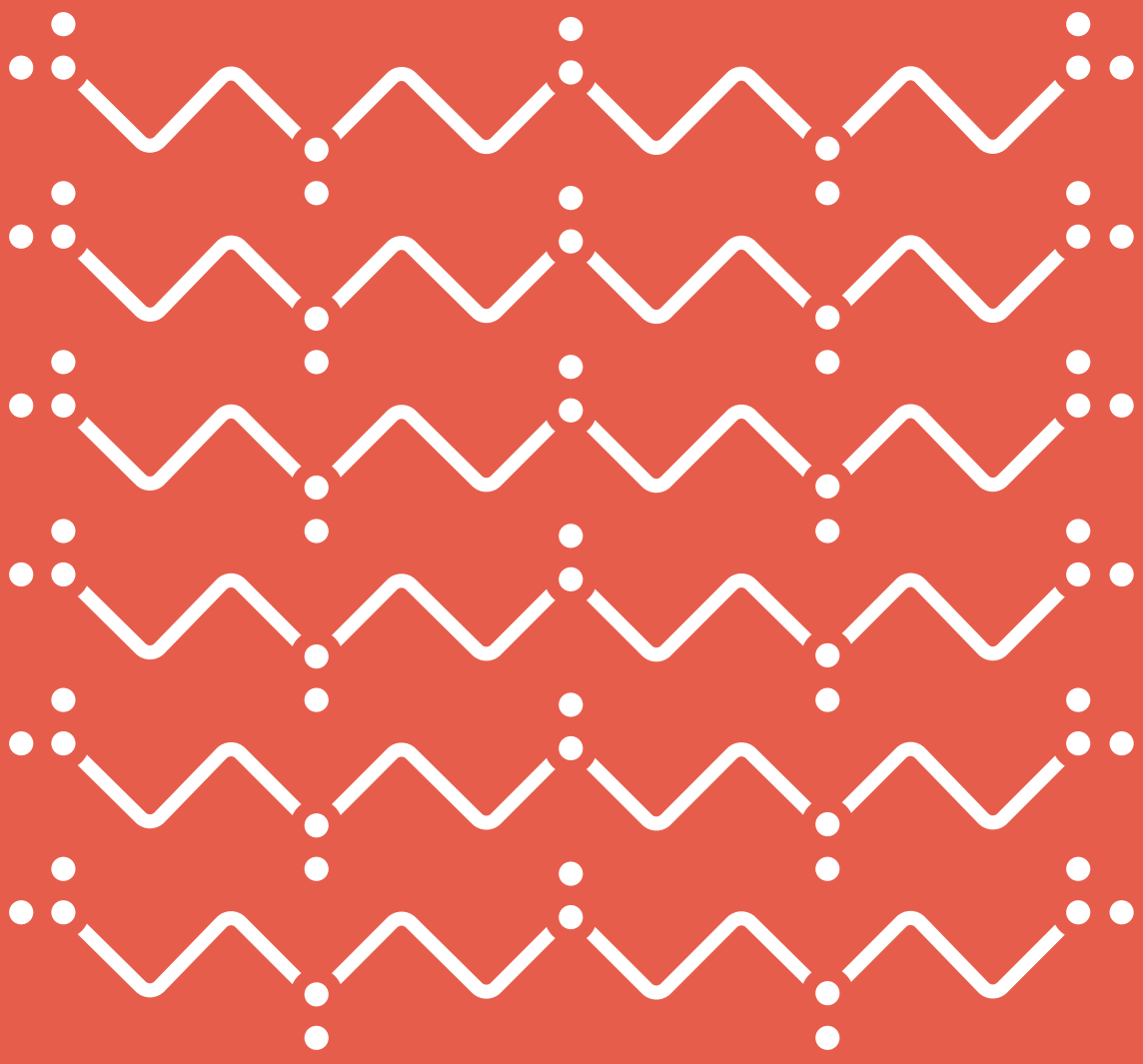

An experimental and computational study of CO_2 absorption in aqueous solutions of tetraethylenepentamine.

by

Rebecca Anne Dowling

to obtain the degree of Master of Science

at the Delft University of Technology,

to be defended publicly on June 30, 2020 at 13:30.

Student number:	4302435	
Project duration:	September 2, 2019 – June 16, 2020	
Thesis committee:	Prof. dr. ir. W. De Jong,	TU Delft, supervisor
	Prof. dr. ir. E. Goetheer,	TNO
	Prof. dr. ir. T. J. H. Vlugt,	TU Delft
	Dr. ir. M. Ramdin	TU Delft
	Ir. J. van Kranendonk,	Zero Emission Fuels

This thesis is confidential and cannot be made public until June 30, 2022

TU Delft

Summary

Capturing CO_2 directly from the atmosphere and subsequently using it to produce hydrocarbon fuels could help decrease mankind's reliance on fossil fuels and mitigate the risks of climate change. Zero Emission Fuels (ZEF), a startup from Delft, is developing a small-scale methanol plant, that uses CO_2 and H_2O vapor captured from ambient air to produce methanol. Their direct air capture unit is based on continuous absorption and stripping, using bulk polyamines as a chemical sorbent. In this study, the vapor liquid equilibrium (VLE) of CO_2 and aqueous solutions of tetraethylenepentamine, a polyamine with 5 amine groups in its molecular structure, is measured and correlated using thermodynamic models.

The equilibrium pressure of aqueous solutions of 30, 70 and 80 wt% TEPA was measured from 313.15 to 393.15 K using a mechanically stirred and temperature controlled autoclave. Using the same set-up, the equilibrium solubility of CO_2 in aqueous solutions of 30 and 70 wt% TEPA was measured at 313.15, 353.15 and 393.15 K. The experimental measurements showed that TEPA can capture up to 2.5 mol CO_2 per mol TEPA. It was observed that the viscosity of TEPA increased with increasing TEPA concentration, decreasing temperature and increasing CO_2 loading. The 70 wt% TEPA results at 313.15 K were discarded, because the liquid phase was too viscous to sufficiently interact with CO_2 and reach equilibrium. Additionally, it was observed that the vapor pressure of H_2O was decreased upon CO_2 absorption, which was attributed to the changing ionic interactions in the liquid phase.

The heat of CO_2 absorption was approximated using the VLE data and the Clausius-Clapeyron equation. For 30 w% TEPA, the heat of CO_2 absorption is approximately 70 kJ/mol at lower temperatures and 75 kJ/mol at higher temperatures. For 70 wt% TEPA, the value lies between 75 kJ/mol and 80 kJ/mol at higher temperatures.

The pressure of the binary TEPA-H_2O mixture was correlated using Wilson's activity coefficient model, with an absolute relative deviation of 4.15%. Furthermore, the equilibrium CO_2 absorption was simulated using the extended Debye-Hückel law for activity coefficients of ionic species. A theory was proposed, which states that the polyamine can be modelled as a multiple of smaller amines, using the ratio of amino groups as a scaling factor. The agreement between developed model and experimental data exhibited an absolute relative deviation of 15.97%.

Both models were applied in a simple process simulation of the absorption and stripping column of the direct air capture unit of ZEF to provide an estimation of the energy demand of the process under different conditions. It was found that under the studied conditions, the lowest regeneration energy demand was 533 kJ/mol CO_2 absorbed, which is approximately 3 times higher than that of monoethanolamine, the current benchmark solvent for amine-based CO_2 capture. However, through the addition of a rich-lean heat exchanger and process optimisation to minimize the required reflux stream, this value could potentially be decreased.

Acknowledgements

There are many people that have been instrumental in the development of this thesis.

First of all, I would like thank Professor Wiebren de Jong, for taking the time to supervise my thesis and providing me with valuable advice and guidance throughout the project.

Also, I want to express my sincere gratitude to Professor Earl Goetheer, for sharing his enthusiasm and expertise on CO_2 capture and utilisation, a topic that we are both passionate about.

Next, I want to thank Mahinder Ramdin, for his daily guidance and continuous support throughout this project. I am thankful for the thoughtful comments and recommendations on this thesis.

Someone who played a decisive role throughout this process is Jan van Kranendonk at Zero Emission Fuels. There is not a problem that he cannot solve. I want to thank him sincerely for inspiring me to think outside the box and always supporting my ideas, especially when I didn't believe in them myself.

I would also like to thank Ulrich Starke, Hessel Jongebreur and Mrigank Sinha for allowing me the opportunity to be a part of the Zero Emission Fuels team and your positive encouragement during the project.

I am also very grateful to Ahmadreza Rhabari, for his valuable help on thermodynamic modelling in Matlab and for proofreading this thesis. I have learned a great deal from him.

I would like to extend my gratitude to Arjen Huizinga from TNO, for providing the VLE set-up and for always being available to answer questions and discuss results.

Lastly, I would like to express my deep appreciation for the loving support of my friends and family during this project and during the challenging times of the coronavirus pandemic. I want to thank my mother, Anna, my father, Tim, my sister, Eveline and my brother, Nikolai for their unconditional support during my studies. I want to thank Wrister for his warmth and patience, as well as for his beautiful design of the front page of this thesis. Special thanks to Laura, Luka, Lucie, Anouk, Marije and Marah, the best roommates anyone could ever wish for, for their moral support and letting me write at their desks for months.

Contents

List of Figures

List of Tables

Chapter 1

Introduction

1.1 Global warming

The climate is changing. In fact, it has been changing throughout the entire history of planet Earth. Evidence from ice cores shows that in the last 650,000 years, there have been 7 alternating glacial and warmer periods [10]. However, the rate at which the earth is currently warming up is unprecedented over decades to millennia [11]. It is estimated that human activities have caused around 1 ℃ of warming compared to pre-industrial levels, due to increased emissions of so-called greenhouse gases (GHGs) [12]. These gases trap the heat that is radiated from Earth towards space, an effect which is enhanced by a higher concentration of GHGs in the atmosphere. These levels of GHGs, such as carbon dioxide, methane and nitrous oxide are higher than they have been in the last 800,000 years [10]. The historical variation of atmospheric CO_2 concentration is shown in Figure 1.1. It is very clear that in the last decades, the CO_2 concentration has increased sharply. The result is global warming [11]. The risks of global warming include shifting ecosystems resulting in mass species extinction, decreased food security, extreme weather events such as coastal flooding, landslides, droughts, water scarcity and much more [11].

To mitigate the risks of climate change and to have a chance at staying below 1.5℃ of warming, a net CO_2 emissions decline by 45% of 2010 levels is required by 2030. Net zero emissions must be reached by 2050 [11]. This requires a rapid system transition on a global scale in all polluting sectors, such as the energy system, transportation and industry. The energy transition from fossil fuels towards renewable energy technologies combined with energy efficiency measures and increased electrification can potentially deliver 90% of the required decline in energy-related CO_2 emissions [13]. Another option is capturing the CO_2 emitted from large, point sources, such as power plants or industrial processes (e.g. cement production) and storing the captured CO_2 in depleted gas reservoirs for example [14]. An entire energy system transition will take time and our dependence on fossil fuels as primary

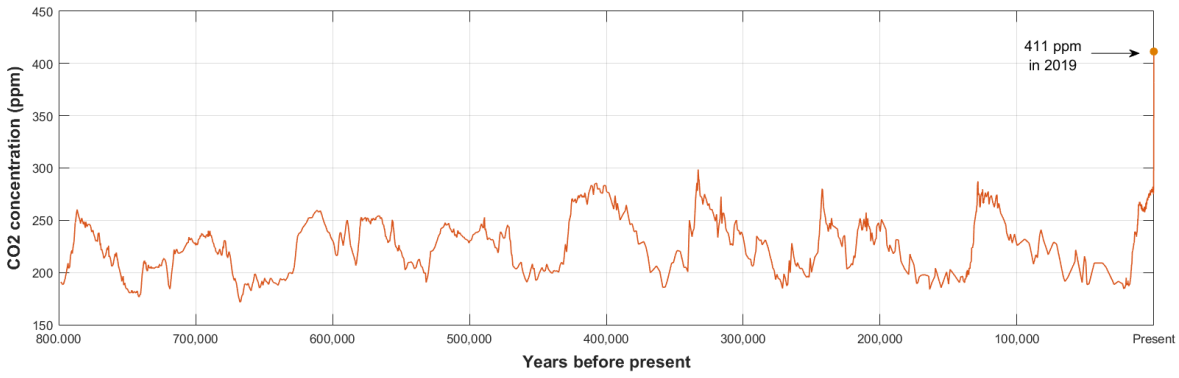

Figure 1.1: Global concentrations of carbon dioxide in the atmosphere in parts per million (ppm) over the past 800,000 years measured from ice cores [1] [2].

energy source will likely continue in the near future. Therefore, technologies to capture and store CO_2 are promising to mitigate the emissions from combustion of fossil fuels in the short-term. The Intergovernmental Panel on Climate Change (IPCC), the internationally accepted authority on climate change, established that carbon capture and storage (CCS) technologies will be necessary in any scenario, if there is to be a chance at staying below 1.5℃ [12].

For the electricity sector, there are multiple options to replace coal and gas power plants, such as solar photovoltaic power and wind power. Currently, electricity is only around 20% of our entire energy demand. However, this number is expected to grow significantly over the coming decades as a result of increased use of electric vehicles, heat pumps and renewable hydrogen [13]. Next to electricity, there will be a continued demand for liquid fuels and feedstock in industry and in transportation. This is especially true for the applications that cannot be easily electrified, such as long-distance aviation, heavy-weight shipping and carbon based chemical processes.

Often the term 'decarbonisation' is used when talking about the energy transition from fossil fuels to renewable fuels. However, in the case of the chemical industry, which relies on carbon feedstock to produce products such as plastics, paints and pharmaceuticals, 'recarbonisation' is necessary. In other words, carbon must be obtained from other sources than fossil fuel, because the industry cannot exist without it! A sustainable carbon source could be biomass, which is in essence a form of naturally stored CO_2. The trouble with biomass is that large plots of land are needed to grow 'fuel crops', which could influence food security and supply. Alternatively, we could capture atmospheric CO_2 from the air or from exhausts [14]. If atmospheric CO_2 is used to produce renewable hydrocarbon fuels, the reliance of mankind on fossil fuels could be decreased and the CO_2 emissions to the atmosphere could be reduced. Increasingly, research efforts are focused on so-called Carbon Capture and Utilisation (CCU). However, due to the very stable C=O double bond in the CO_2 molecule it is very difficult to transform. To convert CO_2 to fuels, it must be reduced, which can be achieved through photo-chemical, electrochemical or thermal hydrogenation methods [15].

1.2 Carbon neutral methanol

An example of a synthetic hydrocarbon fuel is methanol. Presently, around 90% of methanol is produced from steam reforming of natural gas [16], which yields synthesis gas (syngas), a mixture of CO and H_2. The produced syngas is then used as a feedstock for methanol synthesis. Methanol is mainly used for the production of chemicals such as formaldehyde, fuel additives and acetic acid [16]. Alternatively, methanol could be synthesized from atmospheric CO_2 and H_2 in the following hydrogenation reaction:

$$CO_2 + 3\ H_2 \leftrightarrow CH_3OH + H_2O \tag{1.1}$$

This yields carbon neutral methanol if it is produced using green hydrogen, which is the product of water electrolysis using renewable energy. Other sustainable methanol synthesis options include direct aqueous electrolysis [17] or photo-electrochemical reduction of captured CO_2 [18].

In 2004, Geoge Olah (1994 Nobel laureate in chemistry) proposed the methanol economy, in which carbon neutral methanol is a feasible and economic alternative to oil [19]. The required CO_2 can be captured from different sources, such as exhausts from power plants, chemical plants and even directly from the air (see Section 2.1.3). Methanol can be used as a liquid fuel in combustion engines, as a

feedstock for carbon-based industry or as a means of energy storage if the methanol is used in a direct oxidation methanol fuel cell (DMFC) to produce electricity again [20].

The methanol economy has several advantages over the hydrogen economy. Both provide ways of storing electrical energy in the form of chemicals, but methanol is a liquid at atmospheric conditions, while hydrogen is a volatile gas. Therefore, methanol storage and transport is much more straightforward and more safe. Additionally it can be used in the existing infrastructure, while hydrogen would necessitate the development of costly and complex infrastructure. Furthermore, methanol can function as a raw material for the chemical industry, while CO_2 from the atmosphere is being recycled, mitigating global warming [20]. Despite its potential, the production of green methanol from atmospheric carbon is currently too costly to be commercially viable [21].

1.3 Zero emission fuels

Zero Emission Fuels B.V., or ZEF for short, is a startup from Delft, whose aim is produce methanol from nothing more than air and sunlight. Their unique concept is a small scale methanol plant that is powered by a solar panel. Methanol can be produced on a large scale by adding these micro plants onto a field of solar panels. The advantage of scaling out, instead of scaling up, is that it makes the process more dynamic, responding better to the intermittent photovoltaic power input. Additionally, the small units can be mass manufactured. This brings down the costs of the unit by taking advantage of economies of scale.

The ZEF methanol factory roughly consists of five subsystems: a direct air capture (DAC) unit, fluid machinery, an alkaline electrolysis cell, a methanol synthesis reactor and a distillation unit, see Figure 1.2. Firstly, in the DAC, CO_2 and H_2O are captured from the ambient air through chemisorption by an amine sorbent. Next, the captured gases must be desorbed from the amine to be used in the subsequent steps. Desorption occurs at high temperatures and low pressures. After desorption, the regenerated solvent is pumped back to the absorber to capture CO_2 again. The captured H_2O is used in the alkaline electrolysis cell to produce H_2 and O_2. The captured CO_2 is compressed and traces of H_2O vapor are removed using fluid machinery. Subsequently, the H_2 together with the CO_2 are fed to the methanol synthesis reactor, producing methanol and water, following Reaction 1.1. Finally, the reaction products are separated in a distillation step and pure methanol is the final product.

Multiple direct air capture concepts have been developed at ZEF. The first two concepts were based on solid supports impregnated with polyethyleneimine (PEI) under temperature-vacuum swing operation. These prototypes had many disadvantages, such as pressure leakage, uneven distribution of the adsorbent, many moving parts and high energy requirement [22]. Due to such difficulties, it was decided to develop a continuous system, where liquid polyamines flow down over a vertical surface, while ambient air is fanned over the absorbent in the opposite direction. Polyamines, such as polyethyleneimine (PEI) and tetraethylenepentamine (TEPA), are of interest to ZEF, for two reasons. They have a potentially high CO_2 capture capacity, due to the many amine groups in these molecules, compared to the more commercially used amines such as monoethanolamine (MEA) [23]. Furthermore, amine loss is avoided because of their very low volatility. Previous research at ZEF [22] [9] points out that TEPA has more favorable characteristics than PEI in terms of CO_2 capture kinetics, capacity, viscosity and cost.

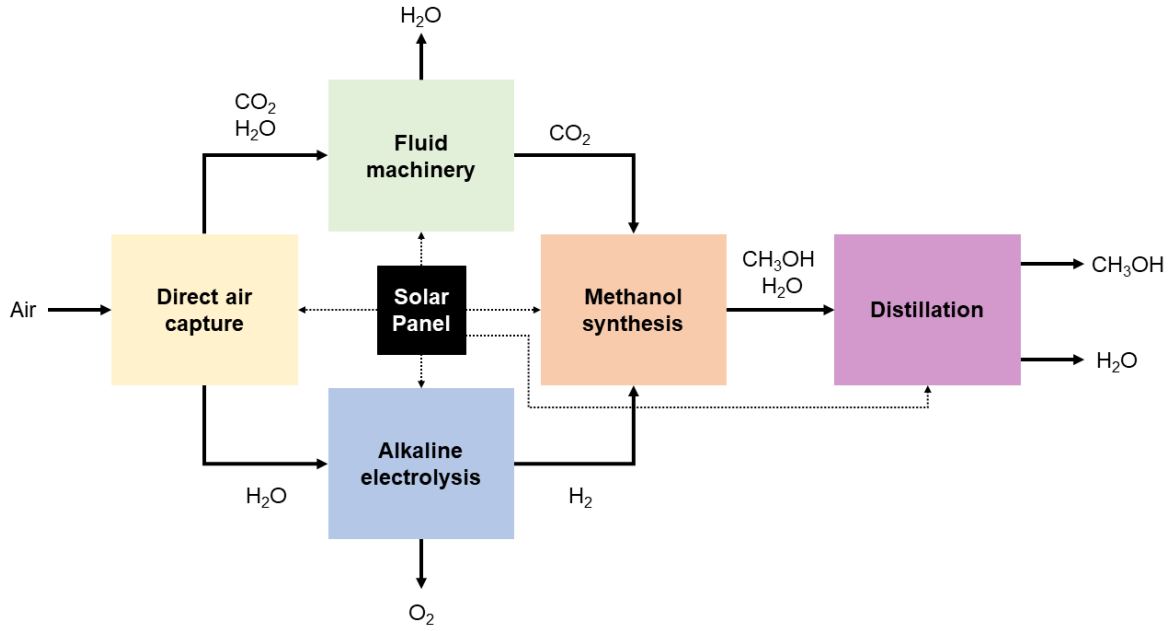

Figure 1.2: A schematic overview of the five subsystems in the ZEF process. During direct air capture, CO_2 and H_2O are captured from the atmosphere and separated from the sorbent. Most of the H_2O goes into the alkaline electrolysis cell to produce H_2, while the CO_2 stream is compressed and purified. H_2 and CO_2 react to form a mixture of methanol and H_2O, which is separated in the distillation unit.

1.4 Aim of this thesis

This thesis deals with the direct air capture subsystem of the ZEF methanol plant, focussing on the vapour liquid equilibrium (VLE) of the three components in the DAC: TEPA, H_2O ans CO_2. The VLE of the three components dictates the composition of the vapour phase and the liquid phase at a certain temperature and pressure. An accurate description of the VLE is the starting point for proper simulation and design of an absorption and desorption process. The VLE in question is particularly complicated, due to the chemical equilibrium reactions occurring in the liquid phase. Ionic species are formed, which results in highly non-ideal phase behavior due to electrostatic interactions.

Therefore, the aim of this thesis is twofold: to measure the VLE of TEPA-H_2O-CO_2 at different compositions and temperatures and to develop a thermodynamic model of the VLE of the TEPA-H_2O-CO_2 system, by fitting it to the acquired experimental VLE data.

1.5 Research questions

To break down the main research aim of this thesis into more specific sections, the following research questions were formulated:

1. How does the VLE of TEPA-H_2O-CO_2 depend on the composition, temperature and pressure?
2. Which thermodynamic model is the most suitable to simulate the phase behaviour of the TEPA-H_2O-CO_2 system?

3. What are the implications of the experimental and modelling results for the design of the direct air capture unit of ZEF?

1.6 Methodology

The first research question is answered by measuring the binary VLE of H_2O and TEPA and the ternary VLE of CO_2, H_2O and TEPA using a VLE set-up provided by TNO (Netherlands Organisation for Applied Scientific Research). Secondly, a suitable thermodynamic model is selected based on a literature review of available models, specifically those applied in the field of amine based CO_2 capture. Following this, sub-questions are addressed by reproducing the selected model in Matlab and applying it first to a mature amine, to ensure the code works properly. Once the model is validated, the code is modified to suit TEPA. The model is regressed using the acquired VLE data from the experiments. The implications of the experimental and modelling results are addressed by applying the equilibrium models to a process simulation of the direct air capture system of ZEF.

1.7 Report outline

This thesis is structured as follows. Chapter 2 provides the theoretical background of the research field and concepts discussed in the following chapters. This includes the relevant thermodynamics and amine chemistry. Chapter 3 describes the experimental methods used for all the measurements performed in this work. In Chapter 4 the selected thermodynamic models are explained in detail, in terms of equations and assumptions. The experimental and simulation results are reported and discussed in Chapter 5. Chapter 6 contains the case study of the direct air capture unit of ZEF. The conclusions of this thesis are listed in Chapter 7. Finally, recommendations for further research are given in Chapter 8.

Chapter 2

Background

This chapter provides all the background information and research that is relevant for this study. First, an overview of the field of carbon capture is given with a particular focus on direct air capture strategies. Second, amine chemistry and the selection criteria for amine-based carbon capture solvents are discussed, followed by a detailed description of the amine used in this work: tetraethylenepentamine. Third, important thermodynamics concepts such as phase equilibria and chemical equilibria are explained, as well as the basic of electrolyte thermodynamics. A brief literature review of the available electrolyte models supports the decision made for the electrolyte model used in this work: the specific ionic interaction theory.

2.1 CO_2 capture

In recent years, carbon dioxide, or CO_2, has received widespread attention as the main greenhouse gas to cause man-made climate change. Therefore, the field of carbon capture is developing fast [3], for it could serve two very important purposes. First and foremost, if combined with CO_2 sequestration, it is a promising strategy to reduce CO_2 emissions to the air. This is called Carbon Capture and Storage (CCS). Secondly, captured CO_2 could potentially be used as an alternative feedstock for the carbon-based industry. These technologies are classified as Carbon Capture and Utilisation (CCU).

In this section, the question will be addressed of how CO_2 is captured from different sources. First a brief overview is given of CO_2 capture technologies and the most mature technology is discussed in more detail, followed by an analysis of direct air capture.

2.1.1 CO_2 capture from combustion processes

CO_2 can be captured from different sources of CO_2. It is generally more cost-effective to separate CO_2 from high concentration gas streams [24]. Therefore, CCS technology is focused on capturing CO_2 from the exhausts of industrial plants involving combustion processes [25]. For example, the waste gas streams of steel production, cement production, oil refining or fossil-fueled power plants contain high levels of CO_2. Often, three different approaches are distinguished for CCS technologies:

- **Postcombusion capture**: The CO_2 in the flue gas stream from the combustion of fossil fuels is captured. The advantage of this approach is that the capture system can be retrofitted to existing power plants [3].
- **Precombustion capture**: The fossil fuel is gasified first, followed by a water gas shift reaction which turns CO and H_2O into H_2 and CO_2. This CO_2 is then captured, while the H_2 rich fuel is combusted [25].
- **Oxy-fuel combustion**: Fossil fuels are combusted with a oxygen rich gas stream, which produces mostly CO_2 and H_2O, which can be easily purified. The main bottleneck for implementation of this technology is the high cost of a continuous oxygen supply [25].

The separation of CO_2 from these types of gas streams can be achieved by different methods, such as absorption, adsorption and membrane separation [26]. The best method of CO_2 capture depends on the CO_2 source, which can vary greatly in scale, concentration, pressure and temperature. In the context of CO_2 capture, absorption is described as the separation of a specific gas from a gas mixture, by means of a solvent, while adsorption refers to the process of separating a specific component in a gas or liquid by adhesion to a surface, usually a porous solid material [26]. Absorption is a bulk process, while adsorption is a surface process. Since this work deals with absorption of CO_2, adsorption and membrane separation technologies are outside the scope of this thesis.

Two types of absorption are distinguished: physical and chemical absorption. Physical absorption is a non-reactive process, which depends on the properties of both the liquid and the gas. It is based on Henry's law and takes place at high pressures and low temperature, while the reversed process, called desorption, takes place at low pressure and high temperature [26]. During chemical absorption, the solvent forms reversible chemical complexes with the absorbed CO_2. This is often preferred over physical absorption for low pressure applications. To reverse the chemical reaction so the CO_2 can be desorbed, heat must be supplied. This is called solvent regeneration.

2.1.2 CO_2 absorption by liquid amines

The most mature and promising CCS technology is post-combustion capture by means of chemical absorption in liquid amines [25]. They are a widely researched class of solvents, which have already been employed on a commercial scale [3][24]. A conventional amine-based CO_2 absorption system consists of an absorber and a regenerator or stripper. A generic process flow diagram is shown in Figure 2.1. The absorber is fed with aqueous amine solution at the top which is contacted with the CO_2 containing gas stream flowing up. Though a series of chemical reactions, the CO_2 is absorbed into the solvent, which now called "rich", since it is enriched with CO_2. The rich solvent flows from the bottom of the absorber column to the top of the stripper column. The reboiler, located at the bottom of the stripper, generates steam which flows up through the column, thereby heating up the rich solvent. This causes the chemical reactions in the solvent to reverse and the CO_2 to desorb out of the solvent. The solvent is now called "lean", because it contains smaller concentrations of CO_2. The lean solvent is pumped back to the absorber. A heat exchanger placed between the lean and rich solvent flow enables the lean solvent heat to be used to pre-heat the rich solvent. The gases that have been "stripped" from the solvent and the remaining steam are collected at the top of the stripper column and are condensed.

2.1.3 State-of-the-art direct air capture

While the largest part of worldwide CO_2 emissions are caused by large point sources such as thermal power generation plants and industrial processes, the remainder is caused by distributed sources such as cars, aircrafts and household heating [27]. To reduce these emissions, direct air capture (DAC) could provide a solution as it extracts CO_2 from ambient air [28]. Additionally, DAC could be combined with onsite technologies that use CO_2 as a feedstock (CCU technologies). This would eradicate the need for CO_2 storage and infrastructure, as a DAC processes are not location-specific [29]. An important benefit of DAC, compared to post-combustion capture, is that the sorbent does not have the same issues of contamination of other concentrated gases in the waste stream, such as sulfur- or nitrous oxides. However, as Sanz-Pérez et al. noted well, when comparing DAC and post-combustion capture technologies, one should keep in mind these technologies are different because they have different end goals [29]. It should not be a question of either the one or the other technology. Due to the vast scale of the climate change crisis, both technologies need to be developed and implemented side by

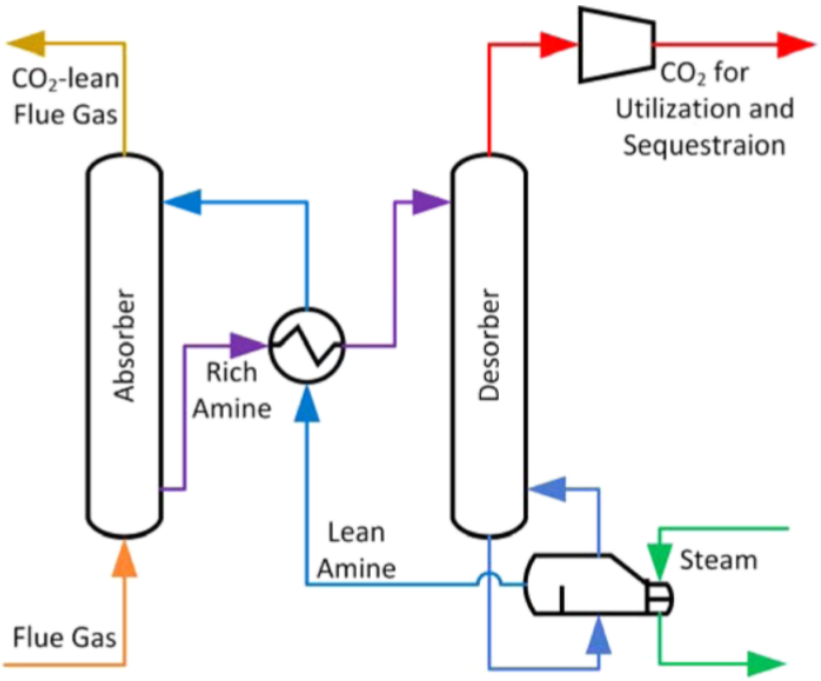

Figure 2.1: Flow sheet of a typical amine scrubbing process used in post-combustion capture of CO_2. In the absorber column, the lean amine solution chemically absorbs CO_2 at low temperature. In the reboiler, steam is heated. This passes through the desorber or stripping column to heat the rich amine solution, which causes release of CO_2 and regeneration of the lean amine solution [3].

side [29].

The main challenge of DAC is the low partial pressure of CO_2 in the air, approximately 400 parts per million. Additionally, atmospheric air can fluctuate in humidity, temperature and composition [27]. Therefore, a sorbent is needed that is inexpensive, physically and chemically stable in atmospheric conditions, selective for CO_2 over the other gases in the air, that can bind CO_2 strong enough, but also weak enough to be released without a huge energy demand during regeneration of the sorbent [28].

In general, chemical sorbents with strong CO_2 binding affinities are more effective for DAC than physical sorbents at low partial pressures of CO_2 [29][30]. In the review of DAC technologies by Broehm et al [27], three separation techniques are distinguished that appear to be the most technically and economically viable options for direct air capture of CO_2.

- Aqueous solutions of hydroxides
- Solid amine adsorbents
- Inorganic solid adsorbents

Besides these three technologies, there are others that are still in the research stage. Therefore, these will not be discussed further.

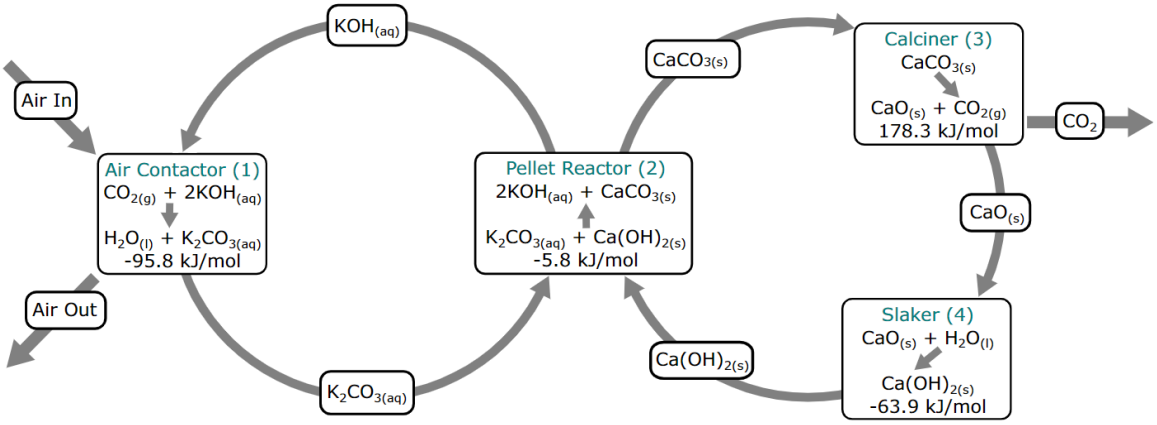

Figure 2.2: Process diagram of the Carbon Engineering DAC process. The titled boxes show the 4 main process steps. In side the boxes, the materials and the reactions are shown, together with the reaction enthalpy. [4]

Aqueous solutions of hydroxides

This technology is relatively mature, as it has been employed in other industries in the past, such as the paper industry, where it is called the Kraft process [27]. Different caustic solutions have been used, such as NaOH, KOH and $Ca(OH)_2$. When brought into contact with an air flow, the bases take up CO_2 through a chemical reaction. The company Carbon Engineering (CE) has been developing an aqueous DAC system, using alkaline aqueous solutions of potassium hydroxide (KOH) as a chemical absorbent [4] and calcium hydroxide, $Ca(OH)_2$ to regenerate the KOH. The process consists of two chemical loops, see Figure 2.2. In the first loop, the air is contacted with a KOH solution and the CO_2 is absorbed through an acid base reaction, in which carbonates are formed. In the second loop, $Ca(OH)_2$ is used to form a precipitate of $CaCO_3$. This $CaCO_3$ is heated up to 900 ℃ to release the CO_2 again. CaO is formed in this process, which is hydrated or ”slaked” to produce $Ca(OH)_2$ again.

The advantages of using liquid sorbents include continuous operation of the contactor, cheap contactor design using readily available cooling-tower hardware and long contactor lifetimes [4]. However it also suffers from high energy consumption of the regeneration step, which causes more CO_2 emissions, as well as evaporative water losses [4]. Additionally, buildup of calcium precipitates inside equipment can pose a problem [27].

Solid amine adsorbents

These type of technologies usually consist of a single DAC unit, which is used both as an absorber and a desorber, by cycling through different conditions in two steps [30]. First, ambient air is fanned through the unit until the sorbent is saturated with CO_2. Second, the system is sealed and the conditions are changed to desorb the CO_2 from the sorbent. The type of sorbent determines the optimal desorption conditions. These can be low pressure, high temperature, high moisture or a combination of these [27].

The largest number of publications have been investigating solid supported amine sorbents [29]. Mainly, the focus of research is on the identification of a suitable amine material and an effective support structure [27]. Previously, they have been divided into three classes, depending on the way the amine is bonded to the support structure [29]. Class 1 are structures where the amine is impregnated into the pores of a substrate material, which means the amine is physically bonded to the surface, often

through hydrogen bonds. Class 2 consists of amines bonded to the walls of the structure with covalent bonds. Class 3 sorbents involves amine monomers that have been polymerised inside the pores of the support structure, thereby covalently bonding polyamine structures to the walls [29]. These three classes are visualised in Figure 2.3.

The advantages of solid supported amine sorbents are their strong bonding of CO_2 at low partial pressures, as well as a high selectivity towards CO_2, compared to physical sorbents [29]. Compared to aqueous solutions of bases, solid sorbents generally require a lower energy input and lower operating costs [4]. However, a disadvantage is the potentially short lifetimes of the amine materials, as they are prone to degradation and evaporation (in case of class 1 sorbents) [30]. Also, the air capture unit design is much more complex compared to that of continuously flowing liquid sorbents, because it must allow for the cycling of the conditions of absorption and desorption in a single chamber. Keith et al describe the main challenge of solid sorbents as the inherently conflicting demands of high sorbent performance, low cost and long economic life in air [4].

Global Thermostat is a company that currently employs a patented amino-polymer adsorbent in multiple pilot and demonstration plants [30]. Climeworks, a Swiss company, is another well-known example of a company that has launched a pilot direct air capture plant, using a cellulose fiber support structure functionalized with amine molecules [30].

Inorganic solid adsorbents

Other solid adsorbents besides amines have been researched, that can reversibly bond CO_2, such as zeolites and Na or Ca based compounds [27]. Zeolites are microporous aluminosilicate structures. Their advantage is the low temperature for regeneration. However, they are very sensitive to atmosphere humidity [27]. Na an Ca based solids take up CO_2 in a similar way to the aqueous bases containing Na an Ca, discussed above. However, issues of slow kinetics and deterioration upon cycling have been reported, especially for CaO systems [27].

The Dutch company Antecy, which has recently joined forces with Climeworks [31], has developed and absorption process based on potassium carbonate (K_2CO_3), which is a cheap material that can be regenerated at a lower temperature, because it uses a moisture-aided desorption reaction [30].

2.1.4 Direct air capture at Zero Emission Fuels

The start-up Zero Emission Fuels BV (ZEF) has been introduced in Section 1.3 as a company working on a small scale methanol factory, which uses only air and sunlight as inputs. The first step in the ZEF process is the capture of H_2O and CO_2 from ambient air. After developing and testing multiple prototypes, which used solid supported amine adsorbents, the direct air capture research has taken a new direction towards continuous capture systems based on liquid polyamines. This is a class of amines that has previously only been applied in the field of solid amine sorbents. This way ZEF takes advantage of the maturity of chemical absorption in liquid amines, a technology widely applied in post-combustion capture of CO_2, but using sorbents that have proved very promising in the field of DAC.

Two polyamine sorbents have been the focus of research at ZEF: polyethyleneimine (PEI) and tetraethylenepentamine (TEPA). The liquid properties and CO_2 absorption characteristics of aqueous solutions of these polyamines have been characterised and compared [22][9]. It was found that TEPA had more favorable characteristics, such as higher absorption rate, higher equilibrium solubility of CO_2 at the same conditions.

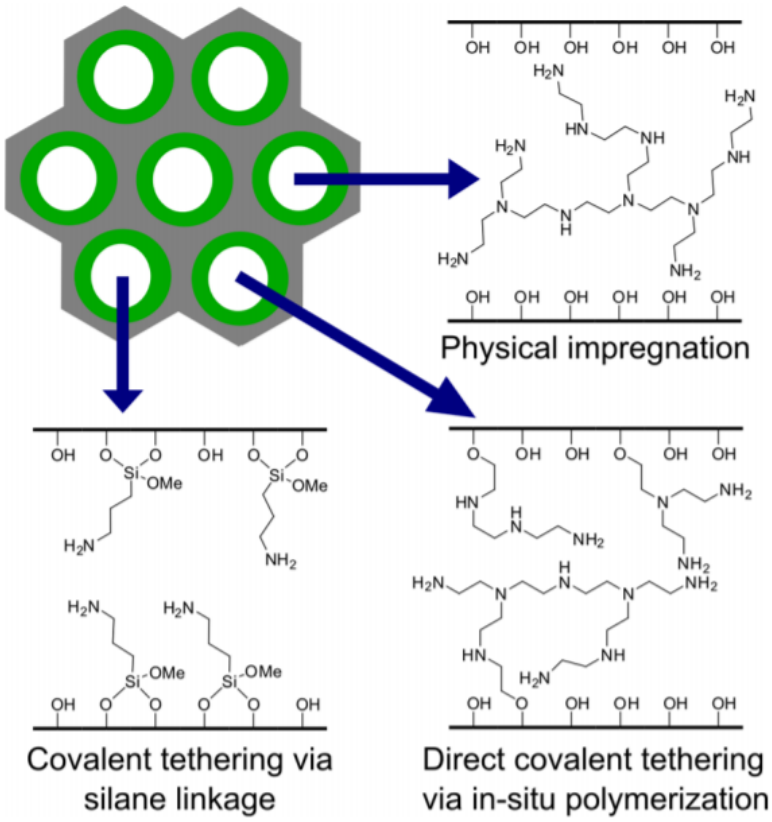

Figure 2.3: Three classes of amine functionalized silica. Class sorbents 1 are porous structures physically impregnated with amine (top right). Class 2 sorbents consist of amine molecules chemically bonded to the surface of the support (bottom left). Class 3 sorbents contain in-situ polymerized and covalently bonded amines (bottom right). [5]

2.2 Amine solvents for CO_2 capture

2.2.1 Primary, secondary, tertiary and sterically hindered amines

An amine is a chemical species which contains an amino group: a nitrogen atom, to which zero, one or two hydrogen atoms are connected. Four types of amines are distinguished: primary, secondary, tertiary and sterically hindered amines. Primary amines are connected to one organic substituent, such as an alkyl or aryl group, and two hydrogen atoms. Secondary amines have two organic substituents and one hydrogen atom. Tertiary amines are connected to three organic substituents. This is shown in Figure 2.4, where R denotes an organic substituent. A sterically hindered amine is a compound in which the adjacent groups in the molecule are ”in the way”, preventing reactions from occurring at the nitrogen atom, as a result of repulsive forces between overlapping electron clouds. Primary amines connected to a tertiary carbon and secondary amines attached to a secondary or tertiary carbon atom are sterically hindered [32].

Primary and secondary amines can form stable carbamates when contacted with CO_2, through the same reaction mechanism. First a zwitterion, an ion with both a negative and positive charge, is

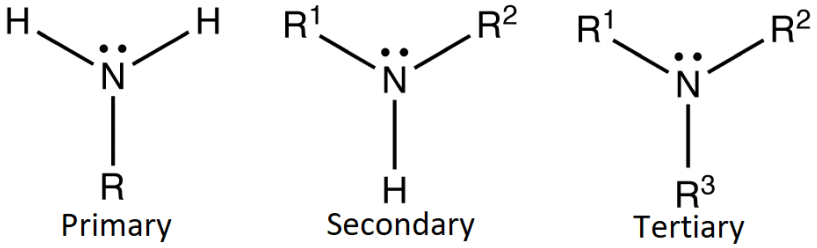

Figure 2.4: General structure of primary, secondary and tertiary amines.

formed [33].

$$R_1R_2NH + CO_2 \leftrightarrow R_1R_2NH^+COO^- \tag{2.1}$$

Next, the proton from the zwitterion is transferred to another amine, which then becomes protonated [33]. The zwitterion has become a carbamate.

$$R_1R_2NH + R_1R_2NH^+COO^- \leftrightarrow R_1R_2NH_2^+ + R_1R_2NCOO^- \tag{2.2}$$

The carbamate can be hydrolysed, resulting in the formation of bicarbonate and regenerating a free amine [33].

$$R_1R_2NCOO^- + H_2O \leftrightarrow R_1R_2NH + HCO_3^- \tag{2.3}$$

Because two amines are necessary to form one carbamate species, the maximum loading at low pressures is 0.5 mole of CO_2 per mole of amine. These reactions occur at a relatively high rate, compared to the CO_2 absorption reaction with tertiary amines [33].

Tertiary amines undergo a different reaction mechanism, because they don't have a proton as a leaving group [34]. They form bicarbonates directly.

$$R_1R_2R_3N + CO_2 + H_2O \leftrightarrow R_1R_2R_3NH^+ + HCO_3^- \tag{2.4}$$

Because of this mechanism, the maximum loading is theoretically 1 mole of CO_2 per mole of amine, twice as high as that of primary and secondary amines. Also, the heat of absorption of this reaction is lower which makes the regeneration energy demand lower for tertiary amines, compared to primary and secondary amines. However, this reaction has a lower reaction rate [34].

Conventional amines used for the capture of CO_2 include monoethanolamine (MEA), which is often used as a benchmark, diethanolamine (DEA), N-methyldiethanolamine (MDEA) and 2-amino-2-methyl-1-propanol (AMP) [35].

2.2.2 Selection criteria for CO_2 capture solvents

The ideal CO_2 capture solvent should have the following characteristics:

- A high CO_2 absorption capacity
- Low regeneration heat duty
- Fast reaction kinetics

The total heat required to regenerate the amine solution in the stripper column is the sum of three different energy terms [36]:

$$E_{\text{regeneration}} = E_{\text{absorption}} + E_{\text{sensible}} + E_{\text{vaporization}} \tag{2.5}$$

The first term is the heat of absorption. This accounts for the heat released during the reaction (or the heat required to reverse the reaction), the heat of physical dissolution of CO_2 and the heat of non-ideal mixing, which is a result of the new interactions being formed in the mixture. The second term is the sensible heat. This is the energy required to increase the temperature of the lean amine solution to that of the reboiler. The third term, the heat of vaporisation, is the heat required to produce the amount of stripping steam that is *not* condensed on its way up in the column. The heat of the steam that *has* condensed on its way up the column has supplied the heat of absorption, stripping the acid gases off the amine solution [36].

These three different components of the regeneration heat requirement are all important for determining the overall heat duty and therefore the cost of the CO_2 capture process. These three enthalpies are not mutually exclusive, since they depend on one another and on the specific process parameters. Therefore, it is not sufficient to only focus on selecting a solvent with a low heat of absorption, without taking the overall process in which the solvent is used into consideration [36].

As described in the previous section, no single, primary secondary or tertiary amine solvent satisfies all three of these requirements [37]. Fortunately, research has shown that blends of primary/secondary amines and tertiary amines improve reaction rates with respect to the pure tertiary amine and reduce the overall heat of absorption, compared to the pure primary or secondary amine[33] [37] [38]. In other words, these blends offers best of both worlds! Sterically hindered amines also offer such favorable characteristics. They can form carbamates of low stability, due to the presence of large groups in the proximity of the nitrogen atom [39]. The consequence is that the bicarbonate route is preferred over the carbamate route, which results in a higher CO_2 capture capacity than that of unhindered primary/secondary amines [39].

Besides the aforementioned main requirements of a solvents for CO_2 capture, there are other properties that should be evaluated:

- Density and viscosity of the solvent. These are important for estimating mass transfer rate in the liquid
- Corrosive behaviour of the solvent. This can do serious damage to process equipment.
- Degradation of the amine. Thermal degradation can occur because of the high temperature swing the amine is subjected to, while oxidative degradation happens in the presence of oxygen in the absorber. Degradation products can also worsen the corrosive behavior of the solution [40].
- Vapor pressure of the solvent. Although in vapor-liquid equilibrium models the amine vapor pressure is often neglect, highly volatile amines can result in high amine losses in practice [39].
- Cost of the solvent.

2.2.3 Polyamines

A polyamine is a molecule that has more than two amino groups, which can be primary, secondary or tertiary. Therefore, it can react with more than two CO_2 molecules per polyamine molecule. Their

potential for CO_2 capture is very dependent on the molecular structure of the amine [41].

A few papers have been published that study and compare the performance of different aqueous polyamine sorbents. Muchan studied the effect of the number of amino groups in the polyamine on the absorption and desorption of CO_2, by comparing the behavior of ethylenediamine (EDA), diethylenetriamine (DETA), triethylenetetramine (TETA) and tetraethylenepentamine (TEPA) [23]. It was found that a higher number of amino groups resulted in a higher equilibrium CO_2 loading per molecule of amine, a higher initial absorption rate and a decreasing basicity. Also, the heat duty for sorbent regeneration was estimated based on the absorption data. This estimation showed a decrease in heat duty with increasing number of amino groups. This was explained by the fact that secondary carbamates and dicarbamates form weaker bonds that primary carbamates and are therefore easier to break down. Therefore, TEPA showed the most promise as a CO_2 capture sorbent. Aronu also reported that TEPA at low concentrations showed great CO_2 capture potential, with fast reaction rates and a high absorption capacity [6]. Due to the higher number of amino groups per molecule, TEPA could remove 3 times more CO_2 per cycle than MEA at the same concentration [6]. Kim studied the properties of six aqueous triamines varying only substituents at the amino groups and their mixtures with other mono- or di-amines and found that 3,3'-iminobis(N,N-dimethylpropylamine) (IBDMPA) exhibited high cyclic capacity, low regeneration duty and moderate CO_2 rate, although it was prone thermal degradation [41].

Unfortunately, only limited information is available about the species distribution of polyamines, which would provide insight into the reactions mechanisms and support modelling efforts. Hartono qualitatively studied the speciation of the DETA-CO_2- H_2O system using ^{13}C NMR spectra [42] and modelled the CO_2 absorption [43]. Kim et al measured ^{13}C-NMR and ^{1}H-NMR spectra for the CO_2 absorption in aqueous 3-methylamino-propylamine (MAPA), DETA, TETA and TEPA solutions. Because DETA, TETA and TEPA have more NH-groups than MAPA, they can form many more possible species with CO_2. For TETA and TEPA, the multitude of species could not clearly be distinguished in the ^{13}C-NMR spectra [35].

2.3 Thermodynamics of amine-based CO_2 capture

2.3.1 Vapor-liquid equilibrium

A vapor-liquid equilibrium (VLE) is defined as the state of coexistence of a liquid and a gas phase. For mixtures, the VLE describes the relationship between the quantities of temperature, pressure and composition of both phases [44]. Usually, given a set of these quantities for a certain mixture, the goal is to calculate the others. For example, given a specified binary mixture at a given temperature and pressure, it is possible to calculate the compositions of the liquid and the vapor phase. This information is particularly important in the field of separation technology. Proper design of a separation process requires detailed knowledge of the phase equilibrium behavior as a function of T, P and composition of the mixture that needs to be separated [45]. Other types of phase equilibria can be distinguished, such as solid-liquid equilibria (SLE), liquid-liquid equilibria (LLE) or vapor-liquid-liquid equilibria (VLLE), but these are outside the scope of this thesis. The thermodynamic phase equilibrium is defined by the so-called iso-fugacity condition which must hold for every component *i* in the mixture:

$$f_i^V = f_i^L \tag{2.6}$$

where f is the fugacity, V stands for vapor and L for liquid [44]. Generally, the task is to relate the fugacity of the seperate components in the mixture to the composition of that mixture. The fugacity

coefficient for components in the vapor phase is defined as

$$\phi_i^V = \frac{f_i^V}{y_i P} = \frac{f_i^V}{p_i} \tag{2.7}$$

The fugacity of a component in the gas phase can be considered as the ”effective partial pressure” exerted by that component in a non-ideal gas mixture. The fugacity coefficient can be interpreted as a measure of deviation from the ideal gas behavior. For an ideal gas mixture, ϕ_i would equal unity. For components in the liquid phase, the fugacity of component *i* is related to its mole fraction in the liquid phase through the activity coefficient.

$$\gamma_i = \frac{a_i}{x_i} = \frac{f_i}{x_i f_i^0} \tag{2.8}$$

Activity of a component in the liquid phase can be considered as the ”effective concentration” of that species, note the analogy of this concept to that of fugacity. The first term of Equation 2.8 shows that the activity coefficient is analogous to the fugacity coefficient for components in the liquid phase, as it is a measure of deviation from ideality. In an ideal solution, the activity would equal the mole fraction and the activity coefficient would equal unity. The f_i^o, in the second term, is the standard state fugacity of component *i*. Usually, for convenience, the standard state is that of the pure liquid at system temperature and pressure [44]. This can be calculated:

$$f_i^0(T, P, x_i = 1) = P_{\text{vpi}}(T)\phi_i^s(T)\exp\int_{P_{\text{vpi}}}^{P} \frac{V_i^L(T, P)}{RT} dP \tag{2.9}$$

where P_{vpi} is the pure component saturation vapor pressure and ϕ_i^s is the pure component fugacity coefficient. The exponential term is called the Poynting factor, which can be usually neglected, as a liquid is nearly incompressible [44].

Putting all these formulas together into the iso-fugacity condition results in the well known VLE relation for each component:

$$y_i P = \gamma_i x_i P_{\text{vpi}} \frac{\phi_i^s}{\phi_i} \exp\int_{P_{\text{vpi}}}^{P} \frac{V_i^L dP}{RT} = \gamma_i x_i P_{\text{vpi}} \mathscr{F} \tag{2.10}$$

Often, this relation is simplified, by assuming the correction factor $\mathscr{F}$ equal to unity, which is justified at low to moderate pressures. This relation is then called the modified Raoult’s law.

$$y_i P = \gamma_i x_i P_{\text{vpi}} \tag{2.11}$$

When the activity coefficient is also set to unity, Raoult’s law is the result.

$$y_i P = x_i P_{\text{vpi}} \tag{2.12}$$

For binary systems, a plethora of equilibrium data is available. However, for multi-component systems, much less data is available, because it is very time consuming to measure[45]. To illustrate, for a 10-component system, if one measures the normal boiling points of all possible combinations (also considering binary, ternary quaternary etc. system) in 10 mol% steps one would require 92378 data points. Assuming 10 measurements can be performed a day, this would take 37 years to measure. For this reason, many thermodynamic models have been developed that greatly reduce the required experimental data points, for example, by only using binary data as an input [45].

2.3.2 Chemical equilibrium

Next to vapor-liquid equilibrium, chemical equilibrium is an important concept in this thesis.

Consider the generic reaction,

$$aA + bB \leftrightarrow cC + dD \tag{2.13}$$

The thermodynamic equilibrium constant defines the composition of this reaction mixture at equilibrium. For a general reaction in the liquid phase, this equilibrium constant would be defined as the ratio of activities.

$$K_{eq} = \frac{a_C^c a_D^d}{a_A^a a_B^b} = \frac{c_C^c c_D^d}{c_A^a c_B^b} \frac{\gamma_C^c \gamma_D^d}{\gamma_A^a \gamma_B^b} \tag{2.14}$$

where a_i is the activity, c_i the concentration and γ_i the activity coefficient of component i. The equilibrium constant only varies with temperature. This variation can be calculated using the Van 't Hoff equation [45].

$$\frac{d\ln K}{dT} = \frac{\Delta H_R^0}{RT^2} \tag{2.15}$$

This can be integrated to the following form, assuming the reaction enthalpy ΔH_R^0 to be constant of the temperature range.

$$\ln K(T) = \ln K(T_0) - \frac{\Delta H_R^0}{R} \left(\frac{1}{T} - \frac{1}{T_0} \right) \tag{2.16}$$

2.3.3 Electrolyte thermodynamics

Electrolytes are substances that dissociate into positively charged cations and negatively charged anions, when dissolved in a polar solvent, such as water [46]. Strong electrolytes dissociate completely, whereas weak electrolytes only dissociate partially.

Kontogeorgis cites two scientists in the field of molecular simulation [47]. The first says: "Life is too short for electrolytes". The second: "All my life I have tried to keep myself away from water and electrolytes" [47]. He introduces the field of electrolyte thermodynamics as one defined by many uncertainties and difficulties. This topic is relevant in many different sciences and engineering fields and finds application in amongst others water desalination, fertilizer production, biotechnology and CO_2 capture [48]. The dissolution of CO_2 into aqueous amines results in the formation of different charged species, such as bicarbonate, carbamates and protonated amines, therefore this by definition is an electrolyte system.

There are multiple differences between electrolyte solutions and non-electrolyte solutions. First of all, the behavior of electrolyte solutions deviates more from ideality compared to solutions containing only molecular species, because the electrostatic Coulomb forces between ions have a longer range than the van der Waals and related forces between molecules [48]. This Coulomb force between two ions *i* and *j* is expressed as:

$$F_{ij} = \frac{q_i q_j}{4\pi\epsilon_0 \epsilon r_{ij}^2} \tag{2.17}$$

where q is the electric charge, ϵ_0 is the permittivity of vacuum, ϵ is the relative permittivity of the medium and r is the ionic radius [45]. As can be seen from the equation, the effect of electrostatic forces becomes larger as the ion valency increases.

Secondly, in electrolyte solutions, one must always account for the constraint of electroneutrality. This means that the total amount of positive and negative charge cancel each other out. If the electrolyte

dissociates into ν_- anions and ν_+ cations with a valance of Z_- and Z_+, the electroneutrality condition can be described as:

$$\nu_- Z_- + \nu_+ Z_+ = 0 \tag{2.18}$$

The implication of this constraint is that the concentrations of two ions cannot be varied independently from each other. Additionally, one cannot make a solution of only 1 type of ion. It is more meaningful to define a mean ionic chemical potential for an electrolyte solution, instead of a chemical potential for the cations or anions separately, since this $\mu_\pm$ can be determined experimentally [45].

$$\mu_\pm = \frac{\nu_+ \mu_+ + \nu_- \mu_-}{\nu} \tag{2.19}$$

where $\nu = \nu_+ + \nu_-$, $\mu_\pm$ is the mean ionic chemical potential, μ_+ is the chemical potential of the cation and μ_- is the chemical potential of the anion. The mean ionic molality is defined as

$$m_\pm^\nu = m_+^{\nu_+} m_-^{\nu_-} \tag{2.20}$$

and the mean ionic activity coefficient is defined as

$$\gamma_\pm^\nu = \gamma_+^{\nu_+} \gamma_-^{\nu_-} \tag{2.21}$$

The mean ionic activity of a solution $a_\pm$ is defined as

$$a_\pm^\nu = (\frac{m_\pm}{m^\circ})^\nu \gamma_\pm^\nu \tag{2.22}$$

This mean ionic activity is related to the mean ionic chemical potential through:

$$\mu_\pm = \mu_\pm + RT \ln a_\pm \tag{2.23}$$

Thirdly, the concentrations of electrolyte solutions are usually expressed in terms of molality, which is defined as the number of moles of solute per kg of solvent. The reason for the popularity of molality is that the numbers are often more practical (between 0 and 20 for most), compared to the mole fractions which are small [49]. Due to the use of molality, different standard states are used for the solvent and the solute. For example, for water, often the solvent in electrolyte applications, the standard state is its pure form, where $\gamma_i \to 1$ as $x_i \to 1$. However, for ions we need a different approach, since we cannot have an ion in its pure form, due to the electroneutrality condition. Therefore, the reference state for ions is that of infinite dilution, such that $\gamma_i^* \to 1$ as $x_i \to 0$ [49].

2.3.4 Overview of electrolyte models used for CO_2 capture

This section provides an overview of different approaches to model the equilibrium absorption of CO_2 in aqueous solutions of amines. These models simultaneously solve the chemical equilibria in the liquid and the phase equilibrium of the entire system. Usually, the results are presented in a graph showing the partial pressure of CO_2 as a function of loading, defined as the number of moles CO_2 absorbed per moles of amine.

The different approaches to modelling amine-H_2O-CO_2 systems can be divided into three categories: semi-empirical models, activity coefficient models and electrolyte equations of state. The overview presented below is not an exhaustive list, but introduces the most commonly used models in literature.

Simple semi-empirical models

- **Danckwerts and McNeil** [50]: This model, together with the Kent and Eisenberg model [51], was one of the first widely applied models used to calculate vapor- and liquid phase compositions in amine-CO_2-H_2O systems [48]. The equilibrium constants of the reactions occurring in the liquid phase were fitted to functions of ionic strength without taking into account non-ideality of either phase, using experimental data.
- **Kent and Eisenberg** [51]: In this simple model, the liquid phase activity coefficients and vapor phase fugacity are set equal to 1, while the equilibrium constants of the reactions are fitted to experimental data. This way, the non-ideality of the system is lumped into these K-values.
- **Gabrielsen** [52]: Instead of accounting for all the different chemical equilibria separately, the model proposed by Gabrielsen considers one overall chemical equilibrium. This means only one explicit equation has to be solved for the CO_2 partial pressure over aqueous alkanolamine solution, with only 3 to 4 adjustable parameters. The fit for three different types of amines is relatively good, especially considering the simplicity of the model [52].

Activity coefficient models

- **Debye-Hückel theory**: This theory is the first successful model of ion-ion interactions, which dates back to 1923 when Peter Debye and Erich Hückel described the thermodynamics of ideal electrolyte solutions [49]. The theory is based on many assumptions. First, it only takes the ionic interactions into account, therefore neglecting the ion-dipole interactions with the solvent, for instance. Next, it assumes that ions are point charges, and their electric field is spherical. The ions do not influence the permittivity of the solution, thus it is equal to the permittivity of the solvent [45]. In other words, the solvent is a di-electric continuum, it has no structure. The electrolyte is assumed to be strong, so it is fully dissociated. The distribution of ions around another ion is governed by Boltzmann's law [45]. The derivation of the full theory can be found in [48] and [49]. However, most textbooks describe the so-called extended DH equation:

$$ln\gamma_i^* = -Z_i^2 \frac{A\sqrt{I}}{1 + Ba\sqrt{I}} \tag{2.24}$$

where I is the ionic strength, a measure of the of ion concentration of a solution. The molar ionic strength is calculated by:

$$I = \frac{1}{2} \sum_{i=1}^{n} m_i z_i^2 \tag{2.25}$$

where m_i is the molarity of the ion and z_i the charge of the ion. A is the Debye-Hückel parameter

$$A = (2\pi N_A d_o)^{1/2} (\frac{e^2}{4\pi\epsilon k_B T})^{3/2} \tag{2.26}$$

and B is defined as

$$B = (\frac{2e^2 N_A d_0}{\epsilon k_B T})^{1/2} \tag{2.27}$$

This usually gives a good approximation of the activity coefficient up to I $\leq$ 0.1 molal [49].

The Debye Hückel Limiting Law is an even further simplified version.

$$log\gamma_{\pm}^m = -A_m |z_+ z_-| I^{1/2} \tag{2.28}$$

The limiting law only holds at very low values of the ionic strength. It is said to be valid approximately up to an ionic strength of I$\leq$ 0.001 molal [45].

- **Specific ion interaction theory (SIT)**: As an electrolyte solution becomes more concentrated, short-range non-electrostatic interactions become more important. This theory, first proposed by Brønsted [53] and further developed by Guggenheim [54] and Scatchard [55], is a correction of the extended Debye-Hückel law. An extra linear term is added to the equation of the activity coefficient, which accounts for concentration dependent short-range ionic interactions.

$$log\gamma_i = -\frac{z_i^2 A\sqrt{I}}{1 + 1.5\rho^{-1/2}\sqrt{I}} + \sum c_j \epsilon_{ij} \tag{2.29}$$

  In their 2013 paper, Puxty and Maeder [7] found that the SIT model describes the VLE behavior of MEA, AMP and PZ up to high concentrations (10 M) as good, if not better than the more complex models, such as e-NRTL or e-UNIQUAC [7].

- **Pitzer**: The Pitzer model was the first major engineering model for electrolytes [48]. It produces accurate results for aqueous electrolyte solutions up to concentrations of 6 mol/kg. The disadvantage of the model is that it is complex. It contains a large number of binary and ternary adjustable parameters, that need to be determined by regression of experimental data. Regression is a difficult task for a system with multiple liquid phase solute species. These parameters are highly dependent on temperature, so they may only be used in the conditions at which they have been regressed. Furthermore, the amine-water system should be treated as a mixed solvent of variable composition, whereas Pitzer's method is more suitable for single solvent systems [56].

- **e-NRTL**: The electrolyte nonrandom-two-liquid (e-NRTL) model was originally proposed by Chen and co-workers in 1982 [57], as a modification of the conventional NRTL concept, developed by Renon and Prausnitz in 1968 [58]. In turn, this concept is based on the local composition theory proposed by Wilson [59], which states that the composition around a molecule is different from the overall composition, because of intermolecular forces.

  Two important principles underlie the e-NRTL model. The first is the like-ion repulsion assumption. This entails that the concentration cations near another cation is zero and same goes for anions, due to large repulsive electrostatic forces. The second is the local electroneutrality assumption, which states that around a central molecule, the concentrations of anions and cations is such that the net ionic charge is zero [48].

  The activity coefficient is calculated from the excess Gibbs energy, which is the sum of three contributions. The first is the Pitzer-Debye-Hückel term. The second is the Born expression. The third contribution is the local composition term [45].

$$g^E = g^{E,DH} + g^{E,Born} + g^{E,LC} \tag{2.30}$$

  E-NRTL has been widely used to model CO_2-H_2O-amine systems [48]. It is available in most commercial process simulators, such as the Aspen Plus software. According to Aspen Inc, the model can handle mixed solvent systems, and both weak and strong electrolytes at any concentrations [60].

- **e-UNIQUAC**: The extended UNIQUAC model, described by Thomsen and co-workers [61] is an extension of the regular UNIQUAC theory to electrolyte applications through the addition of an

extended-DH term to account for ion-ion interactions [48]. The model consists of three terms:

$$G^{ex} = G^{ex}_{combinatorial} + G^{ex}_{residual} + G^{ex}_{extended\ D\text{-}H} \tag{2.31}$$

It has been successfully applied to CO_2-water-amine systems [62] [6], showing excellent correlation of the equilibrium pressure over a large range of loadings and temperatures. The main difference between e-UNIQUAC and e-NRTL is that e-UNIQUAC uses ion-specific parameters, while e-NRTL uses salt-specific parameters [48].

Electrolyte equations of state

Electrolyte equations of state (e-EoS) have emerged as a new generation of electrolyte models [47]. They could potentially be a more generally applicable alternative to activity coefficient models with a more theoretically sound foundation [47]. Another benefit of an e-EoS is that it can be used to treat the liquid and gas phases equally, while activity coefficient models require the use of a separate model for the gas phase. To date, these types of models have rarely been used in the field of CO_2 absorption in amines. Nevertheless, two examples are described below.

- **Fürst and Renon**: [63]: This e-EoS is derived from an expression of the Helmholtz free energy, which contains a non-electrolyte term, a short-range and a long-range ionic term [63]. It has been used in several different variations to model chemical CO_2 absorption by amines. For example, Vallée applied it to the VLE of CO_2-H_2O-DEA mixtures [64].
- **SAFT-VR** [65]: MacDowell et al. describe the application of the statistical associating fluid theory for potentials of variable range (SAFT-VR) to the VLE of CO_2 absorption in aqueous amine solutions. Like other SAFT equations of state, this model is derived from statistical mechanical methods, specifically thermodynamic perturbation theory. It considers molecules as chains of identical spherical segments which interact with one another [48].

2.3.5 Selection of suitable electrolyte model

The thermodynamic model chosen for the purpose of this work must describe the partial pressure of CO_2 above a highly concentrated solution of TEPA over a wide range of temperatures and CO_2 loadings. It is not crucial to be able to predict liquid phase speciation. To the author's knowlegde, no study has previously attempted to model the VLE of CO_2 absorption in TEPA. Therefore, a model is selected from the electrolyte models that have been applied to CO_2 absorption in other amine solutions. The selection of a suitable thermodynamic model is fundamental, as this decision will have a big impact on the results.

The different electrolyte models have different advantages and disadvantages. The semi-empirical models are very straightforwards and simple to implement and have proven reliable to estimate the partial pressure of CO_2. However, they cannot be reliably extrapolated outside the range used for parameter estimation nor can they accurately predict the chemical speciation [56]. In that regard, activity coefficient models are a better choice. The major drawback of activity coefficients is that often a large number of parameters need to be fitted to experimental data, which means that a substantial data set is required for regression and the model is more computationally complex [7]. Compared to activity coefficient models, e-EoS have the advantage of a more theoretically sound foundation and better predictive capability [48]. However, their relative immaturity renders these models more explorative in nature and a much smaller body of work has been devoted to the subject in the context of chemical CO_2 absorption.

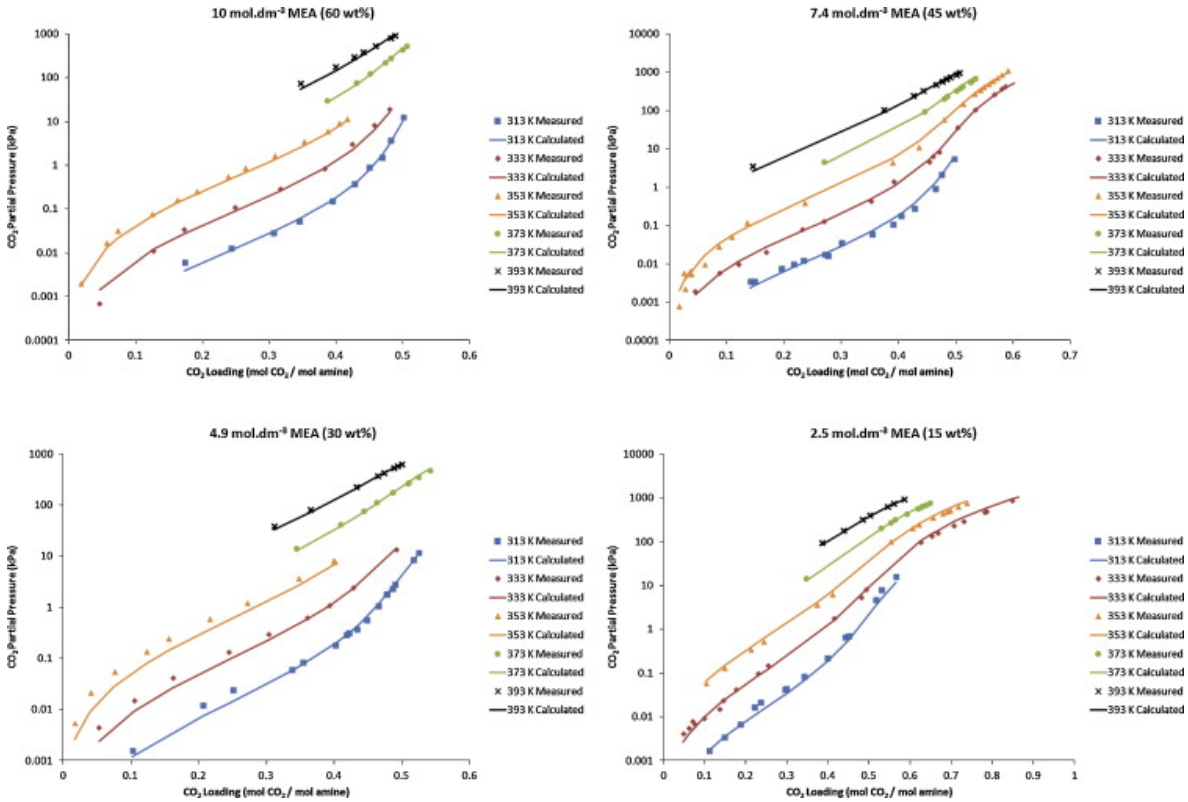

Figure 2.5: Experimental datapoints from Aronu et al (2011) [6] and model calculated lines for CO_2 partial pressure as a function of CO_2 loading in aqueous MEA, as calculated by Puxty and Maeder (2013) [7].

Taking all these considerations into account, the model of choice is the **specific ionic interaction theory (SIT)**, as described in the paper by Puxty and Maeder [7]. In their models, the short-range interaction term was set to zero, as it did not improve the accuracy of the correlation. This reduces the theory to the **extended Debye-Hückel law**. This model is chosen due to its comparable performance compared to complex thermodynamic electrolyte models such as e-NRTL, ex-UNIQUAC and Pitzer, but its relative simplicity. They found that the SIT model describes the VLE behavior of MEA, AMP and PZ up to high concentrations (10 M) as good, if not better than the more complex models [7]. The excellent agreement of the model prediction and the experimental VLE data for CO_2 absorption in aqueous MEA solutions is demonstrated in Figure 2.5.

Chapter 3

Experimental methods

In this chapter, the materials and the method used to measure the vapor-liquid equilibrium (VLE) of TEPA, H_2O and CO_2 are described. First, the experimental set-up is explained in detail, followed by a description of the planning, procedure and assumptions underlying the CO_2 loading and the vapor curve measurements.

3.1 Experimental setup

A schematic of the setup is shown in Figure 3.1. It consists of an autoclave (Büchi glasuster cyclone 300), whose temperature is controlled by a liquid bath around the vessel (Huber Ministat 230) and a separate liquid bath for the lid (Julabo F32GB) with a temperature stability of $\pm$0.02 K and $\pm$0.01 K, respectively. The solvent is injected through an opening in the lid. The gas is injected by a mass flow controller (Bronkhorst Flowbus). A temperature sensor is placed directly in the liquid to measure the temperature of the solvent, while another temperature sensor measures the temperature of the vapour phase. The pressure is measured by WIKA P30 pressure sensor, with an accuracy of 0.5% over the entire range from 0 to 6 bar. The solvent is mechanically stirred to ensure good mixing between the gas and the liquid, which is especially useful when dealing with viscous liquids such as TEPA. A vacuum pump is connected to evacuate the chamber at the start of the experiment.

This set-up was used to perform two types of experiments: vapor curve measurements and CO_2 loading measurements. These are discussed in detail in the next two sections.

3.2 Vapor curve measurements

The aim of these experiments is to measure the equilibrium of TEPA and H_2O without the addition of any CO_2.

3.2.1 Design of experiment

The only variable that could be varied in this experiment was the composition of the mixture. The temperature range studied was 298.15 unitl 393.15 K (or 25℃ - 120℃).

Table 3.1: Experimental plan for vapor curve measurements.

Concentration	**Temperature**
wt %	K
30	298.15 - 393.15
70	298.15 - 393.15
80	298.15 - 393.15

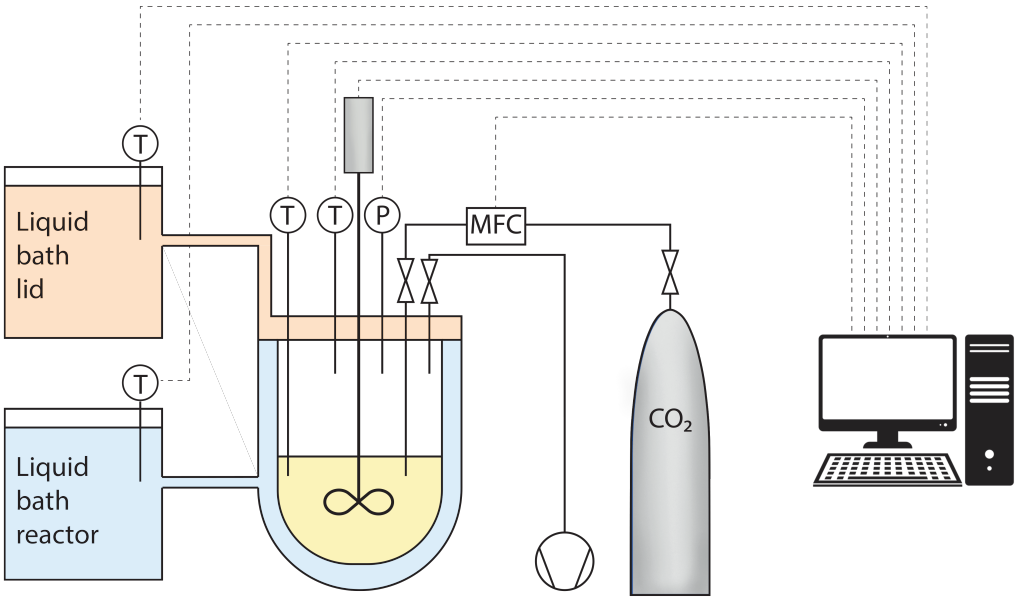

Figure 3.1: Schematic of the VLE apparatus, consisting of a mechanically stirred autoclave heated by two separate liquid baths. The CO_2 gas is injected from the gas bottle into the autoclave using a mass flow controller. A vacuum pump is connected as well. The mass flow controller, liquid baths and stirrer as well as all pressure and temperature sensors are controlled by the computer software.

3.2.2 Procedure

During a vapor curve measurement, no CO_2 is added. Only the equilibrium pressure of the TEPA solution was measured as a result of changing temperature.

1. The solution was loaded into the vessel through a plastic funnel. The remaining solvent on the funnel and in the sample flask is measured on the mass balance to determine the exact weight of solution inside the vessel.
2. The stirring mechanism was set to 500 rpm.
3. The liquid baths were set to 298.15 K. Once the liquid reached this temperature, the vessel was evacuated for 5 minutes.
4. The solution was left to stabilize for at least 1 hour.
5. Then, the temperature of the liquid baths was increased manually with at least 1 hour between every step. The liquid bath of the lid was set slightly higher than that of the vessel.
6. After the last step, the solution was cooled down and cleaned according to the procedure detailed in section 3.3.2.

3.2.3 Data processing

The data output of a vapor curve experiment is a raw data file containing per second data of the temperature in the liquid phase, the temperature in the gas phase and the pressure inside the autoclave. A Matlab file was created to find the points in the curve where the temperature was increased to the next step. An average over 3 minutes before this point is calculated, which is assumed to be the equilibrium

pressure of the mixture at this temperature. The Matlab script is provided in Appendix A.

3.3 CO_2 loading measurements

The objective of these experiments was to measure the vapor liquid equilibrium between TEPA, H_2O and CO_2 at different temperatures and compositions. This was done by adding pulses of CO_2 to a mixture of TEPA and H_2O. After every pulse, the pressure in the autoclave increased sharply, followed by a quick decrease in pressure, as the CO_2 was absorbed by the solvent. Once the pressure became stable between certain stabilisation margins, the software recognized that equilibrium was achieved and added a new CO_2 pulse to the system, which continued until either the set number of steps or a maximum pressure of 4.5 bar was reached.

3.3.1 Design of experiment

The two independent variables that could be changed for each experiment were the concentration of TEPA in the solution and the temperature of the system. The ZEF process will make use of very concentrated TEPA, as this will not evaporate over time. Therefore the experiments were carried out at high concentrations of TEPA. Currently, the desorption unit is a distillation column, with different stages containing different compositions of TEPA and H_2O. Therefore, a range of different concentrations were investigated. Since previous experiments in the group have been performed at 30wt% TEPA using a different set-up, these were repeated to validate the apparatus used in this work.

Since absorption is likely to occur at ambient conditions, it is important to know the CO_2 absorption behavior of TEPA at low temperatures and very low partial pressures of CO_2, because air contains approximately 400 ppm CO_2, which corresponds to approximately 0.4 mbar. Desorption of the CO_2 from the loaded solvent will occur at high temperatures (around 373.15 - 393.15 K) and low pressures (500 mbar). Therefore, the experiments covered a wide range of temperatures. Taking all these requirements into account as well as time constraints, the following experimental plan was devised, as shown in Table 3.2.

Table 3.2: Experimental plan for CO_2 loading measurements

Concentration	**Temperature**		
wt %	K		
30	313.15	353.15	393.15
70	313.15	353.15	393.15

3.3.2 Procedure

The experimental procedure consists of 3 general steps: sample preparation, CO_2 loading and the cleaning of the vessel. These are discussed in the following section.

Sample preparation

1. The TEPA solution of approximately 250 mL was prepared by measuring the required mass of H_2O and TEPA on an analytical balance (Mettler AT460) with a linearity of $\pm$0.08 mg. Precision weighing was achieved using a Pasteur pipette.

2. The sample was then put in a sonication bath (Grant XUB) in degassing mode for 15 minutes and sonication mode for 10 minutes, to release any absorbed inert gases. After this step, the solution should be clear and no bubbles should be visible. If this was not the case, some bubbles had not yet escaped the viscous solution, then the sonication step was repeated for another 10 minutes.

CO_2 loading

1. The solution was loaded into the vessel through a plastic funnel. The remaining solvent on the funnel and in the sample flask is measured on the mass balance, to determine the exact weight of solution inside the vessel.
2. The stirring mechanism is turned on to 500 rpm, which is high enough to move the sample around, but not so vigorously that a vortex is created.
3. The sample was then cooled down to 298.15 K and the vessel was evacuated for 5 minutes to remove most of the air inside it.
4. Then, the sample was heated to 313.15 K and evacuated again for 5 minutes, to ensure that all the absorbed gases were removed.
5. The liquid baths were set to the temperature required for the experiment. The most stable temperatures and pressures were achieved by setting the vessel's liquid bath to external control, while setting the liquid bath of the lid to internal control at a slightly higher temperature than the vessel.
6. The pressure and temperature were allowed to stabilise for 3 hours, before the first CO_2 pulse was added, which means TEPA and H_2O have reached equilibrium.
7. CO_2 is injected by the mass flow controller in pulses. After one pulse the pressure in the vessel sharply increases, followed by a sharp decrease as the CO_2 is absorbed.
8. Once the pressure remains within a certain range for a specified amount of time, as entered in the software, equilibrium is assumed to be reached and the next pulse of CO_2 is added.
9. The CO_2 pulses are repeated, until the experiment is stopped or the pressure inside the vessel reaches 5 bar.

Cleaning the vessel

After either type of experiment, the vessel was cleaned thoroughly according to the following procedure.

1. Once the experiment was stopped, the pressure in the vessel was released slowly.
2. The solution was diluted with hot tap water and stirred vigorously.
3. The vessel was rinsed once more with hot tap water.
4. Then, the vessel was filled with demiwater heated to 373 K. This was kept boiling for 10 minutes.
5. With the hot water still in the vessel, a short CO_2 pulse was given to make sure no TEPA was blocking the tube of the mass flow controller.
6. Next, the vessel was flushed twice with cold demineralized water.

7. Then, the vessel was filled with ethanol, which was stirred for 10 minutes and then drained.
8. Lastly, the vessel was dried with pressurized air and evacuated for 15 minutes to dry it.

3.3.3 Data processing

The software produces two files. One raw data file, where all the experimental data are logged every second. The pressure in the tank, the temperature in the gas and liquid phase, as well as the temperature in the liquid baths, the torque of the stirring mechanism and the flow of CO_2 through the mass flow controller are logged every second. The other file is the VLE file, which only logs the partial pressure in the tank just before the next CO_2 pulse, which is the equilibrium pressure, as well as the exact size of the CO_2 pulse.

It was found that the equilibrium pressure taken from the VLE file was rather dependent on the noise in the pressure sensor and was not very representative of the average pressure just before the next CO_2 pulse. Therefore it was decided to create a Matlab script to convert the raw data to VLE data instead.

Since spreadsheets provide a more clear overview of the data, a spreadsheet was created for each experiment, which converts the VLE data from the experiment to the conventional format of reporting an absorption isotherm, which is a CO_2 loading vs. CO_2 partial pressure curve. CO_2 loading is defined as the moles of CO_2 absorbed per mole amine or per mole nitrogen atoms in the molecule.

The equilibrium partial pressure of CO_2 is calculated by:

$$p_{\mathrm{CO_2,eq}} = P_{\mathrm{total,eq}} - p_{\mathrm{H_2O,eq}} \tag{3.1}$$

The vapor pressure of water, $p_{H_2O,eq}$, is equal to the pressure measured before the first CO_2 pulse. The amount of CO_2 added to the system is calculated from the mass flow controller data, which is given in normal liters. A normal liter is defined as a liter of gas at standard temperature and pressure (STP): 100 kPa and 273.15 K Therefore the MFC data can be converted to moles using the ideal gas law.

$$n_{\mathrm{pulse}} = \frac{P_{\mathrm{STP}} V_{\mathrm{pulse}}}{R T_{\mathrm{STP}}} \tag{3.2}$$

The total amount of CO_2 in the system is calculated by summing all the gas pulses up to that point.

$$n_{\mathrm{total}} = \sum_{\mathrm{i}} n_{\mathrm{pulse,i}} \tag{3.3}$$

The amount of CO_2 in the gas phase is calculated from the equilibrium pressure in the reactor, using the ideal gas law.

$$n_{\mathrm{CO_2,g}} = \frac{p_{\mathrm{CO_2,eq}}(V_{\mathrm{vessel}} - V_{\mathrm{solution}})}{RT} \tag{3.4}$$

It follows that the amount of CO_2 in the liquid phase can be calculated by:

$$n_{\mathrm{CO_2,abs}} = n_{\mathrm{CO_2,total}} - n_{\mathrm{CO_2,g}} \tag{3.5}$$

The loading is calculated by:

$$\alpha_{\mathrm{CO_2}} = \frac{n_{\mathrm{CO_2,abs}}}{M_{\mathrm{solution}} V_{\mathrm{solution}}} \tag{3.6}$$

A Matlab script was written to automate the process of filling in the spreadsheet with the experimental data and the specific composition of the sample required to make all the calculations. The flow of information is shown in the diagram in Figure 3.2. The Matlab script is given in Appendix B. The Excel spreadsheet templates are provided in Appendix C.

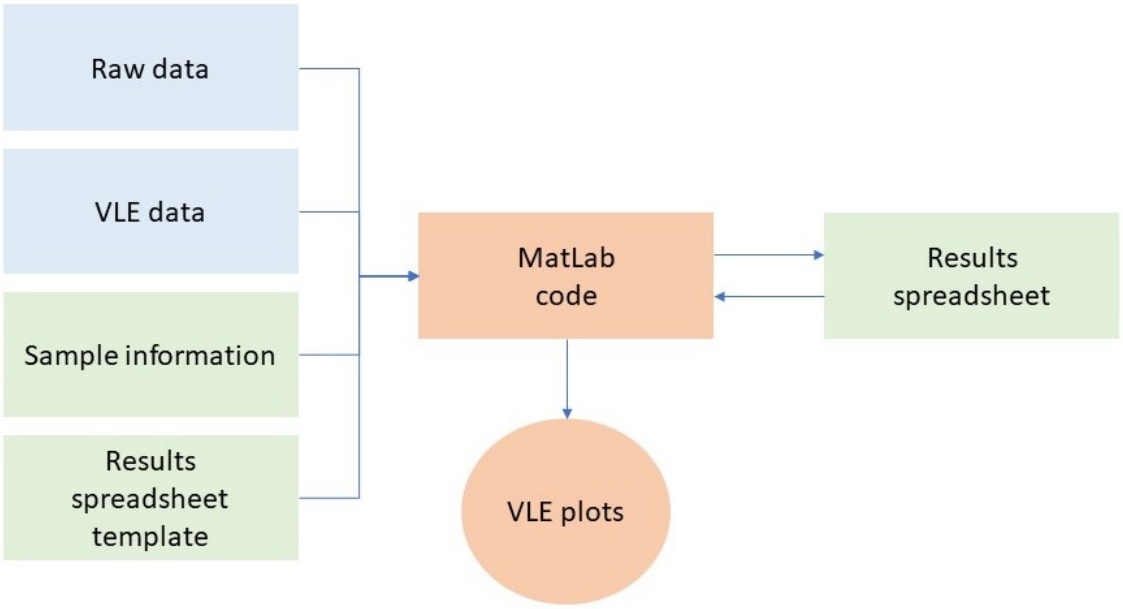

Figure 3.2: Flowchart of the data processing scheme for CO_2 loading experiments. The raw data, VLE data from the experiment, as well as the Excel spreadsheets templates are loaded into the Matlab file, which exports the manipulated experimental data into the results spreadsheet. The calculated results are then imported back into the Matlab code to create plots.

3.3.4 Assumptions

Converting the experimental data to loading and partial pressure data requires a few assumptions. These assumptions are listed below.

- The vapor pressure of H_2O is assumed to be constant during the entire run of the experiment. This implies that the addition of CO_2 in the system, which causes the formation of ions in the liquid phase, has a negligible influence on the amount of H_2O in the gas phase. This makes it possible to calculate the equilibrium partial pressure of CO_2 using Equation 3.1.
- The ideal gas law is used to convert the partial pressure of CO_2 to moles. This is a reasonable assumption at low pressures.
- The volume above the liquid is assumed to be constant during the experiment. This implies that the liquid volume and therefore the density of the liquid does not change. However, temperature, H_2O and CO_2 loading all have an influence on the density of the liquid.
- Equilibrium is assumed to occur when the pressure variation remains within 7 mbar for 90 minutes.
- It is assumed that the stirring mechanism causes homogeneous loading of CO_2 inside the sample.
- It is assumed that the reactor vessel is leak tight and that there is no condensation of H_2O occurring.
- It is assumed that the initial evacuating of the vessel causes negligible H_2O evaporation. The

ratio of H_2O to amine is assumed to remain unchanged.

Chapter 4

Model Description

Three different models are described in this chapter. Firstly, Wilson's activity coefficient model is explained, which was used to model the binary mixture of TEPA and H_2O. Secondly, the CO_2 absorption model developed for MEA is described. Thirdly, a similar but more elaborate model is detailed, based on a quantitative structure activity relationship for CO_2 absorption in TEPA.

4.1 Binary TEPA-H_2O model

Using the experimental data of the TEPA-H_2O VLE, a simple binary model was developed, based on the modified Raoult's law and the Wilson equation.

4.1.1 Model equations

The modified Raoult's law is, as the name suggests, an extension of the Raoult's law, which is generally valid for a mixture of chemically similar compounds. However, in the case of H_2O and TEPA, the regular Raoult's law would not hold. The modified Raoult's law allows for the correction of liquid phase non-idealities [44].

$$y_i P_{\text{tot}} = x_i \gamma_i P_i^{\text{sat}} \tag{4.1}$$

where y_i is the vapor phase mole fraction, ϕ_i is the fugacity coefficient, x_i is the liquid phase mole fraction, γ_i is the activity coefficient and P_i^{sat} is the pure component saturation vapor pressure of component i. P_{tot} is the total pressure in the system.

The pure component vapor pressure of H_2O was calculated using the Antoine's Equation [44].

$$\log_{10} P_{H_2O}^{\text{sat}}(T) = A - \frac{B}{C + T} \tag{4.2}$$

The Antoine coefficients were taken from the Dortmund Databank [66] and are shown in Table 4.1.

Table 4.1: Antoine coefficients for the temperature dependence of pure water vapor pressure in two different temperature and pressure units.

	Antoine coefficients			
	mmHg and °C		mbar and °C	
	$T < 100$ °C	$T > 100$ °C	$T < 100$ °C	$T > 100$ °C
A	8.07131	8.14019	8.196213	8.265093
B	1730.63	1810.94	1730.755	1811.065
C	233.426	224.485	233.5509	244.6099

Because no literature values of Antoine coefficients for pure TEPA were found, a different method was used. The vapor pressure of TEPA was calculated using the Clausius-Clapeyron equation, because

information on the boiling point and the heat of vaporization of TEPA was available. The Clausius-Clapeyron equation allows for the calculation of the pure component vapor pressure, using the heat of vaporization and one known vapor pressure (P_{ref}) at a known temperature (T_{ref}). It is easiest to use the boiling point of TEPA as the reference temperature, because then the vapor pressure must equal atmospheric pressure [44].

$$\ln\left(\frac{P^{sat}_{TEPA}(T)}{P_{ref}}\right) = \frac{\Delta H_{vap}}{R}\left(\frac{1}{T} - \frac{1}{T_{ref}}\right) \tag{4.3}$$

The following boiling point and heat of vaporisation data was used, which is shown in Table 4.2. It is taken from the National Institute of Standards and Technology [67].

Table 4.2: TEPA properties required to calculate the vapor pressure of TEPA using the Clausius-Clapeyron equation.

Quantity	**Value**	**Units**
H_{vap}	71.3	kJ/mol
T_{boil}	613.15	K

The activity coefficients were calculated using Wilson's equation. This model was chosen, due to its relative simplicity. Only two parameters need to be fitted. Next to that, Wilson's equation has been shown to be in excellent agreement with the experimental data of a wide variety of binary mixtures and often works better than other simple activity correlations, such as Margules' or Van Laar's equation [68]. Additional advantages are the built-in temperature dependence and the extension to multi-component equilibria using only binary data [68].

In the next equations, H_2O is referred to as species 1, and TEPA as species 2. According to Wilson's theory, the activity coefficients for a binary system are calculated using the following semi-empirical equations [68]:

$$\ln\gamma_1 = -\ln(x_1 + \Lambda_{12}x_2) + x_2\left[\frac{\Lambda_{12}}{x_1 + \Lambda_{12}x_2} - \frac{\Lambda_{21}}{x_2 + \Lambda_{21}x_1}\right] \tag{4.4}$$

$$\ln\gamma_2 = -\ln(x_2 + \Lambda_{21}x_1) - x_1\left[\frac{\Lambda_{12}}{x_1 + \Lambda_{12}x_2} - \frac{\Lambda_{21}}{x_2 + \Lambda_{21}x_1}\right] \tag{4.5}$$

where Λ_{12} and Λ_{21} are the Wilson parameters, which are defined as:

$$\Lambda_{12} = \frac{v_2^L}{v_1^L} e^{-(\lambda_{12}-\lambda_{11})/RT} \tag{4.6}$$

and

$$\Lambda_{21} = \frac{v_2^L}{v_1^L} e^{-(\lambda_{12}-\lambda_{22})/RT} \tag{4.7}$$

where λ_{12} is the interaction energy between molecules of species 1 and 2, λ_{11} of 2 molecules of species 1 an λ_{22} of 2 molecules of species 2. v_1^L and v_2^L are the molar liquid volumes of pure components 1 and 2, respectively [68].

The model calculates the total pressure using the modified Raoult's law, neglecting the vapor phase non-ideality.

$$P_{tot}(T, x) = x_1\gamma_1 P_1^{sat}(T) + x_2\gamma_2 P_2^{sat}(T) \tag{4.8}$$

Using the experimental P-T-x data from the vapor curve experiments, the values of $(\lambda_{12} - \lambda_{11})$ and $(\lambda_{12} - \lambda_{22})$, that determine the Wilson parameters, were fitted by minimizing the sum of the squared residuals:

$$\text{SSQ} = \sum_{i=1}^{n} \left(P_{\text{tot},i}^{\text{exp}} - P_{\text{tot},i}^{\text{model}} \right)^2 \tag{4.9}$$

A Matlab script was written and is provided in the Appendix D. Using the MultiStart feature combined with the fminunc solver, the combination of parameters was found that provided the best fit to the data.

4.2 Ternary MEA-H_2O-CO_2 model

As explained in Chapter 2, the chemical model proposed by Puxty and Maeder [7] was selected to model the VLE of TEPA, H_2O and CO_2. In their 2013 paper, they describe the application of this model to different types of amine solutions, including MEA and piperazine. In this work, their MEA model was reproduced, to serve as a basis for the development of a model for TEPA. MEA was selected because it is a simple mono-amine, with an abundance of VLE data available in literature. Additionally, the model parameters are already provided by the paper by Puxty and Maeder [7].

4.2.1 General model overview

The model proposed by Puxty et al. is a simple chemical model. Given the total concentrations of the three main species - amine, H_2O and CO_2 - it solves for the concentrations of species inside the liquid phase, which are governed by equilibrium constants, mass balances and activity coefficient correlations. The activity coefficient are calculated using the specific ionic interaction theory. However, the second term in this equation is not used, because it was found that this had a negligible influence on the accuracy of the model [7]. The specific ionic interaction model simplifies to the extended Debye Hückel law.

The calculated free concentration of CO_2 is used to calculate the partial pressure of CO_2 above the solution, using the Henry constant of CO_2 in water, see Figure 4.1. By comparing the model partial pressure with the experimental partial pressure at the same conditions, the model's parameters are fitted. These parameters determine the value of equilibrium constants as a function of temperature for the reactions involving amine species. Since the equilibrium constants for the CO_2-H_2O system have been thoroughly researched already [69], they don't need to be fitted.

4.2.2 Model equations

Inputs

To regress the model parameters, VLE data is required as input. For the model developed here, the VLE data from Aronu [6] was used, because these cover a large range of concentrations and temperatures and were also used by Puxty and Maeder for parameter regression [7]. Every VLE datapoint contains the following information:

- The temperature of the system, T, given in K.
- The concentration of MEA in the solvent, w_{MEA}, given in weight percentage.
- The loading of CO_2 in the solution, α, defined as mol CO_2 per mol MEA.

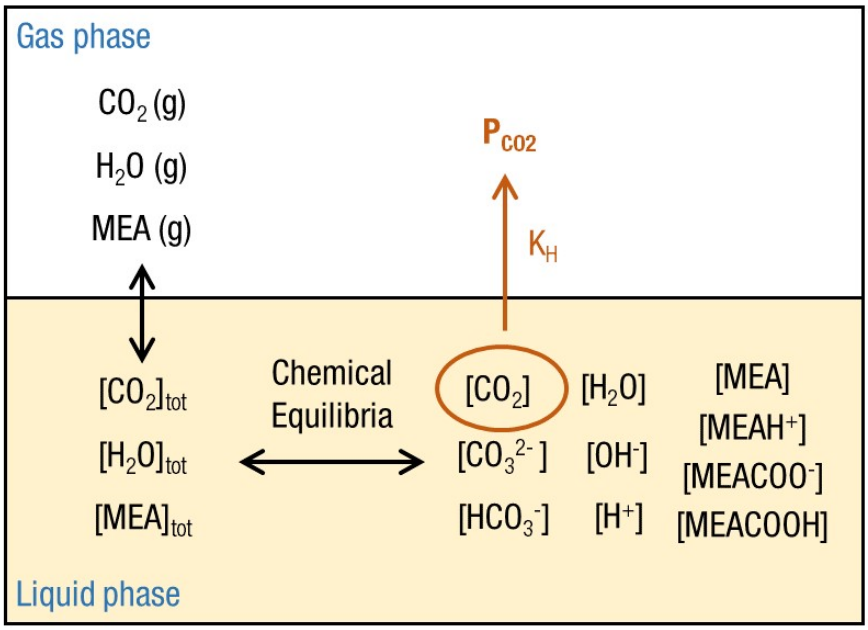

Figure 4.1: Visualisation of the chemical model described by Puxty and Maeder [7].

- The partial pressure CO_2, p_{CO_2} given in kPa.

The model works with molarities. For the mass balances, the total MEA, total CO_2 and total water molarity can be calculated for every data point using the following equations:

$$c_{\text{MEA}}^{\text{total}} = \frac{\frac{w_{\text{MEA}}}{MW_{\text{MEA}}}}{\frac{w_{\text{MEA}}}{\rho_{\text{MEA}}} + \frac{(1-w_{\text{MEA}})}{\rho_{\text{H}_2\text{O}}}} \tag{4.10}$$

$$c_{\text{H}_2\text{O}}^{\text{total}} = \frac{\frac{(1-w_{\text{MEA}})}{MW_{\text{H}_2\text{O}}}}{\frac{w_{\text{MEA}}}{\rho_{\text{MEA}}} + \frac{(1-w_{\text{MEA}})}{\rho_{\text{H}_2\text{O}}}} \tag{4.11}$$

$$c_{\text{CO}_2}^{\text{total}} = \alpha c_{\text{MEA}}^{\text{total}} \tag{4.12}$$

The above equations are based on two assumptions. First, the vaporization of water or MEA is assumed to have a negligible effect on their total concentration inside the liquid phase. Since the overhead volume in the experimental set up used for VLE experiments is usually small relative to the liquid volume, this is a reasonable assumption. Second, the volumes of MEA and H_2O are assumed to be additive and do not depend on temperature. In other words, the non-ideal mixing between MEA and H_2O is neglected and the density is assumed independent of temperature.

Chemical equilibria

Six chemical equilibria occur in the liquid phase. The H_2O and CO_2 equilibria are:

$$H^+ + CO_3^{2-} \xleftrightarrow{K_1} HCO_3^- \tag{4.13}$$

$$H^+ + HCO_3^- \overset{K_2}{\longleftrightarrow} CO_2 + H_2O \tag{4.14}$$

$$H^+ + OH^- \overset{K_3}{\longleftrightarrow} H_2O \tag{4.15}$$

MEA is a mono-amine: it has one nitrogen group. This group can either act as a base or form a carbamate in the presence of CO_2. Therefore, the chemical equilibria involving MEA are:

$$H^+ + MEA \overset{K_4}{\longleftrightarrow} MEAH^+ \tag{4.16}$$

$$HCO_3^- + MEA \overset{K_5}{\longleftrightarrow} MEACOO^- + H_2O \tag{4.17}$$

$$H^+ + MEACOO^- \overset{K_6}{\longleftrightarrow} MEACOOH \tag{4.18}$$

The chemical equilibria are described by the infinite dilution equilibrium constant. At infinite dilution, all activity coefficients are assumed to be unity and the ionic strength is zero. This is a hypothetical reference state. When the concentrations increase, the ionic strength increases and the value of the activity coefficients are no longer equal to 1. To be able to calculate the concentrations at equilibrium outside of this reference state, two approaches can be used. Either an iterative approach is used or a computer program is used to simultaneously solve the concentrations and activity coefficients. The latter is the strategy used in the model described here.

The infinite dilution equilibrium constants of the chemical equilibria of MEA, H_2O and CO_2 relate the concentrations of the species and the activity coefficients according to the following equations.

$$K_1^0 = \frac{c_{HCO_3^-}}{c_{H^+} c_{CO_3^{2-}}} \frac{\gamma_{HCO_3^-}}{\gamma_{H^+} \gamma_{CO_3^{2-}}} \tag{4.19}$$

$$K_2^0 = \frac{c_{CO_2}}{c_{H^+} c_{HCO_3^-}} \frac{1}{\gamma_{H^+} \gamma_{HCO_3^-}} \tag{4.20}$$

$$K_3^0 = \frac{c_{H_2O}}{c_{H^+} c_{OH^-}} \frac{1}{\gamma_{H^+} \gamma_{OH^-}} \tag{4.21}$$

$$K_4^0 = \frac{c_{MEAH^+}}{c_{H^+} c_{MEA}} \frac{\gamma_{MEAH^+}}{\gamma_{H^+}} \tag{4.22}$$

$$K_5^0 = \frac{c_{MEACOO^-}}{c_{HCO_3^-} c_{MEA}} \frac{\gamma_{MEACOO^-}}{\gamma_{HCO_3^-}} \tag{4.23}$$

$$K_6^0 = \frac{c_{MEACOOH}}{c_{H^+} c_{MEACOO^-}} \frac{1}{\gamma_{H^+} \gamma_{MEACOO^-}} \tag{4.24}$$

The K_i^0 values are the equilibrium constants at zero ionic strength. They are dependent on temperature according to the van 't Hoff equation (note the similarity to the Clausius Clapeyron equation). The chemical equilibrium constants in Equation 4.13, 4.14 and 4.15 have been thoroughly researched and their dependence on temperature is taken from literature [69].

$$\log K_1^0(T) = -\frac{-12431.7/T - 35.4819 \log T + 220.067}{2.3026} \tag{4.25}$$

$$\log K_2^0(T) = -\frac{-12091.1/T - 36.7816 \log T + 235.482}{2.3026} \tag{4.26}$$

$$\log K_3^0(T) = -\frac{-13445.9/T - 22.4773 \log T + 140.932}{2.3026} \tag{4.27}$$

The chemical equilibrium constants of the MEA reactions are dependent on 2 parameters, which are the parameters to be fitted in the regression of this model to experimental data. For MEA this means 6 parameters need to be fitted: $\log K^0_{4,\text{ref}}$, ΔH_4, $\log K^0_{5,\text{ref}}$, ΔH_5, $\log K^0_{6,\text{ref}}$ and ΔH_6.

$$\log K^0_4(T) = \log K^0_{4,\text{ref}} - \frac{\Delta H_4}{2.3026R}\left(\frac{1}{T} - \frac{1}{313.15}\right) \tag{4.28}$$

$$\log K^0_5(T) = \log K^0_{5,\text{ref}} - \frac{\Delta H_5}{2.3026R}\left(\frac{1}{T} - \frac{1}{313.15}\right) \tag{4.29}$$

$$\log K^0_6(T) = \log K^0_{6,\text{ref}} - \frac{\Delta H_6}{2.3026R}\left(\frac{1}{T} - \frac{1}{313.15}\right) \tag{4.30}$$

In these equations, R is the gas constant in J/mol K, ΔH_i is the enthalpy of reaction in J/mol, T is the temperature in K and $K^0_{\text{i,ref}}$ is the infinite dilution equilibrium constant at 313.5 K.

Activity coefficient correlation

For each charged species an activity coefficient is calculated by a modified Debye-Hückel equation. This causes the activity coefficient to be equal for species with the same charge. For the species of charge one, the activity coefficient is calculated using:

$$\log\gamma_{HCO_3^-} = \log\gamma_{H^+} = \log\gamma_{OH^-} = \log\gamma_{MEAH^+} = \log\gamma_{MEACOO^-} = -\frac{1^2 A_{DH}(T)\sqrt{I}}{1 + 1.5\rho^{-1/2}\sqrt{I}} \tag{4.31}$$

where I is the ionic strength in mol/dm^3, A_{DH} is the Debye-Hückel parameter in dm$^{3/2}$/mol$^{1/2}$, ρ is the density of water in kg/dm^3.

$$\log\gamma_{CO_3^{2-}} = -\frac{2^2 A_{DH}\sqrt{I}}{1 + 1.5\rho^{-1/2}\sqrt{I}} \tag{4.32}$$

The Debye-Hückel parameter is dependent on temperature according to the relation:

$$A_{DH} = \frac{1.8248 \cdot 10^6}{eT^{2/3}} \tag{4.33}$$

where e is the relative permittivity of water. The ionic strength is defined as:

$$I = \frac{1}{2}(c_{HCO_3^-} + 4c_{CO_3^{2-}} + c_{OH^-} + c_{H^+} + c_{MEAH^+} + c_{MEACOO^-}) \tag{4.34}$$

Mass balances

Finally the mass balances are written for CO_2, amine, protons and hydroxide ions. According to Puxty and Maeder, these are defined as:

$$c_{CO_2}{}^{\text{total}} = c_{HCO_3^-} + c_{CO_3^{2-}} + c_{MEACOO^-} + c_{MEACOOH} \tag{4.35}$$

$$c_{MEA}{}^{\text{total}} = c_{MEA} + c_{MEAH^+} + c_{MEACOO^-} + c_{MEACOOH} \tag{4.36}$$

$$c_{H^+}{}^{\text{total}} = c_{H^+} + c_{HCO_3^-} + c_{MEAH^+} + 2c_{CO_2} + c_{MEACOOH} + c_{H_2O} \tag{4.37}$$

$$c_{OH^-\,\text{total}} = c_{OH^-} + c_{H_2O} \tag{4.38}$$

However, for some reason, the Matlab code did not work properly using this set of mass balances. This problem was solved by replacing the mass balance of protons by the charge balance of the system:

$$c_{H^+} + c_{MEAH^+} = c_{OH^-} + c_{HCO_3^-} + 2c_{CO_3^{2-}} + +c_{MEACOO^-} \tag{4.39}$$

Speciation solver

The system of nonlinear equations consisting of 6 equilibrium constant equations, 4 mass balances and 2 activity coefficient correlations, 12 equations in total, is used to solve the 12 unknowns: 10 species concentrations and 2 activity coefficients for every data point. This is solved using the 'fsolve' tool in Matlab, which uses the Newton-Raphson algorithm to find the root of the function. This function consists of all the nonlinear equations, written in such a way that all equations should equal 0. The solver requires an initial guess of the unknowns, which must be relatively close to the solution, or else the solver will not converge. Therefore, an initial guess, x_0, was taken from running a flash separation in Aspen at 50 kPa and 353.15 K, with a feed containing 29 wt% MEA, 70 wt% H_2O and 1 wt% CO_2. The carbamate protonation reaction was not available in Aspen, thus the values of all species except $c_{MEACOOH}$ were calculated without taking that reaction into account. The value of $c_{MEACOOH}$ was set equal to that of c_{MEACOO^-} for the initial guess. The initial guess values are listed in Table 4.3.

Table 4.3: Initial guess for Newton Raphson algorithm to solve the set of nonlinear equation in the MEA model. Values taken from Aspen.

Unknown	Value	Unit
$c_{HCO_3^-}$	$3.86 \cdot 10^{3}$	mol/dm^3
c_{H^+}	$3.65 \cdot 10^{-10}$	mol/dm^3
$c_{CO_2^{2-}}$	$2.74 \cdot 10^{-3}$	mol/dm^3
c_{H_2O}	37.4	mol/dm^3
c_{CO_2}	$2.03 \cdot 10^{-6}$	mol/dm^3
c_{OH^-}	$8.56 \cdot 10^{-4}$	mol/dm^3
c_{MEAH^+}	0.222	mol/dm^3
c_{MEA}	4.13	mol/dm^3
c_{MEACOO^-}	0.212	mol/dm^3
$c_{MEACOOH}$	0.212	mol/dm^3
γ_1	0.5	-
γ_2	0.5	-

The problem with this system is that the unkowns are badly scaled. This means that they vary across orders of magnitude, which causes problems for the solver to converge. The solution is to scale the system. This was done in two ways. First the unknowns were normalised, so that the solver adjusts them equally. Secondly, the logarithm was taken on both sides of the equilibrium constant equations (Equation 5.19 - 5.24), which doesn't change anything for the solution, but accelerates the computations, greatly reducing the time to run the model.

Regression

Nonlinear regression of the VLE data was used to find the model parameters that fit the data best. The objective function to be minimised was the absolute average relative deviation (AARD%):

$$\text{AARD\%} = 100x\frac{1}{n}\sum_{i=1}^{n}\frac{|p_{CO_2,i}^{exp} - p_{CO_2,i}^{model}|}{p_{CO_2,i}^{exp}} \tag{4.40}$$

The entire Matlab code is given in Appendix E.

4.3 Ternary TEPA-H_2O-CO_2 model

The MEA model described in the previous section was used as the foundation to develop a similar model to describe the ternary mixture of TEPA, H_2O and CO_2. This model is explained in the next section.

4.3.1 General model overview

Similar to the previous model, this model calculates the concentrations of species inside the liquid phase for every data point by solving a set of nonlinear equations consisting of equilibrium constants, mass balances and activity coefficients. The concentration of free CO_2 is then used to calculate the partial pressure of CO_2 above the liquid. Again, the model parameters that are fitted to the data are the parameters of the van 't Hoff equation that determine the value of the equilibrium constants of the amine related reactions as a function of temperature.

The TEPA molecule is quite different to that of MEA, see Figure 4.2a and 4.2b. MEA only has 1 amino group, a primary amino group, while TEPA has 5, two of which are primary and three are secondary amino groups. This means MEA can only form mono-carbamates, while TEPA can also form higher order carbamates, such as di- and tri-carbamates. When the number of amino groups increases, the number of possible reactions and number of ionic species in the liquid increases strongly, when taking into account all the potential combinations of CO_2 and protons binding to the NH-groups of the molecule. For example, a study of CO_2 absorption in an aqueous solution diethyltriamine (Figure 4.2c) showed that 24 species can be formed which participate in a total of 23 reactions [42]. It would be impossible to attempt to take all of the possible species and reactions into account for three reasons. Firstly, because the number of species and reactions are even higher for TEPA than for DETA. Secondly, every reaction that is added to the model adds 2 parameters to be fitted. Thirdly, no speciation data is available for TEPA. With a limited amount of data, this would lead to over-fitting. Additionally, there would be no way of validating the result of the speciation.

Therefore it was decided that the model must be a simplification of the real situation inside the liquid phase. It was postulated that one molecule of TEPA behaves similarly to 2.5 molecules of a diamine. This idea is based on the fact that the CO_2 absorption capacity is mostly determined by the number of amino groups. A solution of 1 M of TEPA would contain the same concentration of amino groups as a solution of 2.5 M of a diamine, such as piperazine (PZ), see Figure 4.2d. PZ was chosen, because the van 't Hoff parameters were available in literature [7].

The advantage of this approach is that the model has to take into account a substantially smaller number of species and reactions, which leads to less unknowns to be solved by the set of nonlinear equations and less parameters to be regressed. The approach could be classified as a quantitative structure activity relationship, as it relates the number of amino groups as a predictor variable to the CO_2 absorption as a response variable.

4.3.2 Model equations

Model inputs

Similar to the MEA model, VLE data is required as input. This time the experimental data from the CO_2 loading experiments is used. The quality of the isotherm 313.15 K 70 wt% TEPA data was questionable, it was omitted. Every datapoint contains the following information:

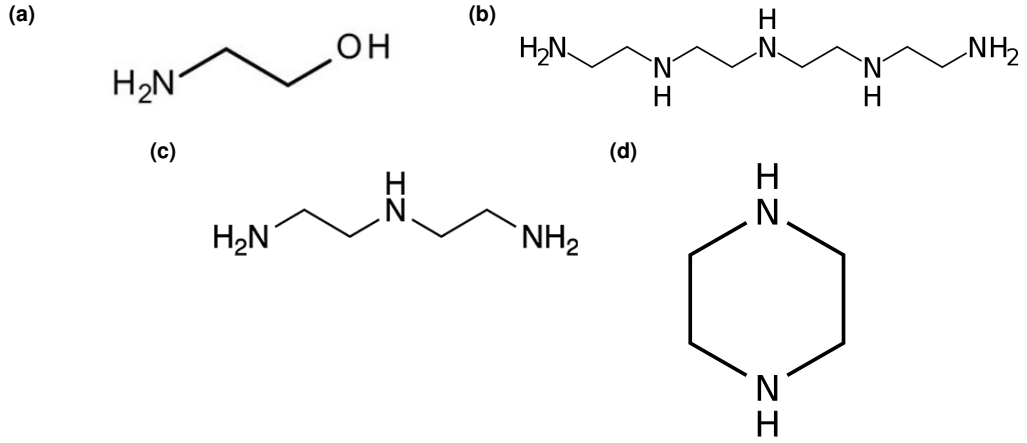

Figure 4.2: (a) Monoethanolamine (MEA) (b) Tetraethylenepentamine (TEPA) (c) Diethyltriamine (DETA) (d) Piperazine (PZ)

- The temperature of the system, T, given in K.
- The concentration of TEPA in the solvent, w_{TEPA}, given in weight percentage.
- The loading of CO_2 in the solution, α, defined as mol CO_2 per mol TEPA.
- The partial pressure CO_2, p_{CO_2} given in kPa.

To convert this information into the required format for the model, the following calculations must be performed:

$$c_{\text{TEPA}}^{\text{total}} = \frac{\frac{w_{\text{TEPA}}}{MW_{\text{TEPA}}}}{\frac{w_{\text{TEPA}}}{\rho_{\text{TEPA}}} + \frac{(1-w_{\text{TEPA}})}{\rho_{H_2O}}} \tag{4.41}$$

$$c_{H_2O}^{\text{total}} = \frac{\frac{(1-w_{\text{TEPA}})}{MW_{H_2O}}}{\frac{w_{\text{TEPA}}}{\rho_{\text{TEPA}}} + \frac{(1-w_{\text{TEPA}})}{\rho_{H_2O}}} \tag{4.42}$$

$$c_{CO_2}^{\text{total}} = \alpha c_{\text{TEPA}}^{\text{total}} \tag{4.43}$$

To model TEPA as a diamine, the amine concentration going into the model must be adjusted accordingly. This 'pseudo diamine concentration' is referred to from here on as 'Am', to avoid confusion.

$$c_{\text{Am}}^{\text{tot}} = 2.5 \cdot c_{\text{TEPA}}^{\text{total}} \tag{4.44}$$

Chemical equilibria

The H_2O and CO_2 equilibria remain the same as those in Equation 4.13-4.15. For the diamine reactions, the following chemical equilibria that were incorporated into the model.

$$H^+ + Am \overset{K_4}{\longleftrightarrow} Am^+ \tag{4.45}$$

$$HCO_3^- + Am \overset{K_5}{\longleftrightarrow} AmCOO^- + H_2O \tag{4.46}$$

$$H^+ + AmCOO^- \xleftrightarrow{K_6} AmCOOH \tag{4.47}$$

$$HCO_3^- + AmCOO^- \xleftrightarrow{K_7} Am(COO)_2^{2-} + H_2O \tag{4.48}$$

$$H^+ + Am(COO)_2^{2-} \xleftrightarrow{K_8} HOOCAm(COO)^- \tag{4.49}$$

The definition of the infinite dilution equilibrium constants for the first three equilibria remains the same as before. For the other reactions, they are defined as:

$$K_4^0 = \frac{c_{AmH^+}}{c_{H^+} c_{Am}} \frac{\gamma_{AmH^+}}{\gamma_{H^+}} \tag{4.50}$$

$$K_5^0 = \frac{c_{AmCOO^-}}{c_{HCO_3^-} c_{Am}} \frac{\gamma_{AmCOO^-}}{\gamma_{HCO_3^-}} \tag{4.51}$$

$$K_6^0 = \frac{c_{AmCOOH}}{c_{H^+} c_{AmCOO^-}} \frac{1}{\gamma_{H^+} \gamma_{AmCOO^-}} \tag{4.52}$$

$$K_7^0 = \frac{c_{Am(COO)_2^{2-}}}{c_{HCO_3^-} c_{AmCOO^-}} \frac{\gamma_{Am(COO)_2^{2-}}}{\gamma_{HCO_3^-} \gamma_{AmCOO^-}} \tag{4.53}$$

$$K_8^0 = \frac{c_{HOOCAm(COO)^-}}{c_{H^+} c_{Am(COO)_2^{2-}}} \frac{\gamma_{HOOCAm(COO)^-}}{\gamma_{H^+} \gamma_{Am(COO)_2^{2-}}} \tag{4.54}$$

The temperature dependence of the infinite dilution equilibrium constant remains the same as well, with the addition of the two van 't Hoff equations for reaction 7 and 8.

$$\log K_7^0(T) = \log K_{7,ref}^0 - \frac{\Delta H_7}{2.3026R}\left(\frac{1}{T} - \frac{1}{313.15}\right) \tag{4.55}$$

$$\log K_8^0(T) = \log K_{8,ref}^0 - \frac{\Delta H_8}{2.3026R}\left(\frac{1}{T} - \frac{1}{313.15}\right) \tag{4.56}$$

The total number of fitted parameters for this model therefore amounts to 8: $\log K_{4,ref}^0$, ΔH_4, $\log K_{5,ref}^0$, ΔH_5, $\log K_{6,ref}^0$, ΔH_6, $\log K_{7,ref}^0$, ΔH_7, $\log K_{8,ref}^0$ and ΔH_8.

Activity coefficient correlation

The activity coefficients for all singly charged species are defined as:

$$\log\gamma_{HCO_3^-} = \log\gamma_{H^+} = \log\gamma_{OH^-} = \log\gamma_{AmH^+} = \log\gamma_{AmCOO^-} = \log\gamma_{HOOCAm(COO)^-} = -\frac{1^2 A_{DH}\sqrt{I}}{1 + 1.5\rho^{-1/2}\sqrt{I}} \tag{4.57}$$

where I is the ionic strength in mol/dm^3, A_{DH} is the Debye-Hückel parameter in dm$^{3/2}$/mol$^{1/2}$, ρ is the density of water in kg/dm^3. For the doubly charged species, the activity coefficient is defined as:

$$\log\gamma_{CO_3^{2-}} = \log\gamma_{Am(COO)_2^{2-}} = -\frac{2^2 A_{DH}\sqrt{I}}{1 + 1.5\rho^{-1/2}\sqrt{I}} \tag{4.58}$$

The ionic strength is defined as:

$$I = \frac{1}{2}\left(c_{HCO_3^-} + 4c_{CO_3^{2-}} + c_{OH^-} + c_{H^+} + c_{AmH^+} + c_{AmCOO^-} + c_{HOOCAm(COO)^-} + 4c_{Am(COO)_2^{2-}}\right) \tag{4.59}$$

Mass balances

The mass balances are defined as:

$$c_{CO_2}^{\text{total}} = c_{HCO_3^-} + c_{CO_3^{2-}} + c_{AmCOO^-} + c_{AmCOOH} + 2c_{HOOCAm(COO)^-} + 2c_{Am(COO)_2^{2-}} \quad (4.60)$$

$$c_{Am}^{\text{total}} = c_{Am} + c_{Am^+} + c_{AmCOO^-} + c_{AmCOOH} + c_{HOOCAm(COO)^-} + c_{Am(COO)_2^{2-}} \quad (4.61)$$

$$c_{OH^-\text{total}} = c_{OH^-} + c_{H_2O} \quad (4.62)$$

The proton balance used by Puxty and Maeder [7], has been replaced by the charge balance of the system:

$$c_{H^+} + c_{AmH^+} = c_{OH^-} + c_{HCO_3^-} + 2c_{CO_3^{2-}} + c_{AmCOO^-} + c_{HOOCAm(COO)^-} + 2c_{Am(COO)_2^{2-}} \quad (4.63)$$

Speciation solver

The set of 8 equilibrium constant equations, 3 mass balances, 1 charge balance and 2 activity coefficient equations was used to calculate the 12 species concentrations and 2 activity coefficients at every data point. For the MEA model, an initial guess was made using Aspen. Since that was not possible in this case, another strategy was devised. A genetic algorithm was used in MATLAB which found plausible values of the unknowns. An objective function was constructed which summed the absolute values of the set of nonlinear equations. The genetic algorithms finds a combination of variables that minimised this sum. Upper and lower bounds were formulated for all variables, so that they would always be positive and not exceed the total concentrations of amine, CO_2 and H_2O. The output of the genetic algorithm was used as an initial guess for the solver.

To improve computational efficiency, only 1 initial guess was made for each isotherm. For the next point on the isotherm, the solution of the previous datapoint was used as an initial guesss. Since the genetic algorithm worked faster with datapoints at high loading, the solver solved the datapoints going from high to low loading, instead of low to high loading.

During the development of this model, it was found that the genetic algorithm did not always find a good initial guess on the first run. A bad initial guess then resulted in divergence of the solver or complex values in the solution of the set of equations. Therefore a threshold of the objective function was implemented, to ensure the initial guess was good enough.

Nonlinear Regression

The same objective function was used to find the parameters that best fit the model to the data: the absolute average relative deviation (%). The parameters for PZ were used as an initial guess.

The entire Matlab code of the ternary TEPA-H_2-CO_2 model is given in Appendix F.

Chapter 5

Results and Discussion

In this chapter, the results of the experiments and the model are discussed. First the vapor curve measurements are discussed, followed by the CO_2 loading experiments. Then, the model results are compared to the experimental results.

5.1 Experimental Results and Discussion

5.1.1 TEPA-H_2O vapor pressure curves

The vapor liquid equilibrium of TEPA and H_2O was measured as explained in Section 3.2. The results are shown in Figure 5.1. The pure water vapor pressure was not measured in this work, but taken from literature [8]. The trend in these curves is as expected. The vapor pressure of the solutions increases exponentially with temperature. Pure TEPA has a much lower vapor pressure than pure water, due to its high molecular weight. Thus, the pressure above the solution with a high TEPA content will be be lower with respect to the pressure above the solution with higher water content.

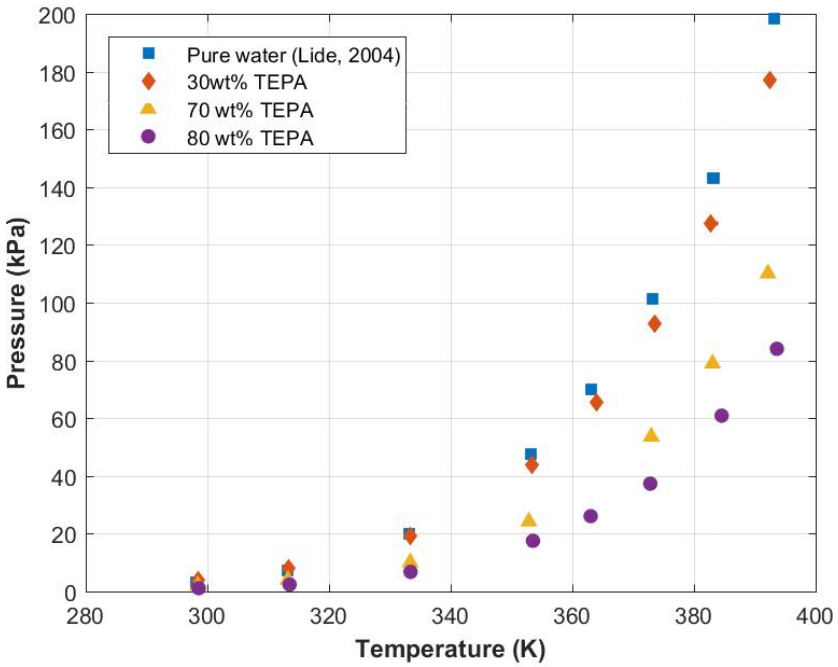

Figure 5.1: The equilibrium pressure of aqueous solution of 30, 70 and 80 wt% TEPA as a function of temperature compared to the saturation vapor pressure of pure water, taken from [8].

Upon closer inspection of Figure 5.1, the 30 wt% TEPA pressure data is slightly higher than that of pure water in the low temperature range. This is probably a measurement error. Likely, this effect is a

result of poor evacuation of the solution and the vessel at the start of the experiment. This would mean that all the measured points of the 30 wt% curve are shifted upwards slightly.

At high temperatures and low water concentrations in the liquid phase (70 and 80 wt% TEPA), the pressure inside the vessel was constantly fluctuating. The lid and the vessel used for these measurements were heated by separate liquid baths and were therefore not always exactly at the same temperature. The instability in the pressure is probably caused by a small reflux of water condensation and evaporation at the top of the vessel due to imperfect insulation of the lid and the pressure sensor. To obtain a approximation of the equilibrium pressure and temperature, the system was given at least 1.5 hours per temperature step to equilibrate and an average of the pressure and temperature was taken over a span of 10 minutes.

The vapor pressure experiments were only performed once for each composition. Therefore, it is not possible to statistically analyse the results. By repeating the experiments once or twice, the reliability of the data could be increased.

5.1.2 CO_2 absorption isotherms

The vapor liquid equilibria of the ternary mixture, consisting of TEPA H_2O and CO_2, were measured as described in Section 3.3. The partial pressure of CO_2 was measured as a function of temperature, loading and TEPA concentration.

30 wt% TEPA

The 30 wt% measurements were used to validate the experimental set-up described in Section 3.1, because the results can be compared to the results of similar experiments performed in a different vapor-liquid equilibrium measurement setup at TNO. Ovaa [9] performed CO_2 loading experiments with 30 wt% TEPA solutions in the solvent screening setup, which is also described in [33]. Figure 5.2 displays the results obtained in this work compared to the reference results from Ovaa. Because the isotherms overlap sufficiently, the experimental setup was validated.

The 30 wt% TEPA experiments were carried out at three different temperatures: 313.15 K (Figure 5.3a and 5.3b), 353.15 K (Figure 5.3c and 5.3d) and 393.15 K (Figure 5.3e and 5.3f). For every temperature, two plots are shown on the next page. The figures on the left show the entire absorption isotherm on a semi-log plot, whereas the figures on the right are closeups of the same data in the low loading region on a linear scale.

When comparing these figures, a clear trend is visible. A higher temperature yields higher CO_2 partial pressures. This means that less CO_2 is absorbed at higher temperatures. It is also clear that the absorption capacity of TEPA is high, especially at lower temperatures. At 313.15 K, loadings of up to 2.3 mol CO_2 per mol TEPA were measured. According to the mechanism of primary and secondary amines, two amine groups are needed to bond one CO_2 molecule. Therefore, a maximum absorption capacity of 2.5 mol CO_2/mol TEPA would be expected, because it has 5 NH-groups per molecule. This means di-carbamates and perhaps even tri-carbamates are formed in the liquid phase.

The duplo experiments show a slight offset from one another in the low loading range of the graph, which is magnified by the logarithmic scale of the y-axis. This offset could be explained by the presence of absorbed gases in the solvent before the addition of CO_2, which are expelled from the liquid phase after the first CO_2 pulse. Although the sonication step in the experimental procedure is supposed to remove these absorbed gases, it is possible that small bubbles did not escape the viscous solution.

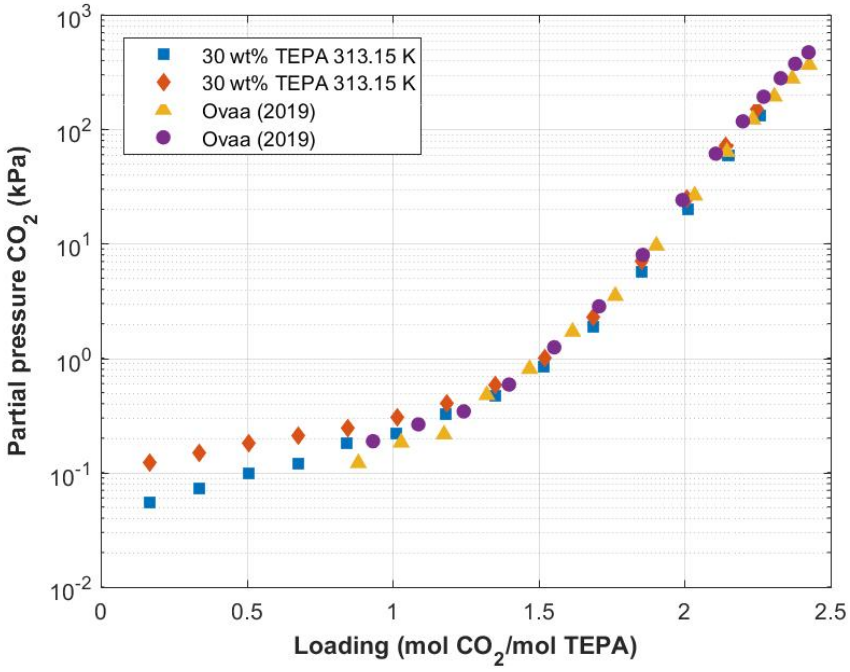

Figure 5.2: Validation of the experimental set-up. The absorption of CO_2 by an aqueous solution of 30wt% TEPA at 313.5 K measured by this work, compared to the data from Ovaa (2019) [9].

The sonication of the sample and two-step evacuation of the vessel apparently results in random errors. Possibly, the sample can be degassed more thoroughly by connecting the solvent sample to a vacuum pump during sonication or by prolonging the sonication time. Additionally, the evacuation inside the vessel could be improved by freezing the sample and evacuating it for a longer time period, so as to not lose a lot of water from the sample.

70 wt% TEPA

The CO_2 absorption isotherms were also measured at a higher TEPA concentration of 70 wt%, at the same temperatures as before: 313.15 K, 353.15 K and 393.15 K.

The isotherm measurements of 70 wt% TEPA at 313.15 K were the most challenging to perform. It took multiple repeat experiments to refine the settings. The high viscosity at these conditions resulted in slow mass transfer of CO_2 into the liquid phase, increasing the time required for the system to reach equilibrium. Additionally, the stirring was less effective at high viscosity. It was therefore uncertain if equilibrium had been reached properly. Also, practically it became very difficult to remove the highly viscous solution from the autoclave. Taking these observations into account, it was decided to limit the loading to approximately 0.7 mol/mol TEPA. The results of these measurements are displayed in Figure 5.4a. In Figure 5.4b, the absolute pressure increase from the first to the second data point of each isotherm is clearly larger than the pressure increase in the consecutive steps. The difference in this jump causes the offset between the duplicate measurements. Again, this initial jump is ascribed to the expulsion of absorbed inert gases still present in the liquid.

The results at 353.15 K are displayed in Figure 5.4c. The strange discontinuity and differences in shape

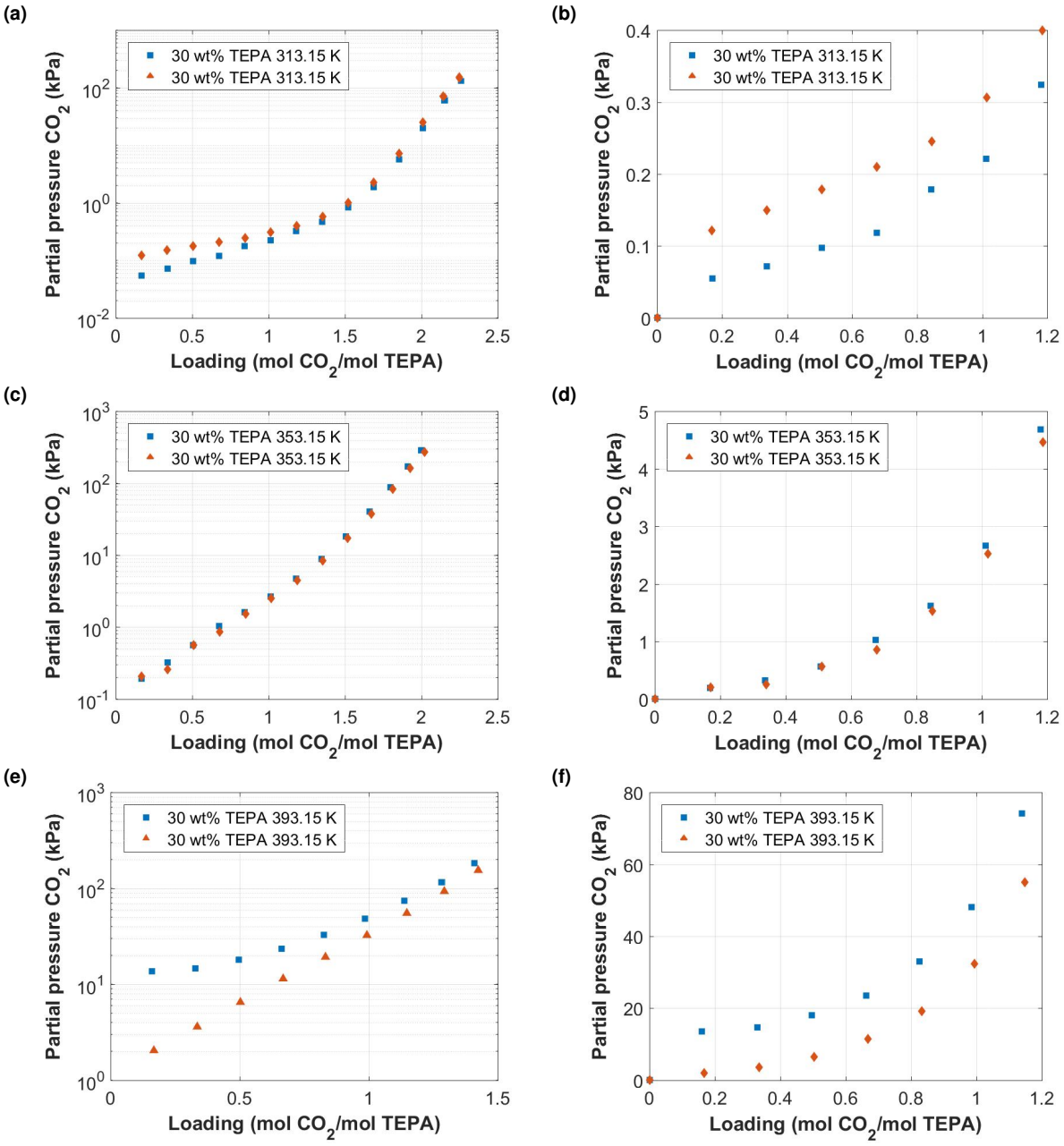

Figure 5.3: Absorption of CO_2 by aqueous solutions of 30 wt% TEPA at different temperatures. The graphs on the left show the full absorption isotherms on a semi-log scale. The graphs on the right show a closeup of the low loading region, with the initial jump in pressure and the offset between the duplo measurements. (a)(b) 313.15 K, (c)(d) 353.15 K, (e)(f) 393.15 K

are explained by looking at the closeup of the lower loading range in Figure 5.4d. Both isotherms show the same and unexpected trend in pressure after the first four or five CO_2 pulses: the pressure in the vessel drops with increasing CO_2 content, before increasing again. The lower curve (the blue squares) show a negative pressure. These points disappear on the semi-log plot in Figure 5.4c. Of course, a negative partial pressure of CO_2 does not exist. This negative pressure is caused by a drop in the total pressure inside the vessel, combined with the assumption that the partial pressure of water at 0 loading is constant throughout the experiment, as explained in Section 4.2.3 and shown in Equation 4.1.

Figure 5.4e shows the isotherms at 393.15 K. Differences in the shape of the curve of the duplicate measurements can be seen in the low pressure range. An initial pressure decrease and negative pressures were measured, similarly to the isotherms of 353.15 K. This decrease of the pressure inside the vessel is most likely caused by water molecules moving from the gas phase to the liquid phase as a result of CO_2 absorption. This means that the vapor pressure of water in the mixture is not constant with an increasing CO_2 loading. It is possible that the absorption of CO_2 and the subsequent increase of ionic species concentrations changes the interactions between the different species in the liquid phase and therefore changes the thermodynamic equilibrium. With the experimental set-up used in this work, it is not possible to quantify this effect properly because has become uncertain what the composition of the vapor phase is. It is challenging but not impossible to measure the vapor phase composition with a different more complex VLE set-up which allows sampling of the vapor phase. An example of such a set-up can be found in [70].

5.1.3 Data corrections

Two pressure effects during the CO_2 loading experiments result in a misrepresentation of the actual partial pressure of CO_2. This first is the disproportionate pressure increase after the first CO_2 pulse, compared to the following pressure steps. The second is the pressure decrease in the low loading ranges of the high temperature and high TEPA concentrations.

Unfortunately, the experimental set-up did not allow for the direct analysis of the gas or liquid phase compositions. Therefore, the pressure data is currently the only source of information to approximate the phase equilibrium. It is possible to apply a few simple corrections to the pressure data, in order to obtain a better approximation of the actual partial pressure of CO_2 and loading. These are explained in the following two sections.

Initial pressure increase correction

To correct for the initial pressure jump in the 30 wt% TEPA data set, the assumption was made that the pressure increase from the first CO_2 pulse (ΔP_1) is equal to that of the second pulse (ΔP_2). In other words, the 'zero point pressure', is adjusted (P_0^*). This correction is visualised in Figure 5.5. The assumption is justified, because at the corrected data points, the concentration of CO_2 is still very small. Therefore, it is reasonable to assume that in this low loading range, the CO_2 species absorbed in the liquid don't interact with each other yet. The absolute change in the equilibrium pressure caused by this correction is only significant relative to the pressure in the low loading range.

To show the impact of the correction on the results, the uncorrected and corrected data of 30 wt% TEPA are displayed in Figure 5.6 and 5.7, respectively. It is clear that the correction causes the duplicate experiments to align and shifts the pressures downwards, which is only visible in the low loading range.

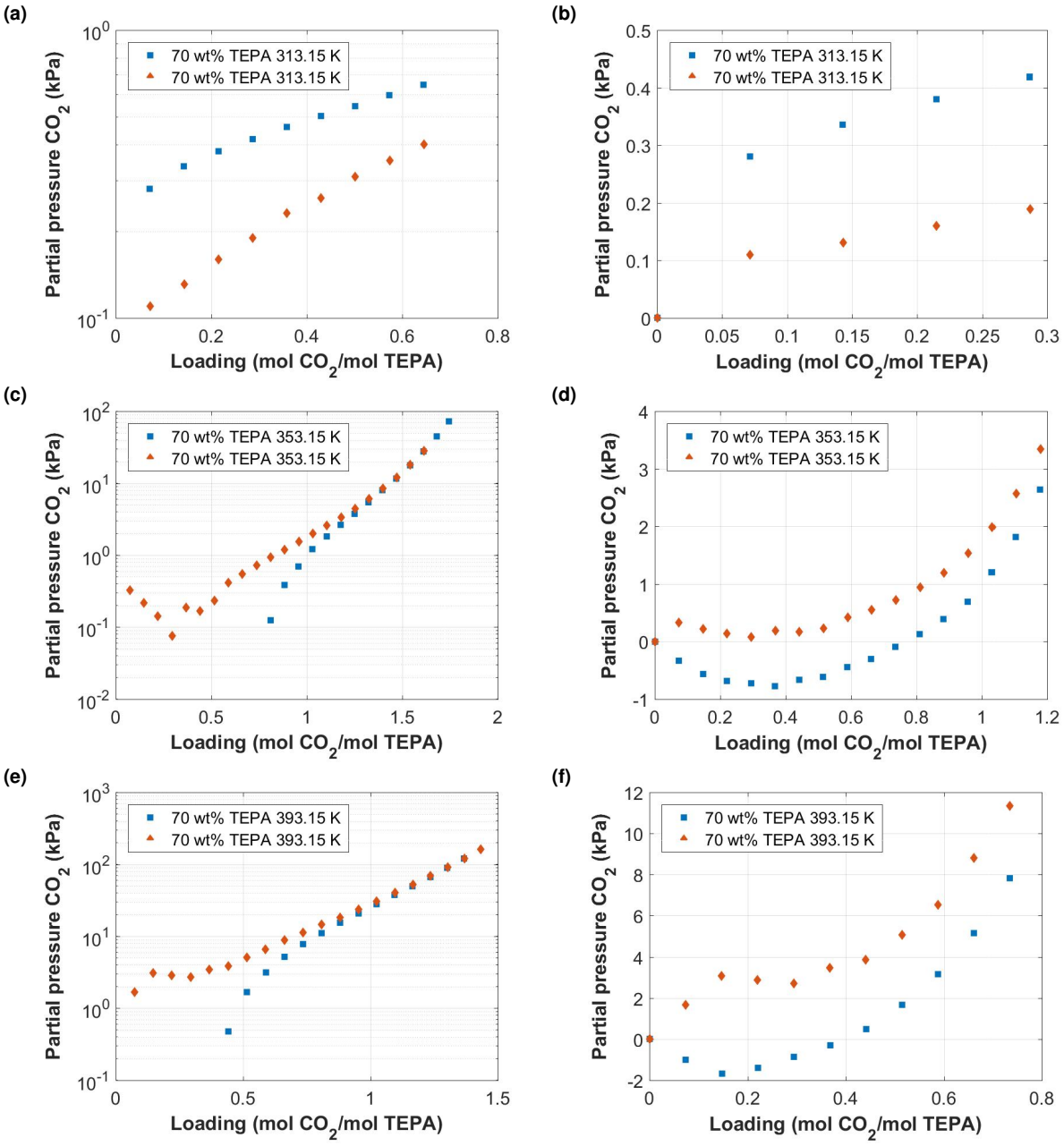

Figure 5.4: Absorption of CO_2 by aqueous solution of 70 wt% TEPA at different temperatures. The graphs on the left show the all measured data points on a semi-log scale. The graphs on the right show a closeup of the low loading region. Duplo measurements show an initial decrease in pressure at 353.15 and 393.15 K and significant pressure offsets. (a)(b) 313.15 K, (c)(d) 353.15 K, (e)(f) 393.15 K

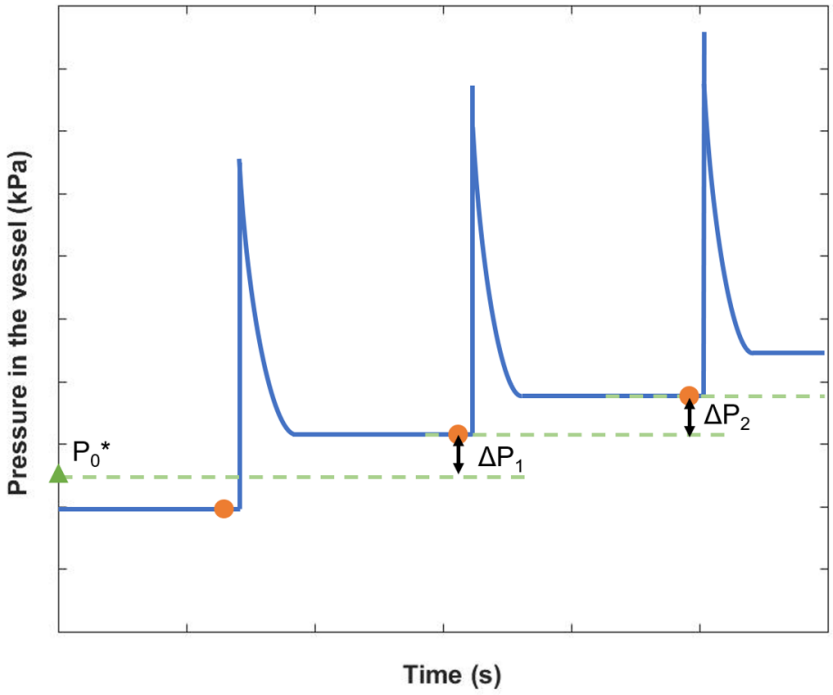

Figure 5.5: Explanation of the data correction of the first pressure data point. The blue graph represents generic raw pressure data, which spikes after each CO_2 pulse, followed by absorption of the CO_2 by the solvent, leading to a new equilibrium state. The orange circles represent the equilibrium pressure. ΔP_1 and ΔP_2 are the pressure differences between two data points. P_0^* is the corrected zero point pressure.

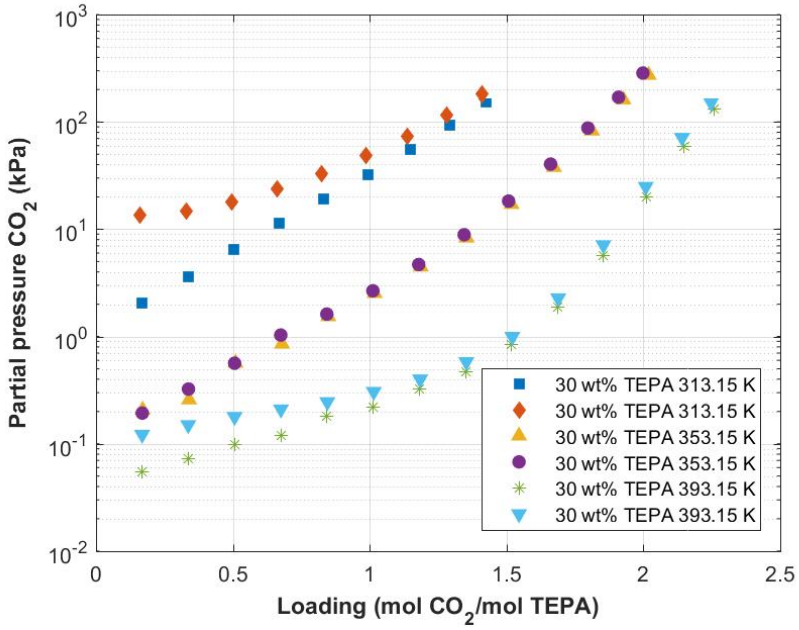

Figure 5.6: Uncorrected CO_2 absorption isotherms of 30 wt% TEPA at 313.15 K, 353.15 K and 393.15 K.

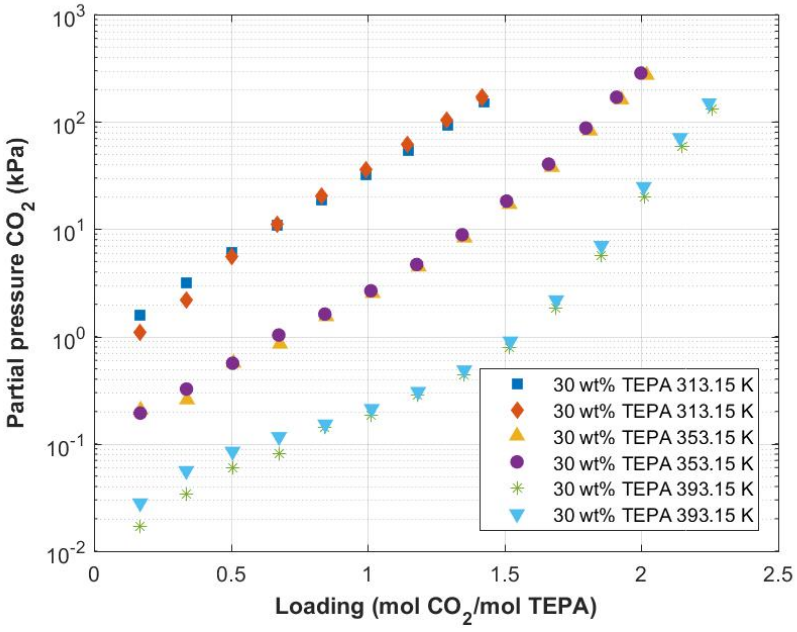

Figure 5.7: Corrected CO_2 absorption isotherms of 30 wt% TEPA at 313.15 K and 393.15 K. No correction was applied to the isotherm at 353.15 K. The correction corrects for disproportionate pressure increases measured after the first CO_2 pulse.

Negative pressure correction

During the measurements of CO_2 absorption in 70 wt% TEPA at 353.15 K and 393.15 K, is was found that total pressure inside the vessel initially decreased after the addition of CO_2 to the system. This was explained by the changing partial pressure of water, as a result of CO_2 absorption by the liquid. Because the partial pressure of CO_2 was calculated as the change in pressure with respect to the pressure at 0 loading, a decrease of the total pressure resulted in a negative pressure of CO_2, which was calculated using the assumption of constant water pressure. This means, that to approximate the actual partial pressure and loading of CO_2 of the system, a different approach must be used.

Similarly to the previous approach, the pressure at 0 loading must be adjusted in order to obtain only positive values of the partial pressure of CO_2. However, this is less straightforward in this case, because it applies to at least the first 5 data points of the isotherm, which show a decreasing pressure trend. The justification of the previous approach at low CO_2 concentration is less valid in this case, because after 5 pulses, the CO_2 concentration is significant and the pressure increase is not likely to be linear anymore. Therefore, the pressure is corrected exponentially in the low loading range, instead of linearly. This correction is visualised in Figure 5.8.

To illustrate the effect of this type of correction, the 70 wt% isotherms are plotted together in one graph, before and after the correction, see Figure 5.9 and Figure 5.10 respectively. The correction for negative pressures was applied to the isotherms of 353.15 and 393.15 K, while the 313.15 K isotherm is corrected only for the initial pressure increase, as described in the previous section.

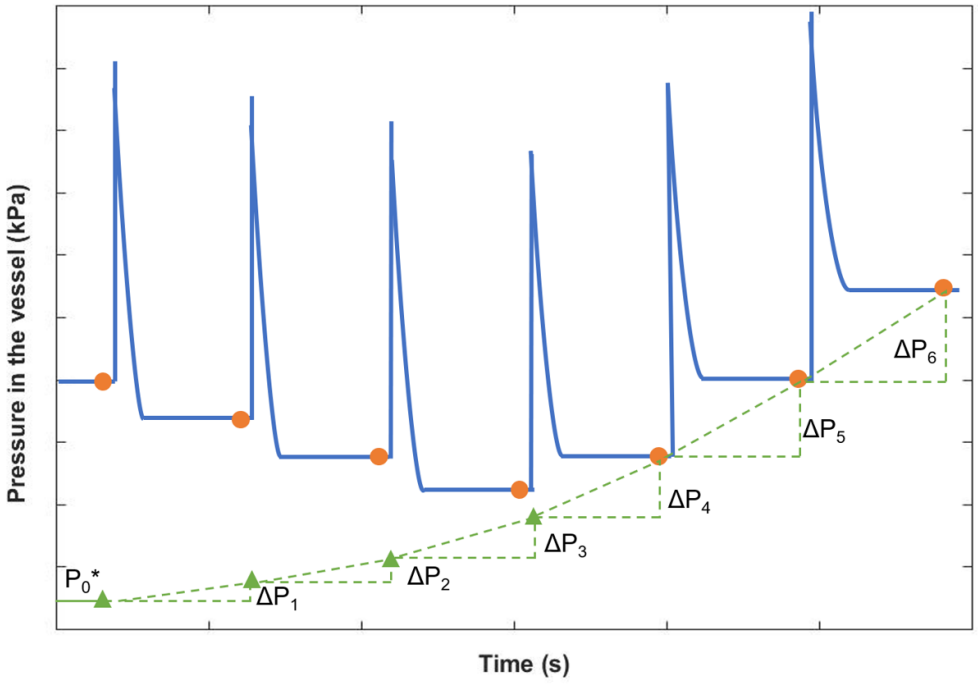

Figure 5.8: Explanation of the data correction of the negative pressures. The blue graph represents generic raw pressure data, which spikes after each CO_2 pulse, followed by absorption of the CO_2 by the solvent, leading to a new equilibrium state. The orange circles represent the equilibrium pressure. ΔP_i are the pressure differences between two equilibrium pressures. P_0^* is the corrected zero point pressure.

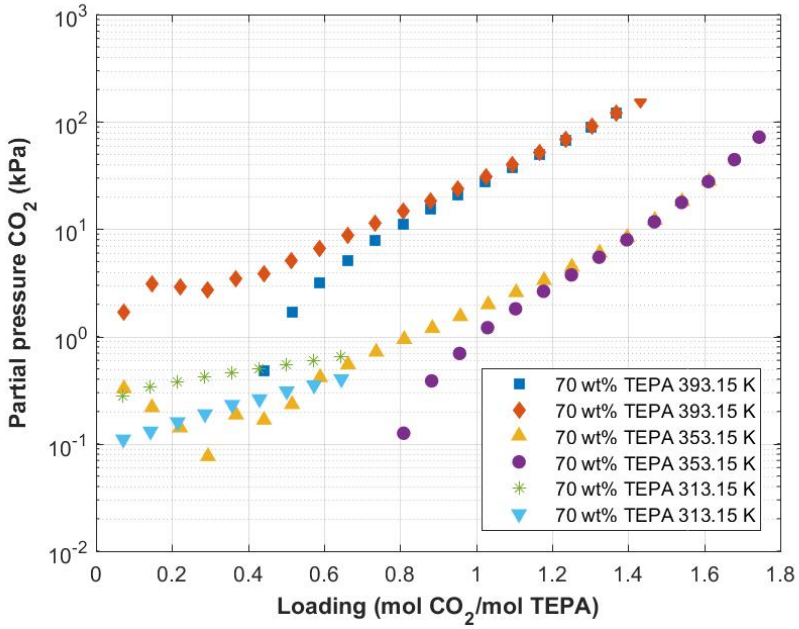

Figure 5.9: Uncorrected CO_2 absorption isotherms of 70 wt% TEPA at 313.15 K, 353.15 K and 393.15 K.

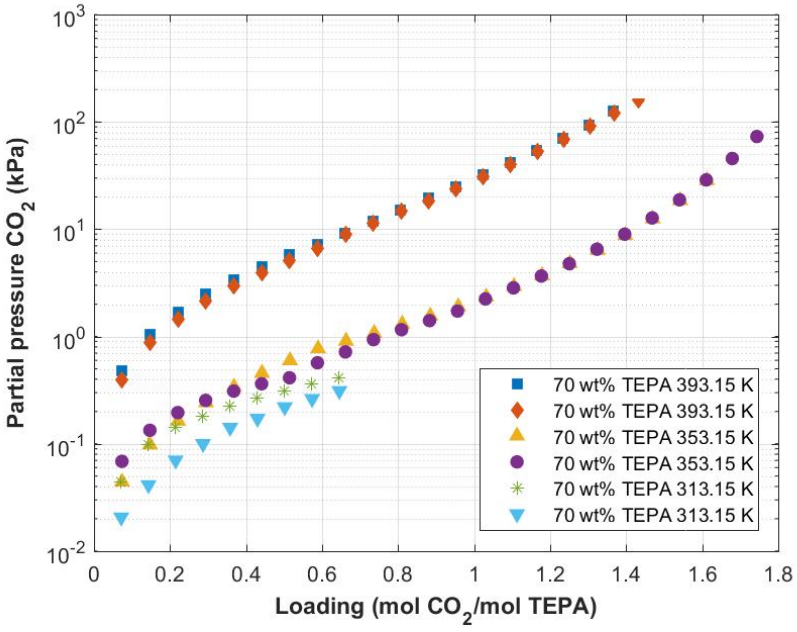

Figure 5.10: Corrected CO_2 absorption isotherms of 70 wt% TEPA at 313.15 K and 393.15 K.

5.1.4 Heat of absorption

The heat of absorption was estimated using the Clausius Clapeyron equation. The enthalpy of absorption H_{abs} is calculated by using the pressure and temperature of two different isotherms at the same loading according to the following equation [35]:

$$\ln\frac{P_2}{P_1} = -\frac{\Delta H_{abs}}{R}\left(\frac{1}{T_2} - \frac{1}{T_1}\right) \tag{5.1}$$

Assuming the loading for the subsequent data points is the same, the heat of absorption was calculated using different combinations of isotherms. Figure 5.11a shows the heat of absorption calculated using the corrected 313.15 and 353.15 K isotherms of the 30 wt% TEPA solution. Additionally, the heat of absorption in Figure 5.11b is calculated using the corrected 353.15 K and 393.15 K isotherms. For the 70 wt% TEPA solutions, heat of absorption was calculated using the data from the corrected 353.15 and 393.15 K. The results of this calculation are shown in Figure 5.11c. The 313.15 K isotherm was not used, as this data set was deemed unreliable. The values of 1-1, 2-2, 1-2 and 2-1 refer to the different combinations of duplo measurements used to calculate the heat of absorption.

Secondary carbamates and primary-secondary dicarbamates are less stable than primary carbamates and will have a lower absorption heat [71]. Since TEPA forms higher order carbamates, the overall heat of absorption is expected to be lower than that of MEA at the same CO_2 loading per mole of amine groups. The graphs show an initial increase in heat of absorption, followed by a decrease. This is not in accordance with literature [72][71][35][73]. It is likely that this is the result of inaccuracy of the VLE data. Kim [73] reported that an accuracy of $\pm$ 2%-3% in the solubility data would result in an order of magnitude increase of uncertainty in the heat of absorption, $\pm$ 20%-30%.

An approximation of the heat of absorption is made by looking at the values at higher loading. For 30 wt% TEPA, the heat of absorption is approximately 70 kJ/mol CO_2 at lower temperatures and 75

kJ/mol at higher temperatures. For 70 wt% TEPA, the value lies between 75 kJ/mol and 80 kJ/mol CO_2 at higher temperatures. A heat of absorption of 84.91 kJ/mol CO_2 (loading = 1.528 mol CO_2 per mol TEPA) for 30 wt% TEPA solutions was measured by Y.E Kim et al [71]. For 30 wt% MEA, the heat of absorption lies between 85 kJ/mol (313.15 K) and 100 kJ/mol (393.15 K)[35]. For 30 wt% DEA, a secondary amine, the heat of absorption is around 70 kJ/mol [72]. The heat of absorption calculated in this work lies between these values for primary-only and secondary-only amines, which is plausible, because the TEPA molecule contains both types of amine groups.

This calculation assumes a constant heat of absorption over the temperature interval used. However, Kim [35] observed that the ΔH_{abs} for MEA and AEEA increased with temperature. Therefore, this calculation only provides an approximation of the heat of absorption. Direct calorimetric measurements of the CO_2 absorption would able to provide more accuracy with regards to heat of absorption and its temperature dependency. Additionally, the assumption of equal loading in the data is not always valid, especially in the higher loading ranges. This could be improved by interpolating the VLE curves and using the partial CO_2 pressures at the exact same loading.

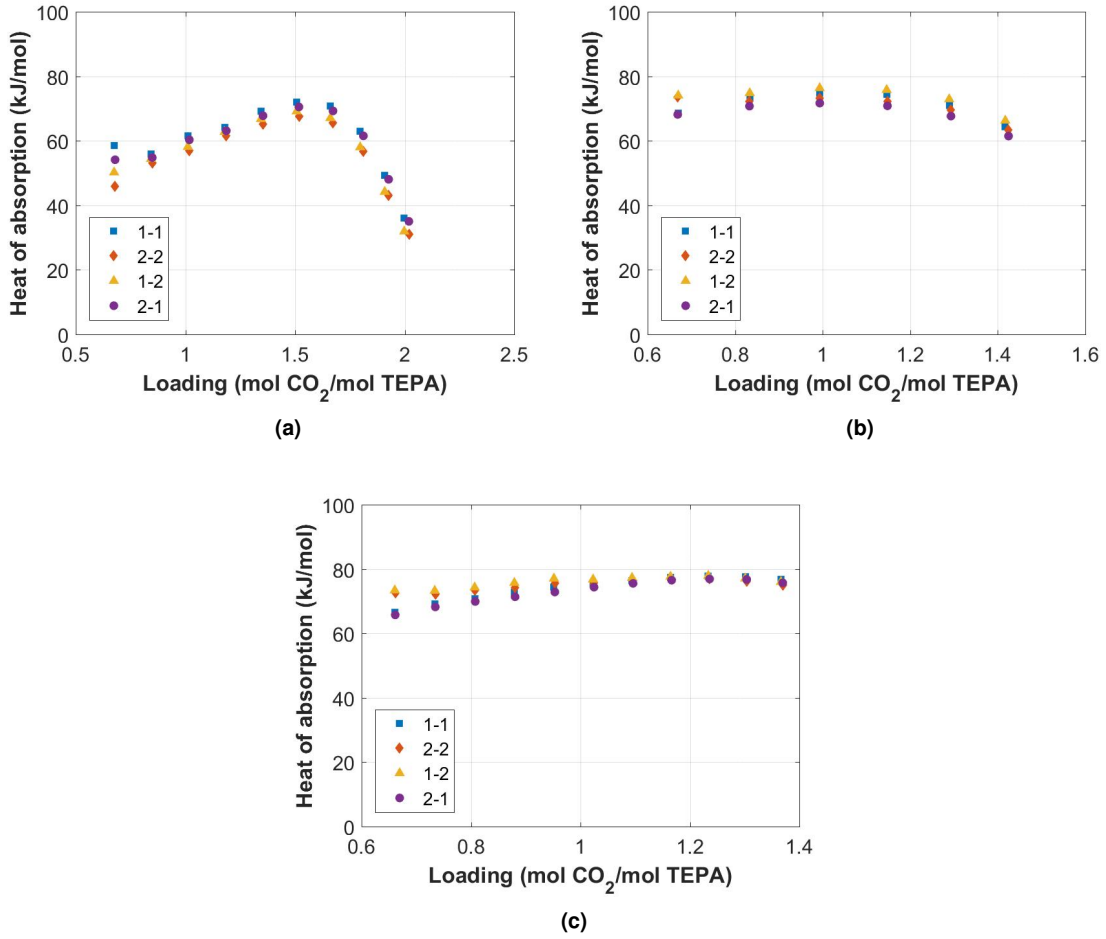

Figure 5.11: Heat of absorption calculated using the Clausius Clapeyron equation and the CO_2 absorption isotherms. The numbers in the legend refer to the different combinations of duplo measurements used for the calculations. (a) 30 wt% TEPA 313.15 K and 353.15 K (b) 30 wt% TEPA 353.15 K and 393.15 K (c) 70 wt% TEPA 353.15 K and 393.15 K.

5.2 Model results and discussion

5.2.1 Binary TEPA-H_2O model

Wilson's activity coefficient model was regressed to the binary TEPA-H_2O VLE data. The fitted parameters that resulted from the regression are given in Table 5.1. It is important to note that the first three data points of the 30 wt% TEPA vapor curve were not taken into account for the regression, because they influenced the fitted result negatively.

The absolute average relative deviation obtained from the model with these parameters is 4.15%, taking into account all measured data points, including the pure water data that was taken from [8]. In Figure 5.12 and 5.13, the excellent agreement between the model and the data is shown.

Table 5.1: Fitted parameters for the Wilson equation to describe the VLE of the binary mixture of TEPA and H_2O.

Fitted parameter	Value	Units
$(\lambda_{12} - \lambda_{11})$	-156.03	J/mol
$(\lambda_{12} - \lambda_{22})$	220.94	J/mol

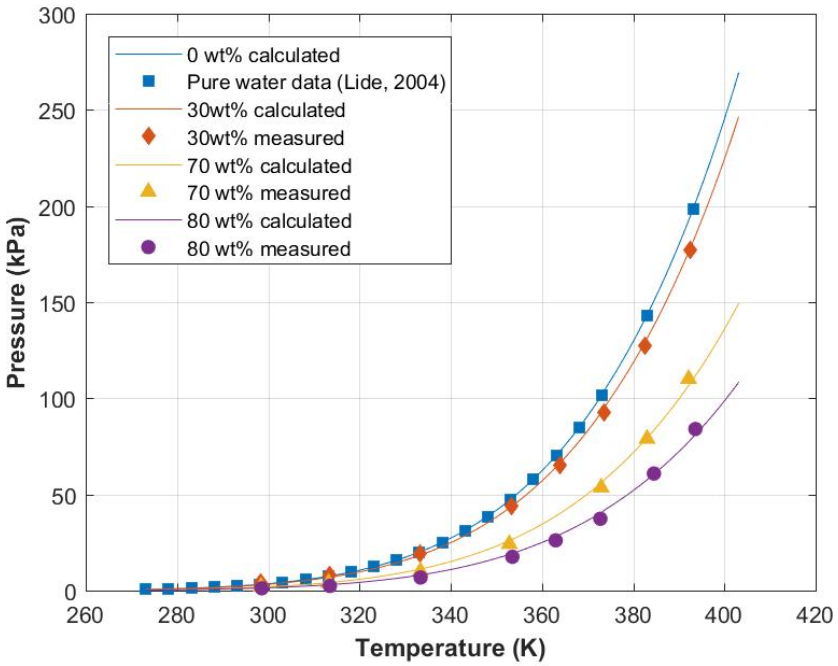

Figure 5.12: The equilibrium pressure of binary mixtures of TEPA and H_2O 30, 70 and 80 wt% TEPA and pure water as a function of temperature, compared to the prediction of the regressed VLE model, using Wilson's equation for activity coefficients.

5.2.2 Ternary MEA-H_2O-CO_2 model

Using the fitted parameters as inputs into the model, the results already looked promising, but they were not as good as the result from the paper [7]. The AARD using the fitted parameters from Puxty

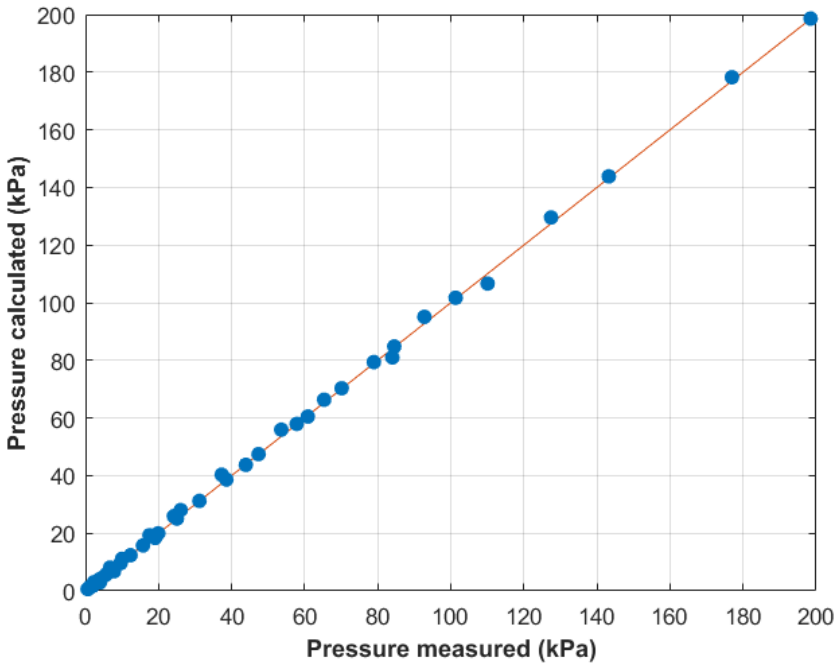

Figure 5.13: Parity plot of the measured versus calculated equilibrium pressure of aqueous solutions of TEPA of different compositions.

and Maeder equalled 23.6%, whereas they obtained an AARD of 15.4% [7]. This discrepancy indicates that the model by Puxty and Maeder was not perfectly reproduced in this work. Since the Matlab script in this work was recreated from scratch, it is possible that a different implementation of the solver and the replacement of the proton balance by the charge balance yields slightly different results.

To improve the agreement between the model created in this work the experimental data, the model parameters were fitted using the parameters from the paper as an initial guess using 'fmincon' from the optimisation toolbox in Matlab. This improved the result to an AARD of 16.6%. The regressed parameters and the results are shown in Table 5.2 and the corresponding plots are given in Figure 5.14. It is clear that the model can predict the partial pressure of CO_2 well across a wide range of MEA concentrations and temperatures. In the parity plot in Figure 5.15, the good agreement between the model and the data is visualised.

The model can not only predict the vapor liquid equilibrium, but also the chemical equilibrium and therefore the concentrations of the different species at a certain temperature and amine concentration. The speciation at 313.15 K and 30 wt% MEA is shown in Figure 5.16.

5.2.3 Ternary TEPA-H_2O-CO_2 model

The model prediction and experimental data of the partial pressure of CO_2 versus the loading in 30 and 70 wt% TEPA solutions are shown in Figure 5.17 and 5.18 respectively. In general, the agreement is very good. In the low loading range the experimental pressure exceeds the model pressure. Figure 5.19 is a parity plot of the calculated and measured pressure. This visualises that the model systematically underpredicts the pressure at low loadings. The experimental uncertainty in the low loading range

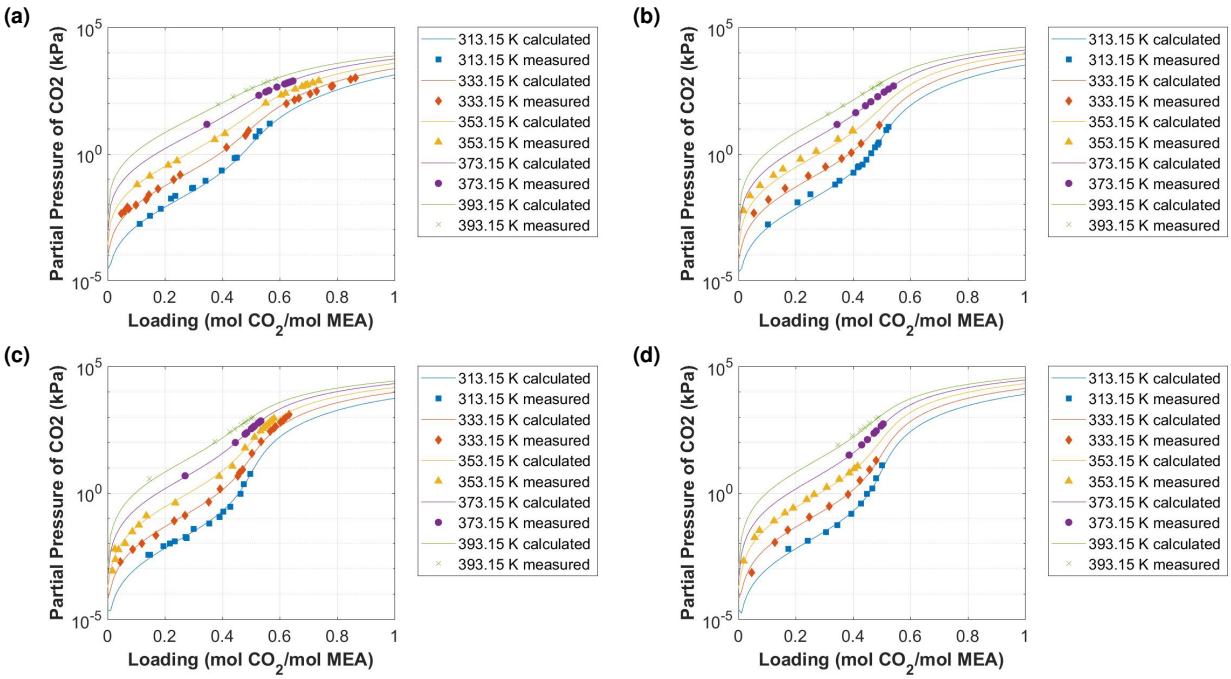

Figure 5.14: Measured versus isotherms for different concentrations of MEA using the ternary MEA-H_2O-CO_2 model. Experimental data from Aronu (2011) [6]. (a) 15 wt% MEA. (b) 30 wt% MEA. (c) 45 wt% MEA. (d) 60 wt% MEA.

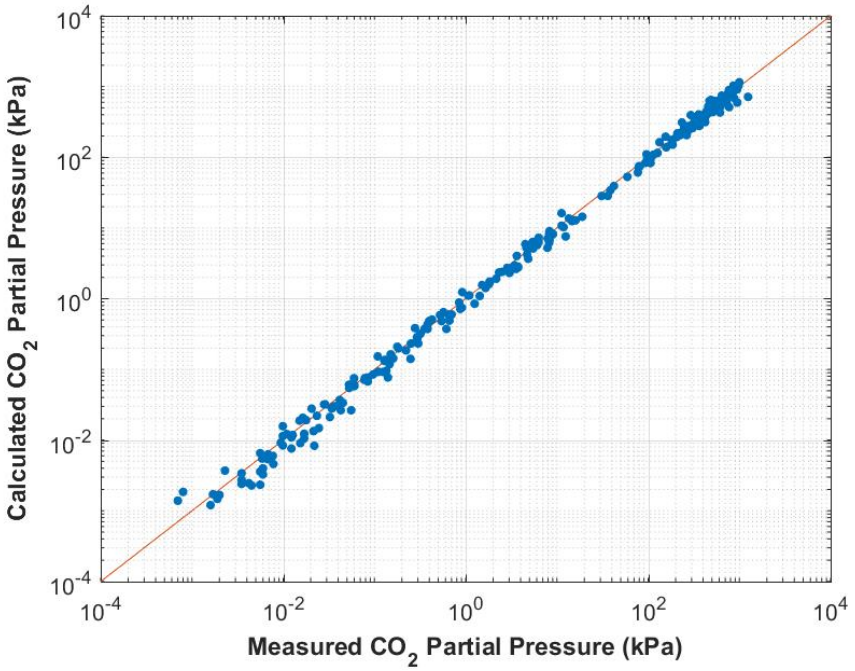

Figure 5.15: Parity plot of the measured partial pressure of CO_2 versus the calculated partial pressure of CO_2 using the ternary MEA-H_2O-CO_2 model.

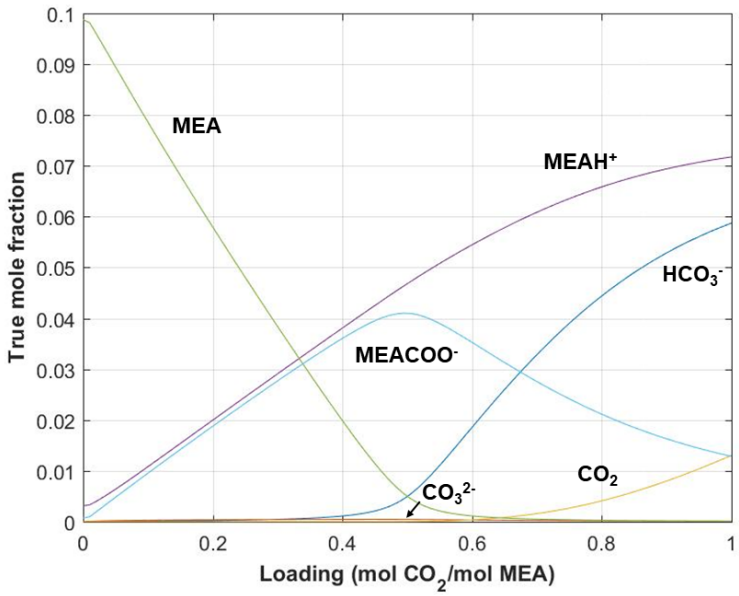

Figure 5.16: Chemical speciation expressed in true mole fraction versus the CO_2 loading in an aqueous solution of 30 wt% MEA at 313.15 K using the Debye-Hückel model prediction.

is high, because this is where the data was corrected and the absolute pressure was in the range of the accuracy of the pressure sensor.

Using the fitted parameters for PZ as an initial guess, the parameters were regressed to the data. However, the setting of parameter boundaries greatly influenced the resulting parameter values and the accuracy of the model. Loose boundaries resulted in better model predictions. Ultimately, the combination of parameters was chosen that provided the best fit, with an AARD of 15.97%.

The approach used in this model was to model TEPA as a diamine. This required the adjustment of the amine concentration by a factor of 2.5. Since this 'pseudo diamine concentration' and its related species do not reflect the concentration of TEPA and multiple carbamates in the liquid, this model cannot be used to predict the speciation in the liquid phase of TEPA. Also, the values of the fitted parameters and the activity coefficients are no longer physically significant.

The model does predict the partial pressure of CO_2 accurately as a function of loading inside the liquid. It allows for confident interpolation between the concentrations of 30 and 70 wt% TEPA and temperatures between 313.15 and 393.15 K. It can be used to extrapolate to concentrations and temperatures outside the liquid, because the model equations are physically logical. However, since no data outside the aforementioned conditions was used for parameter regression, extrapolation is much less reliable.

This model can be used for process simulations. Additionally, the theory of the quantitative structure activity relationship could be applied to other polyamine molecules of which VLE data are available. Hence, this developed model could serve as a potential screening tool to quickly estimate the performance of different prospective solvents for direct air capture.

Table 5.2: Regressed model parameters from this work, compared to the work of Puxty and Maeder and the agreement between the model and the experimental VLE data by Aronu [6] expressed in absolute average relative deviation.

Parameter	Puxty&Maeder (2013)	Regressed parameters (this work)
$logK_4^0$	9.27	9.27
ΔH_4	-53	-46.09
$logK_5^0$	1.44	1.50
ΔH_5	-20	-21.72
$logK_6^0$	7.0	4.17
ΔH_6	-23	-23.03
AARD%	23.6%	16.6%

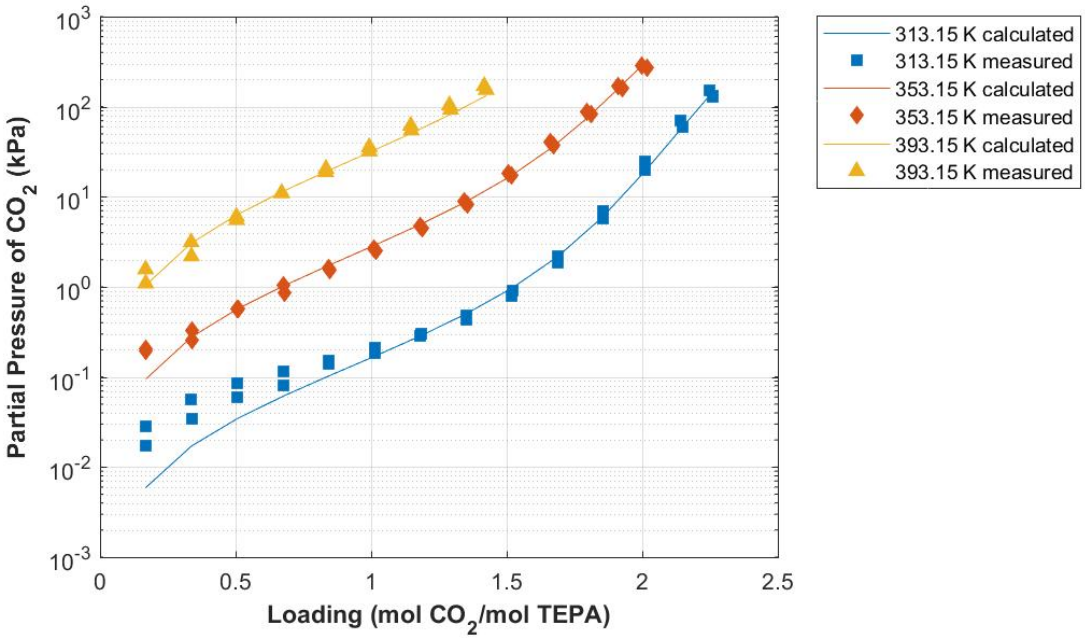

Figure 5.17: Experimental VLE data of the equilibrium CO_2 absorption in an aqueous solution of 30 wt% TEPA at 313.15, 353.15 and 393.15 K versus the ternary TEPA-H_2-CO_2 model prediction.

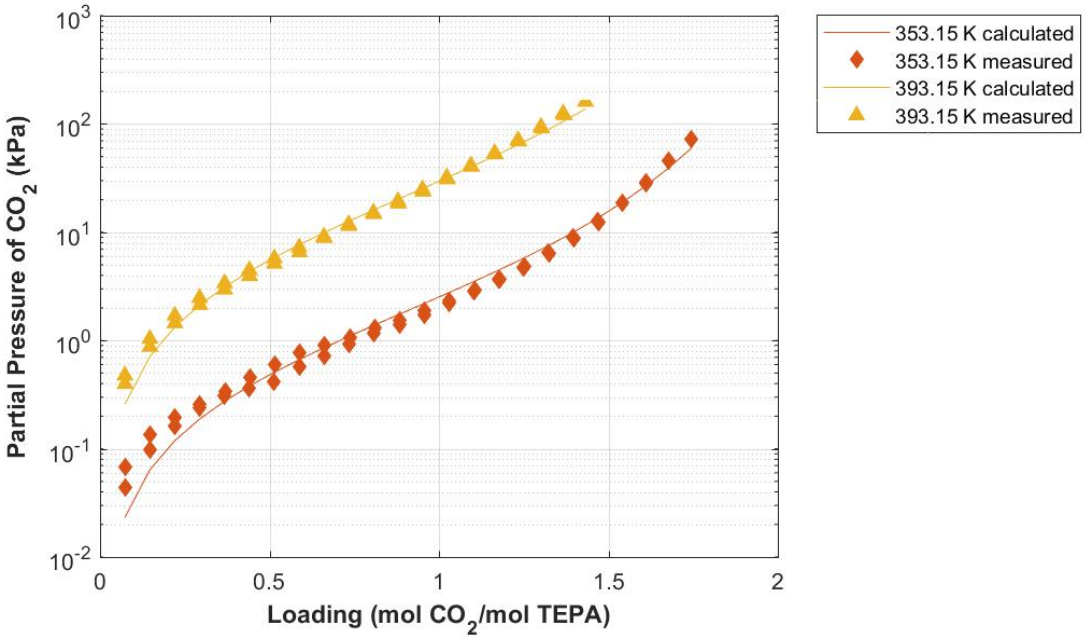

Figure 5.18: Experimental VLE data versus model prediction of the equilibrium CO_2 absorption in an aqueous solution of 70 wt% TEPA at 353.15 and 393.15 K.

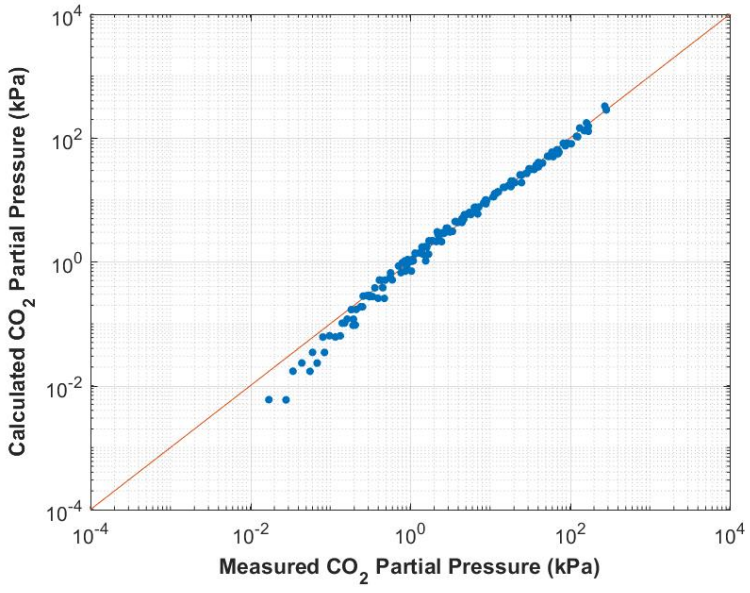

Figure 5.19: Parity plot of the measured partial pressure of CO_2 versus the prediction partial pressure of CO_2 using the ternary TEPA-H_2-CO_2 model described in this work.

Table 5.3: Regressed model parameters from this work, compared to the work of Puxty and Maeder and the agreement between the model and the experimental VLE data of this work expressed in absolute average relative deviation.

Parameter	**PZ parameters [7]**	**Regressed parameters (this work)**
$logK_4^0$	9.3	8.05
ΔH_4	-38	-19.4
$logK_5^0$	1.2	1.05
ΔH_5	-32	-26.37
$logK_6^0$	8.9	8.9
ΔH_6	-18	-26.51
$logK_7^0$	0.8	2.37
ΔH_7	-24	-21.28
$logK_8^0$	8.9	6.74
ΔH_8	-24	-24.53
AARD%		15.97%

Chapter 6

Case Study: ZEF DAC

The aim of this chapter is to provide insight into the performance of TEPA as a direct air capture sorbent, based on results of the equilibrium models developed in this work. First, the process flow diagram of the DAC unit of ZEF is described, followed by an explanation of the methodology and assumptions used for the calculations. Then, the effect of different process parameters on the energy demand is analyzed and discussed. Concrete recommendations for ZEF are listed in the last section. The most important results and findings are highlighted in bold text.

6.1 ZEF DAC unit

As explained in Section 2.1.4, the current research and development in the context of direct air capture at Zero Emission Fuels is focused on using TEPA in a continuous absorption and stripping process. The process flow diagram of the current prototype of the DAC unit is show in Figure 6.1.

Inside the absorption column, CO_2 and H_2O are absorbed by a highly concentrated TEPA stream. Next, the rich amine is heated up in the stripping column by the reboiler. This starts the reversal of the chemical reactions inside the liquid to allow the CO_2 and the amine solvent to be regenerated. Additionally, the reboiler causes water to vaporize. This steam flows up the desorption column and strips the CO_2 out of the liquid phase by decreasing the partial pressure of CO_2 in the vapor phase, resulting in a driving force of CO_2 out of the liquid. H_2O vapor and CO_2 gas exit the top of the stripping column and are separated in a flash tank. Part of the water stream is led back into the stripping column, to ensure the partial pressure of H_2O is high enough.

6.2 Absorption and stripping column calculations

In this section, absorption and stripping calculations are performed using the models developed in this work. These calculations are done with varying conditions inside the absorption and stripping column, to illustrate the effects of the process parameters on the carbon capture performance of TEPA and the associated energy demand of the process.

6.2.1 Assumptions

In order to do these calculations, assumptions need to be made. These are listed below:

- **Thermodynamic equilibrium**: It is assumed that thermodynamic equilibrium has been reached inside the absorption column, the stripping column and the flash tank.
- **Steady state**: It is assumed that no accumulation of mass or energy occurs in the system.
- **Daily CO_2 target of 18.75 mol**: ZEF has specified a daily target of 18.75 mol of CO_2 that needs to be captured in order to make the system cost effective. It is assumed the solar powered micro-plant is operated 8 hours a day. This makes the target mass flow rate of CO_2 2.344 mol/h or 0.103 kg/h.

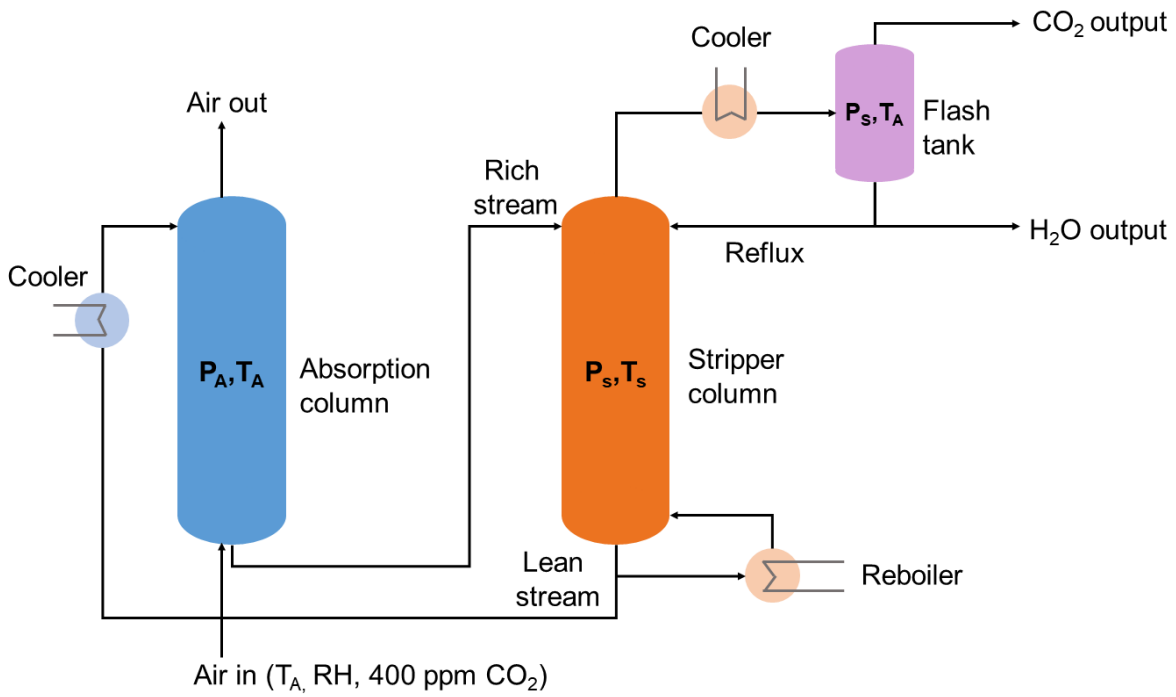

Figure 6.1: Overview of the ZEF absorption and stripping process.

- **Daily H_2O target of 56.3 mol**: H_2 and CO_2 react in the molar ratio 3:1 to form methanol. Therefore, at least 7.031 mol/h of H_2O or 0.127 kg/h needs to be captured to produce the required H_2 for methanol synthesis.
- **Flash tank and absorption column operate at ambient temperature**: It is assumed the hot gaseous stream that comes out of the top of the stripping column is cooled passively by the ambient air down to the ambient temperature. Additionally, the hot solvent coming out of the bottom of the stripping column is assumed to be cooled passively to ambient temperature, before reaching the absorption column.
- **Constant air composition, temperature and pressure**: It is assumed that the outside air conditions, the temperature and relative humidity, are constant during the operation of the process. Ambient pressure is assumed to be 100 kPa.
- **Single-stage stripping column**: The optimal configuration of the stripping column of the ZEF DAC prototype has not yet been found. Different 7-stage, 3-stage and single stage prototypes are being tested currently. Therefore, for simplicity, the stripping column in this chapter is modelled as a single stage flash separator. However, to avoid confusion between this column and the flash tank that separates the H_2O and CO_2 output, the stripping column will not be referred to as a flash tank.
- **No pressure drop in the system**: The gaseous output stream from the top of the stripping column is connected to a flash tank, to separate H_2O and CO_2. It is assumed this flash tank operates at the same pressure as the stripping column.

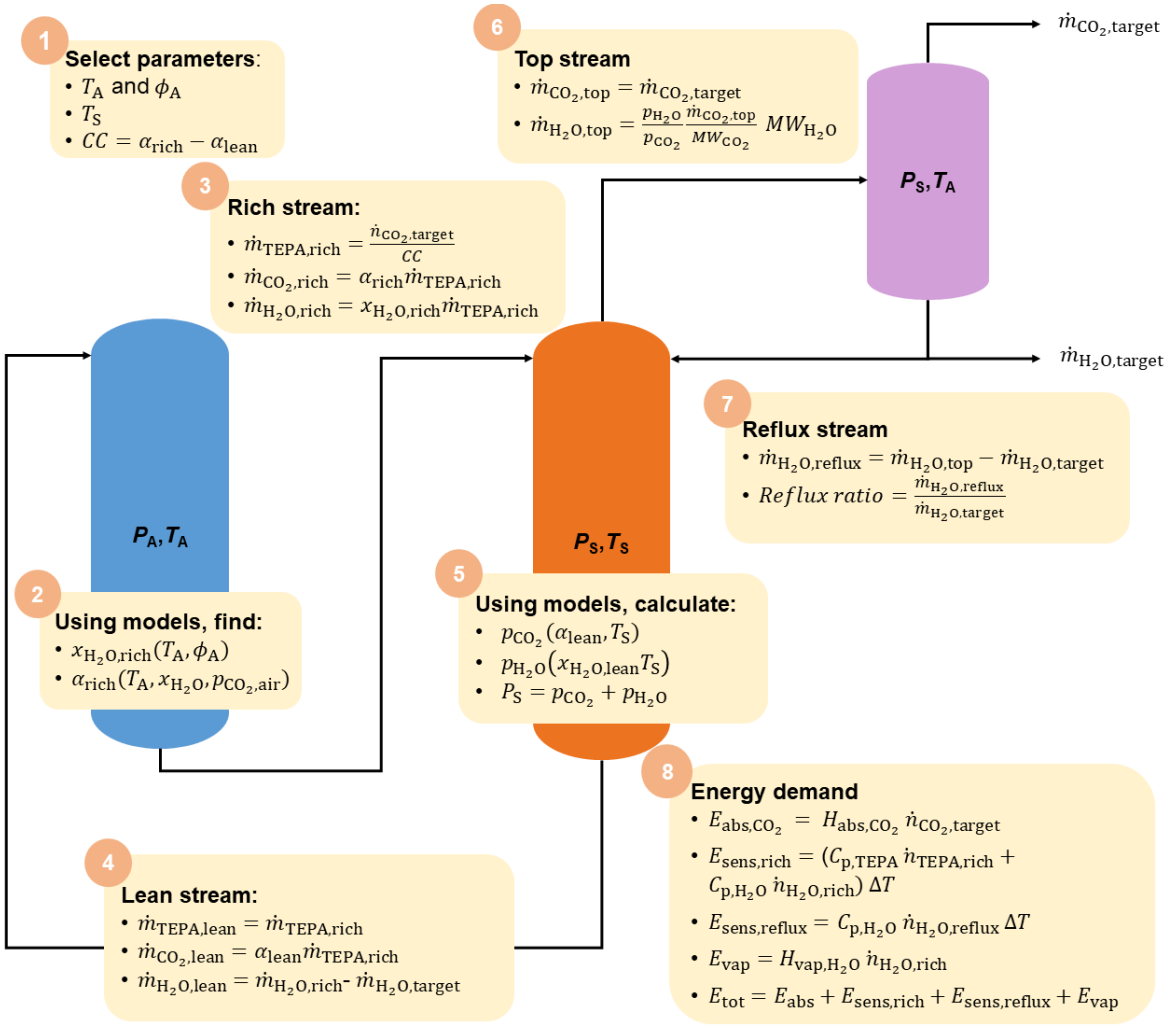

Figure 6.2: Diagram explaining the methodology used to calculate the effect of the selected process parameters on the mass balance and the energy demand of the direct air capture unit of ZEF. The calculations were performed in the order of the numbered steps.

- **Negligible vaporization of TEPA**: It is assumed that the amount of TEPA in the vapor stream exiting the stripping column is negligible.

6.2.2 Calculation methodology

When it comes to the calculation of different scenarios for an absorption and stripping process, there are different process parameters that can be varied separately. Hence, there are many ways to approach this problem. In this chapter, the calculations were carried out using the methodology that is visualised in Figure 6.2. With the design parameters selected in step 1 and the assumptions described in Section 6.2.1, the flow rates of all components of each stream as well as the energy balance can be calculated following the steps in the figure.

A description of all the parameters that are shown in Figure 6.2 can be found in Table 6.1. Additionally, the values of the constants used in the energy balance are given in Table 6.2.

Table 6.1: Nomenclature of the process parameters.

Parameter	Description
T_A	Temperature of the ambient air.
P_A	Pressure of the ambient air.
T_S	Temperature inside the stripping column
P_S	Pressure inside the stripping column
ϕ_A	Relative humidity of ambient air
CC	Cyclic capacity of the process
$\dot{m}_{i,j}$	mass flow rate of component *i* in stream *j*
$\dot{n}_{i,j}$	molar flow rate of component *i* in stream *j*
α	loading of CO_2
x_{H_2O}	loading of H_2O (weight percentage, without taking the mass of CO_2 into account)
rich	The stream that flows from the absorption column to the stripping column
lean	The stream that flows from the stripping column to the absorption column
target	The streams of CO_2 and H_2O that exit from the flash tank
top	The stream containing H_2O and CO_2 that exits the top of the stripping column
reflux	The stream of H_2O that is sent back into the stripping column from the flash tank.

Table 6.2: Values used for the calculation of the total energy demand.

Property	Description	Value	Unit	Source
H_{abs,CO_2}	Heat of absorption of CO_2 from TEPA	75	kJ/mol	This work
C_{p,H_2O}	Specific heat of H_2O	75.3	J/(mol K)	[74]
$C_{p,TEPA}$	Specific heat of TEPA	460	J/(mol K)	[75]
H_{vap,H_2O}	Heat of vaporization of H_2O	40.65	kJ/mol	[76]

6.2.3 Rich loading as a function of ambient conditions

H_2O loading depends more strongly on the relative humidity than on the temperature of air.

TEPA absorbs H_2O as it is exposed to moist air. Using the H_2O-TEPA binary model, the equilibrium water loading of the solution can be calculated as a function of temperature and the relative humidity of air. Relative humidity is defined as the ratio of the partial pressure of water vapor in air to the saturation pressure of water at the air temperature. Therefore, the partial pressure of water can be calculated at air of a specified temperature, T, and relative humidity, ϕ, using the following equation:

$$p_{H_2O} = \phi p^{sat}_{H_2O}(T) \tag{6.1}$$

As the relative humidity goes up, the partial pressure of H_2O in the air increases, which increases the amount of water absorbed by TEPA, see Figure 6.3a. When the temperature increases at constant relative humidity, the water loading in TEPA decreases, see Figure 6.3b. It is clear that the relative humidity has a stronger effect on the water loading than the ambient temperature.

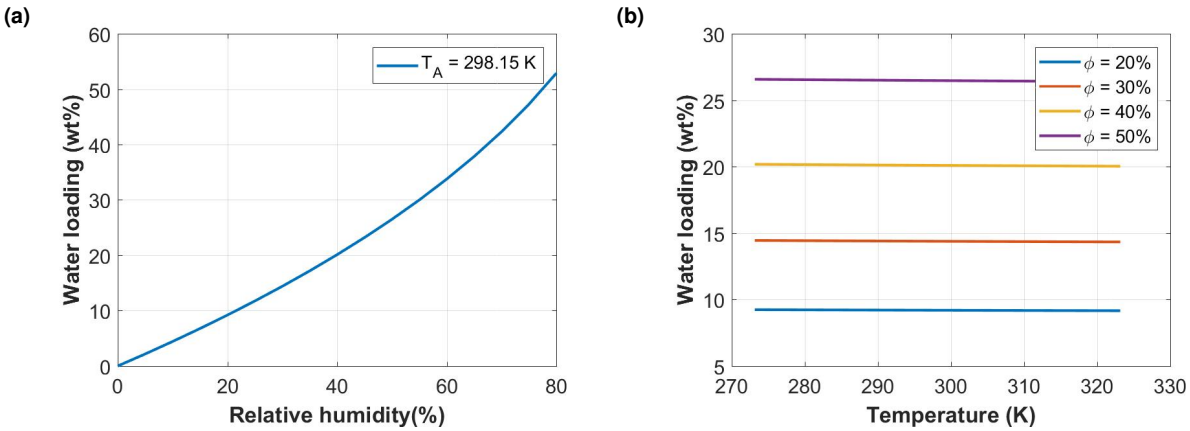

Figure 6.3: (a) Strong effect on the water loading of TEPA as a result of a changing relative humidity of air, at a constant ambient temperature of 298.15 K (b) Weak effect on the water loading of TEPA as result of a changing ambient temperature at different relative humidities.

CO_2 loading depends more strongly on the temperature than on the concentration of the TEPA solution.

The water content of the TEPA solution and the temperature of the solution also have important consequences for the amount of CO_2 absorbed by the solution at equilibrium. Air contains approximately 400 ppm of CO_2 (see Section 1.1). If the pressure of air is 100 kPa, then the partial pressure of CO_2 (assuming ideal gas) must be:

$$p_{CO_2} = 100 \text{ kPa} \cdot \frac{400}{10^6} = 0.04 \text{ kPa} \tag{6.2}$$

The effect of the temperature on the equilibrium loading of CO_2 is shown in Figure 6.4. As the temperature decreases, more CO_2 is absorbed. Table 6.3 additionally shows the effect of the water concentration on the loading. The CO_2 loading decreases slightly with increasing water loading.

Table 6.3: CO_2 loading (mol CO_2/kg TEPA) inside TEPA solution as a function of temperature and water loading of the solution.

Water loading (wt%)	**Temperature (K)**	
	293.15	313.15
10	5.90	3.20
20	5.88	3.17
30	5.84	3.13

6.2.4 Effect of rich composition on energy demand

To illustrate the effect of the rich composition on the rest of the process, four different scenarios are compared in this section.

1. **Dry and cold location:** Ambient temperature of 293.15 K (20℃) and a relative humidity of 25%.

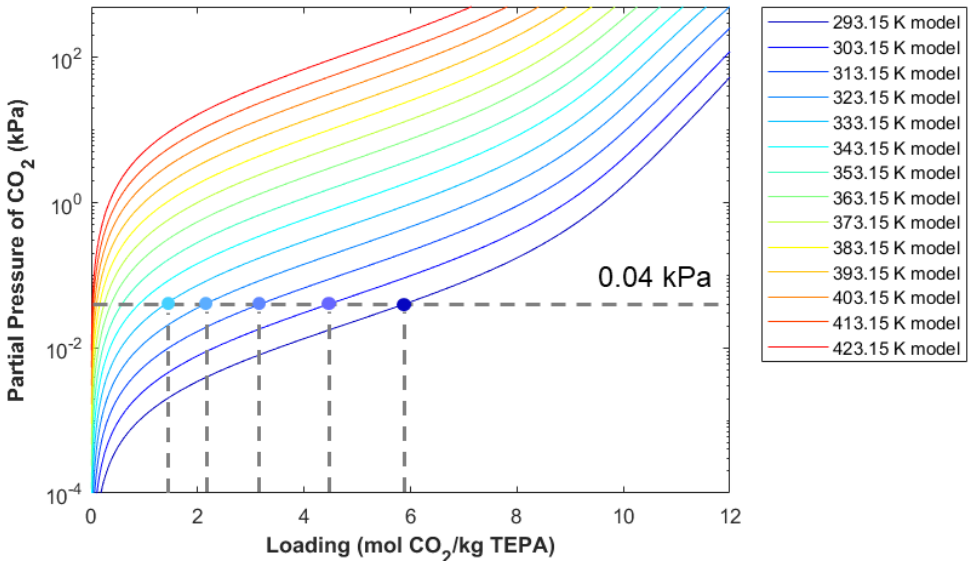

Figure 6.4: Effect of temperature on the rich CO_2 loading of 80 wt% TEPA in equilibrium with ambient air, using extrapolated model developed in this work.

2. **Humid and cold location:** Ambient temperature of 293.15 K (20℃) and a relative humidity of 75%.

3. **Dry and hot location:** Ambient temperature of 313.15 K (40℃) and a relative humidity of 25%.

4. **Humid and hot location:** Ambient temperature of 313.15 K (40℃) and a relative humidity of 75%.

The rest of the process conditions are kept constant, to analyse the effect of these ambient conditions only. Therefore it is assumed that the stripper is operated at 393.15 (120℃) and the cyclic capacity is fixed to 1 mol/kg.

In a dry and cool climate, the H_2O target cannot be met. However, if the climate is too humid, the energy demand increases sharply.

An overview of the results in shown in Table 6.4. The energy demand of the different scenarios is compared in Figure 6.5. A few trends can be deduced from the results. In scenario 1, the cold dry climate, the CO_2 loading is high, but the H_2O is low. This causes the ratio of the partial pressure of H_2O to CO_2 to be below the desired ratio of 3:1. Therefore, in this climate, the system cannot provide the desired H_2O target. Therefore, required reflux stream and ratio were calculated to be negative. The water balance in this scenario is therefore not correct and the lean composition and water output should be solved iteratively. In scenario 2, the cold humid climate, the H_2O loading is much higher. This means that the partial pressure of H_2O in the column must be higher compared to the previous scenario. A reflux stream will be necessary to provide the needed vapor pressure. With respect to the previous scenario, the energy demand is increased, because more water in the feed stream leads to higher sensible heat requirements and more water needs to be vaporised.

Hot and dry conditions result in a more energy efficient process than hot and humid conditions, because less energy is required for vaporisation.

In scenario 3 and 4, the CO_2 rich loading is lower due to a higher ambient temperature, which means the partial pressure of CO_2 in the column goes down and the reflux ratio becomes higher. In scenario 4, this is amplified by the higher water loading, which results in a higher partial pressure of water in the stripping column. Although the sensible heat requirement in scenarios 3 and 4 is lower, because the temperature difference between absorption and stripping is lower, this effect is outweighed by the increase caused by the larger reflux stream.

Cool and moderately humid conditions or hot and dry conditions are the most advantageous in terms of energy demand. However, a trade-off must be made regarding the separation of H_2O and CO_2.

Looking at the overall performance, scenario 1 shows the lowest energy demand, but cannot provide the target H_2O output necessary for ZEF. Therefore scenario 3 has emerged as the best out of the analysis in terms of energy demand. However, a trade-off must be made, because the separation of CO_2 and H_2O in the flash tank is worst in scenario 3, because the pressure is low and temperature high. Ideally, the pressure should be high and the temperature low to facilitate a mostly pure CO_2 and H_2O output stream. This is desirable for the subsequent processing steps in the ZEF process, as H_2O vapor will cause problems for the CO_2 compression, while CO_2 in the H_2O stream increases its acidity, which is disadvantageous for its use in alkaline electrolysis.

Table 6.4: Results of varying the ambient conditions on the H_2O and CO_2 loading and other process parameters.

	Scenarios				
Process parameter	**1**	**2**	**3**	**4**	**Unit**
T_A	20	20	40	40	℃
ϕ	25	75	25	75	%
T_S	120	120	120	120	℃
Cyclic capacity	1	1	1	1	mol CO_2/kg TEPA
$\alpha_{CO_2,rich}$	5.9	5.8	3.2	3.1	mol CO_2/kg TEPA
$\alpha_{CO_2,lean}$	4.9	4.8	2.2	2.1	mol CO_2/kg TEPA
$x_{H_2O,rich}$	11.7	47.3	11.7	47.2	wt%
$P_{CO_2,col}$	22.9	22.4	3.8	3.6	kPa
$P_{H_2O,col}$	32.5	146.6	32.3	146.4	kPa
$\frac{P_{H_2O,col}}{P_{CO_2,col}}$	1.4	6.5	8.6	40.7	-
Reflux ratio	-0.5	1.2	2.0	12.8	-
y_{CO_2} output	0.96	0.99	0.82	0.96	-
E_{abs}	75	75	75	75	kJ/mol CO_2
$E_{sens,feed}$	299	618	239	493	kJ/mol CO_2
$E_{sens,reflux}$	0	27	34	227	kJ/mol CO_2
E_{vap}	58	266	349	1653	kJ/mol CO_2
E_{tot}	431	986	696	2449	kJ/mol CO_2

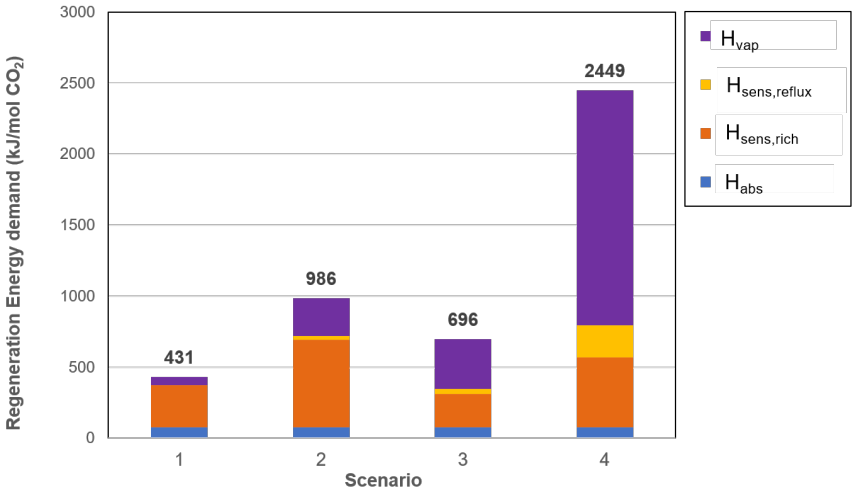

Figure 6.5: Energy demand of the stripping column for 4 different scenarios. The energy must provide sufficient stripping water vapor, heat up the rich and reflux stream from ambient temperature to stripping temperature (393.15 K) and desorb CO_2 from the TEPA solution.

6.2.5 Cyclic capacity and energy demand

In the previous section, the cyclic capacity was fixed to 1 mol of CO_2 per kg of TEPA. However, the system can be designed such that this value is higher or lower, which influences the other process parameters. Therefore, the same calculations were done, but this time the CC was varied, while the other parameters were fixed. The ambient conditions were fixed to 20 ℃ and a relative humidity of 50 % with a stripping temperature of 120 ℃. The results are shown in Table 6.5 and Figure 6.6.

A higher cyclic capacity results in a decrease of pressure in the stripping column and an increasing reflux ratio.

When the cyclic capacity is increased, a lower mass flow rate of TEPA is required to produce the same amount of CO_2. By keeping the H_2O output flow rate the same, the ratio of water to TEPA in the lean stream decreases which decreases the partial pressure of H_2O in the column. Additionally, the lean loading is lower, which means the partial pressure of CO_2 in the column is decreased. Therefore, by only increasing the cyclic capacity, the total pressure in the column goes down. Because the partial pressure of CO_2 decreases more strongly than the partial pressure H_2O with increasing cyclic capacity, the reflux ratio goes up.

A higher cyclic capacity causes the sensible heat requirement to decrease and the vaporisation heat demand to increase.

The change in energy demand with increasing cyclic capacity shows an interesting trend. Due to the increasing ratio of H_2O to CO_2 in the vapor phase in the stripping column, more energy is needed to vaporize water with increasing cyclic capacity (see the purple bars in Figure 6.6). However, at the same time, the sensible heat requirement decreases, because a smaller flow rate of TEPA and H_2O is needed at higher cyclic capacity. This effect is dominant in the first three scenarios, causing the total energy demand to drop. However, the vaporisation becomes dominant after that, increasing the total energy demand again.

Table 6.5: Results of varying the cyclic capacity of the process.

	Cyclic capacity (mol CO_2/kg TEPA)					
Process parameter	**0.5**	**1**	**1.5**	**2**	**2.5**	**Unit**
T_A	20	20	20	20	20	℃
ϕ	50	50	50	50	50	%
T_S	120	120	120	120	120	℃
$\alpha_{CO_2,rich}$	5.9	5.9	5.9	5.9	5.9	mol CO_2/kg TEPA
$\alpha_{CO_2,lean}$	5.4	4.9	4.4	3.9	3.4	mol CO_2/kg TEPA
$x_{H_2O,rich}$	26.5	26.5	26.5	26.5	26.5	wt%
$P_{CO_2,col}$	30.8	22.7	16.8	12.3	8.9	kPa
$P_{H_2O,col}$	95.7	90.9	85.8	80.3	74.4	kPa
$\frac{P_{H_2O,col}}{P_{CO_2,col}}$	3.1	4.0	5.1	6.5	8.3	-
Reflux ratio	0.0	0.3	0.7	1.2	1.8	-
y_{CO_2} output	0.98	0.98	0.98	0.98	0.98	-
E_{abs}	75	75	75	75	75	kJ/mol CO_2
$E_{sens,feed}$	787	394	262	197	157	kJ/mol CO_2
$E_{sens,reflux}$	1	8	16	26	40	kJ/mol CO_2
E_{vap}	126	163	208	265	339	kJ/mol CO_2
E_{tot}	989	639	561	563	611	kJ/mol CO_2

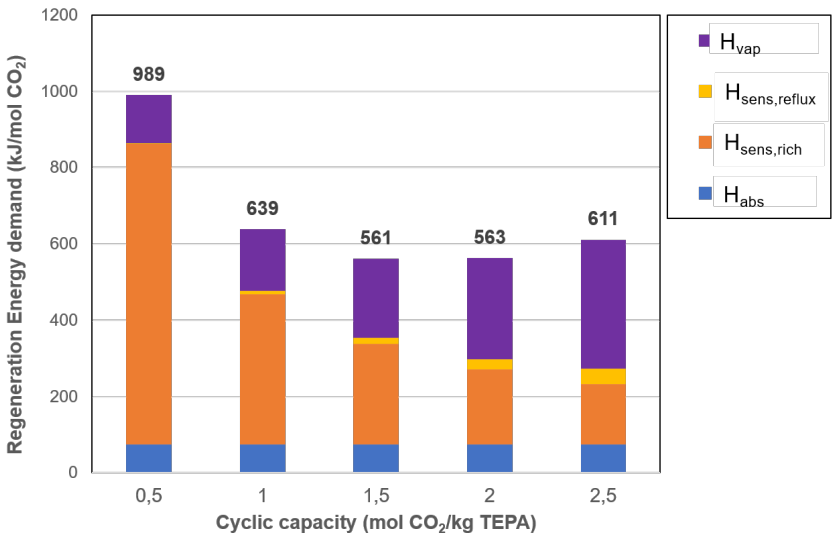

Figure 6.6: Effect of varying the cyclic capacity on the total regeneration energy demand of the direct air capture process.

6.2.6 Stripping column temperature

The last parameter that could be varied (according to the methodology used in this work) is the temperature in the stripping column. Therefore, to illustrate the effect of this on the energy demand, the

stripping temperature was varied from 110, to 120 and 130 ℃, while the other design parameters were kept constant. In this analysis, an ambient temperature of 20 ℃, relative humidity of 50 % and a cyclic capacity of 1.5 mol CO_2/kg TEPA were used.

A higher stripping temperature causes a higher pressure in the stripping column and a decreased reflux ratio.

With an increasing temperature, the following effects can be distinguished. The total absolute pressure inside the stripping column is increased. However, this effect is stronger for the partial pressure of CO_2, compared to that of H_2O. This causes the ratio of H_2O to CO_2 to decrease (in these cases) towards the desired ratio for methanol synthesis. In turn, this means that a smaller reflux stream is required to achieve the pressures inside the column.

A higher stripping temperature results in an increased sensible heat and a decreased vaporisation heat demand.

The effect on the energy demand is twofold. With an increasing temperature difference between the ambient temperature and the stripping column, more energy is required to heat the feed stream. However, simultaneously, the energy required to vaporize water decreases because of the smaller reflux stream, which is dominant in this case. Therefore, the overall energy demand decreases with increasing stripping temperature (see Figure 6.7).

Table 6.6: Results of varying the stripping temperature on the other process parameters.

	Stripping temperature (℃)			
Process parameter	**110**	**120**	**130**	
T_A	20	20	20	℃
ϕ	50	50	50	%
Cyclic capacity	1.5	1.5	1.5	mol CO_2/kg TEPA
$\alpha_{CO_2,rich}$	5.9	5.9	5.9	mol CO_2/kg TEPA
$\alpha_{CO_2,lean}$	4.4	4.4	4.4	mol CO_2/kg TEPA
$x_{H_2O,rich}$	26.5	26.5	26.5	wt%
$P_{CO_2,col}$	5.2	16.8	29.4	kPa
$P_{H_2O,col}$	43.9	85.8	116.5	kPa
$\frac{P_{H_2O,col}}{P_{CO_2,col}}$	8.5	5.1	4.0	-
Reflux ratio	1.8	0.7	0.3	-
y_{CO_2} output	0.96	0.98	0.99	-
E_{abs}	75	75	75	kJ/mol CO_2
$E_{sens,feed}$	236	262	289	kJ/mol CO_2
$E_{sens,reflux}$	37	16	8	kJ/mol CO_2
E_{vap}	344	208	161	kJ/mol CO_2
E_{tot}	693	561	533	kJ/mol CO_2

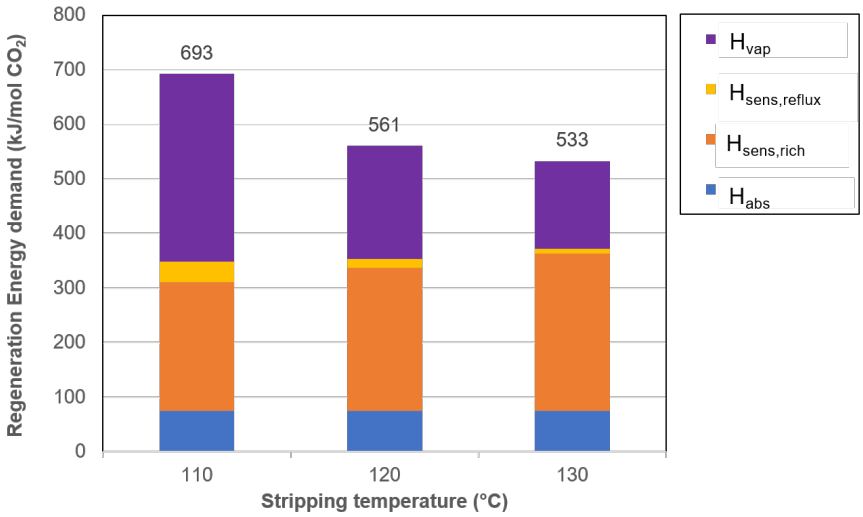

Figure 6.7: Effect of varying the stripping temperature on the energy demand of the direct air capture process.

6.3 Discussion

The most energy efficient scenario was T_A of 20℃, T_S of 130℃, *CC* of 1.5 mol/kg

It is clear that different process parameters can be varied and that an optimum must be found where the energy demand of the process is the lowest. The most efficient result was found when the ambient temperature was 20℃, the stripping temperature was 130℃ and the cyclic capacity was 1.5 mol CO_2/kg TEPA. This yielded an energy demand of 533 kJ/mol CO_2. In this scenario, the separation of CO_2 and H_2O was also satisfactory to provide pure product streams for the next process steps. It should be noted that a stripping temperature over 120℃ is usually not recommended, due to thermal degradation of the amine.

The conditions presented here are by no means the global optimum. This would involve a more thorough parametric study. However, it does indicate that a dry and hot location, such as a desert, would not be the most ideal location for this process.

TEPA has a much higher energy demand than the benchmark solvent MEA

The regeneration energy of an absorption stripping process using 30 wt% MEA is on average 3.9 GJ/tonne CO_2 [77]. Converted to the units used in this chapter, this amounts to approximately 172 kJ/mol CO_2. This comparison is slightly unfair, as the MEA based process is highly optimised and takes advantage of a rich-lean heat exchanger to minimise sensible heat demand. Additionally the MEA system captures CO_2 from much more concentrated gas streams than ambient air, which makes it easier to obtain a high rich loading. As shown in this chapter, a high rich loading is beneficial because it reduces the required water vaporisation and increases the cyclic capacity. In turn, this means that less amine is needed to absorb CO_2, which then decreases the sensible heat demand.

The comparison shows that the energy demand of the TEPA sorbent is high and should be optimised to reduce costs. This can be done in multiple ways. First and foremost, implementation of a rich-lean heat exchanger will reduce the sensible heat demand (see Section 6.4). Additionally, the process should be

designed to ensure that no reflux stream is necessary, to minimise the vaporisation energy demand.

Limitations of the analysis presented in this chapter

The analysis presented in this chapter only serves as a first indication of the process design. However, it is important to highlight the limitations of the method applied in these calculations. As explained in Section 6.2.1, many assumptions were made. As demonstrated during the experiments carried out in this work, TEPA becomes viscous at high concentrations in water, low temperatures and high CO_2 loadings. Therefore, mass transfer will be slow, especially if the liquid is not stirred. It is likely that equilibrium will not be reached. The equilibrium models to predict partial pressure of CO_2 and H_2O are assumed to be accurate even when extrapolated, which has not yet been validated by more experimental data. Additionally, it was assumed that the hot TEPA solution and the hot vapor exiting the stripping column can be cooled passively to the temperature of the surroundings, which is very optimistic. Cooling of the lean stream could be achieved partially by a heat exchanger, but probably the temperature inside the flash tank and the top of the absorption column will be higher than those of the surroundings.

6.4 Recommendations for ZEF

Based on the findings in this chapter, a few recommendations can be formulated with regards to the design of the DAC unit of ZEF.

Use a heat exchanger to reduce sensible heat demand

Firstly, it is recommended to implement a heat exchanger between the lean and rich amine streams in the process, to decrease the sensible heat demand. The modified process is shown in Figure 6.8. To provide a simple estimate of the energy saved, the scenario with the lowest energy demand is used. Assuming an approach temperature of 10 °C on the cold side, the temperature of the lean stream exiting the heat exchanger would be 30 °C. The amount of energy transferred from the lean stream is:

$$Q_{transferred} = (C_{p,TEPA}\dot{n}_{TEPA,lean} + C_{p,H_2O}\dot{n}_{H_2O,lean})(130 - 30) = 454 \text{ kJ/h} \tag{6.3}$$

Assuming, the rich stream is heated up using this amount of energy, the temperature of the rich stream exiting the heat exchanger is:

$$T_{hotrich} = T_{coldrich}\frac{454 \cdot 10^3}{(C_{p,TEPA}\dot{n}_{TEPA,rich} + C_{p,H_2O}\dot{n}_{H_2O,rich})} = 111\,°C \tag{6.4}$$

If it were possible to achieve this, the sensible heat demand in this scenario would decrease by 83%, the difference between the case with and without a heat exchanger is shown in Figure 6.9. Note that this calculation does not take into account the vaporisation of water in the rich stream or any heat losses, which makes it an optimistic estimation.

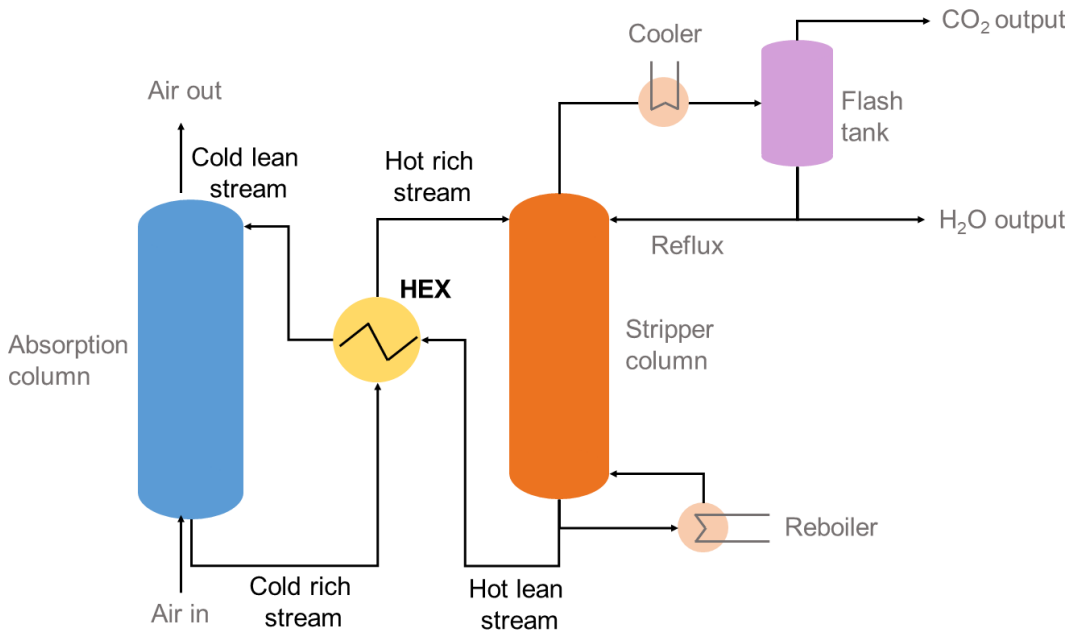

Figure 6.8: Modified overview of the ZEF absorption and stripping process, using a heat exchanger (HEX) to decrease the sensible heat demand.

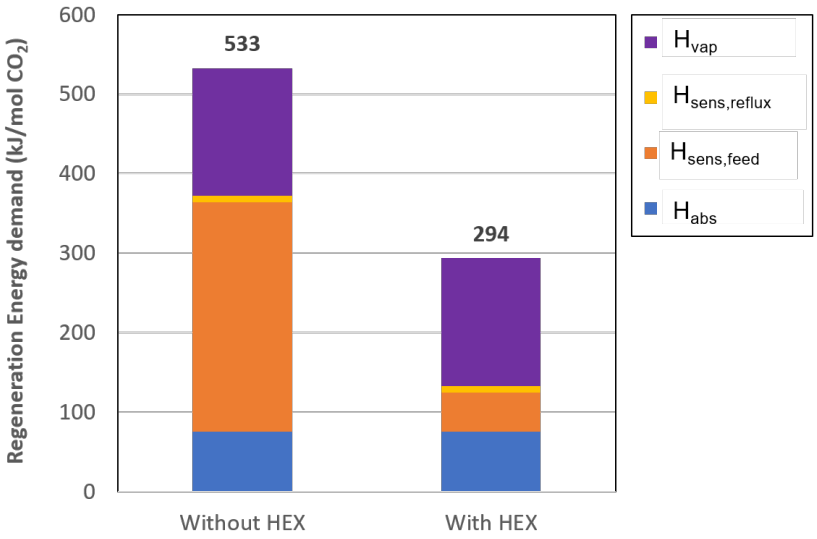

Figure 6.9: Effect of using a heat exchanger (HEX) on the total energy demand of the process.

Take the effects of weather conditions on the process into account when selecting a location for direct air capture.

It was found that absorption should ideally take place at cool temperatures, to ensure a high rich loading and a minimal reflux. Additionally, the relative humidity of the ambient air should not be too low, which results in insufficient production of H_2O which is needed for methanol synthesis, nor too

high, which would result in a higher vaporisation energy demand. Next to temperature and humidity, an important site-specific condition is the solar irradiation, which will power the process. Furthermore, humidity and temperature are properties of air that fluctuate daily as well as seasonally. Therefore the process should be responsive to these fluctuations.

Chapter 7
Conclusions

The aim of this research was to investigate the vapor liquid equilibrium of TEPA, H_2O and CO_2, through experiments and the development of a thermodynamic model. This investigation has provided insight into the specific behavior, as well as the potential of TEPA as a liquid sorbent for direct air capture of CO_2. To conlcude this thesis, the research question are answered.

1. How does the VLE of TEPA-H_2O-CO_2 depend on the composition, temperature and pressure?

The VLE measurements performed in this work provide new information on TEPA, a polyamine that has not yet been extensively studied. The binary VLE of aqueous solutions of 30, 70 and 80 wt% TEPA was measured from 313.15 to 393.15 K. Additionally, the CO_2 absorption of aqueous solutions of 30 and 70 wt% TEPA was measured at 313.15, 353.15 and 393.15 K. The data at low temperature and high TEPA concentration showed poor accuracy and reproducibility in the low loading range. In the higher loading range, the data were validated by the plausible heat of absorption prediction, through the use of the Clausius-Clapeyron equation.

At low temperatures, high TEPA concentrations and high CO_2 loadings, it proved to be a challenging material to work with due it its high viscosity. An interesting phenomenon that was found in the TEPA-H_2O-CO_2 system was that the vapor pressure of H_2O was decreased by the absorption of CO_2, which was attributed to the changing ionic interactions in the liquid phase upon CO_2 absorption.

2. Which thermodynamic model is the most suitable to simulate the phase behaviour of the TEPA-H_2O-CO_2 system?

Firstly, the binary TEPA-H_2O VLE data were correlated using a simple, yet effective activity coefficient model based on Wilson's equations. Secondly, the specific ionic interaction model was selected as the most accurate, yet simple option for modelling the CO_2 absorption in TEPA, inspired by the 2013 paper by Puxty and Maeder [7]. Both thermodynamic models show excellent agreement with the data presented in this work.

Furthermore, a new modelling strategy was developed, based on the assumption that polyamine molecules could be modelled as multiple smaller amine molecules. This approach could be categorised as a quantitative structure activity relationship. It has the advantage that less researched amine solvents can be modelled using the availble information of more well known solvents. It was shown that the CO_2 absorption behavior TEPA could be modelled as that of a diamine (piperazine), by correcting the TEPA concentration by a scaling factor based on the ratio of amino groups.

3. What are the implications of the experimental and modelling results for the design of the direct air capture unit of ZEF?

The two models were applied to a simple process simulation of the direct air capture unit of Zero Emission Fuels. This analysis gave a first approximation of the energy demand of such as process

involving TEPA as a direct air capture liquid sorbent. Compared to monoethanolamine, MEA, the benchmark solvent for post combustion CO_2 capture, TEPA has a energy demand that is 3 times as high. This is largely due to the difficulty in obtaining a high rich loading at the low concentration of CO_2 in air.

Implementation of a rich-lean heat exchanger, as well as optimisation of the process parameters to minimise the reflux stream of H_2O could lead to the decrease of this energy demand. However, it is likely that the high viscosity of TEPA at the optimal conditions for CO_2 absorption will be a bottleneck for its use in a continuous absorption and stripping process.

For ZEF, the models developed in this study have paved the way for the evolution of more complex simulations of the direct air capture unit involving TEPA. In addition, the procedure developed for the measuring and modelling of relatively unknown solvents could be applied to a large range of solvents. As such, it could be developed into a useful screening tool for other amine solvents for direct air capture.

Chapter 8
Recommendations for further research

At the end of this master thesis, different topics for further research are distinguished.

- **Improve the experimental set-up to allow analysis of the vapor phase composition.**
  With respect to the experimental measurement of the VLE of TEPA, H_2O and CO_2, it was found that the assumption of constant water pressure was not valid. However, the composition of the vapor and liquid phase were calculated based on this assumption. Therefore, to facilitate the measurement of these compositions, a different experimental set-up could be used that allows for the sampling of the vapor phase and the determination of its water content.
- **Integrate the two separate VLE models into one.**
  Two separate models were developed in this work, one to predict the partial pressure of H_2O and one to predict the partial pressure of CO_2 as a function of composition and temperature. These were used side by side to predict the total pressure of the ternary H_2O-CO_2 system. However, these models could be integrated together. For example by extending the Debye-Hückel activity model to the specific ionic interaction theory. This would allow to calculate the activity coefficients of all charged and uncharged species using the same model. Additionally, this would enable the consideration of the effect of CO_2 absorption on the phase behavior of H_2O, making it a more complete ternary VLE model.
- **Investigate the possibilities of the amine model further.**
  In this work, a theory was proposed that the CO_2 absorption by polyamines can be modelled as that of a larger concentration of smaller amines. This way, the VLE of less studied amines could be approximated by the VLE of more well-known amines. This theory could be tested and developed further by applying it to other amines.
- **Measure the liquid phase speciation of the TEPA-H_2O-CO_2 system.**
  To date, no speciation data of the TEPA-H_2O-CO_2 system is available. Using H- and C-NMR analysis, it is possible to measure the concentrations of different species in the solution as a function of loading and temperature. This would provide insight into the most important ionic species and chemical equilibria occurring in the liquid phase. This knowledge would enable the development of a more rigorous chemical model, taking into account the real situation in the liquid phase. In turn, this would enable the development of rate-based models for the CO_2 capture by TEPA.
- **Reduce the viscosity of TEPA.**
  The high viscosity of TEPA causes very slow CO_2 capture kinetics. For TEPA to approach equilibrium and to improve the flow in a continuous absorption and stripping process, this problem must be addressed. The investigation of alternative solvents or additives is recommended.

Bibliography

[1] D. Lüthi, M. Le Floch, B. Bereiter, T. Blunier, J.-M. Barnola, U. Siegenthaler, D. Raynaud, J. Jouzel, H. Fischer, K. Kawamura *et al.*, "High-resolution carbon dioxide concentration record 650,000–800,000 years before present," *Nature*, vol. 453, no. 7193, pp. 379–382, 2008.

[2] P. Tans and R. Keeling. Trends in atmospheric carbon dioxide: Mauna loa co2 anual mean data. https://www.esrl.noaa.gov/gmd/ccgg/trends/data.html. Accessed on 03-05-2020.

[3] B. Dutcher, M. Fan, and A. G. Russell, "Amine-based co2 capture technology development from the beginning of 2013 a review," *ACS applied materials & interfaces*, vol. 7, no. 4, pp. 2137–2148, 2015.

[4] D. W. Keith, G. Holmes, D. S. Angelo, and K. Heidel, "A process for capturing co2 from the atmosphere," *Joule*, vol. 2, no. 8, pp. 1573–1594, 2018.

[5] S. A. Didas, "Structural properties of aminosilica materials for co2 capture," Ph.D. dissertation, Georgia Institute of Technology, 2014.

[6] U. E. Aronu, S. Gondal, E. T. Hessen, T. Haug-Warberg, A. Hartono, K. A. Hoff, and H. F. Svendsen, "Solubility of co2 in 15, 30, 45 and 60 mass% mea from 40 to 120 c and model representation using the extended uniquac framework," *Chemical Engineering Science*, vol. 66, no. 24, pp. 6393–6406, 2011.

[7] G. Puxty and M. Maeder, "A simple chemical model to represent co2–amine–h2o vapour–liquid-equilibria," *International Journal of Greenhouse Gas Control*, vol. 17, pp. 215–224, 2013.

[8] D. R. Lide, *CRC Handbook of Chemistry and Physics*. CRC press, 2004, vol. 85.

[9] B. Ovaa, "Direct air capture: An experimental approach on the desorption of co2 and h2o from pei and tepa," Zero Emission Fuels, Delft University of Technology, 2019.

[10] NASA, "Global climate change: Vital signs of the planet," https://climate.nasa.gov/evidence/. Accessed on 7-10-2019.

[11] R. K. Pachauri and L. Meyer, "Climate change 2014 synthesis report-summary for policymakers," 2014.

[12] T. Masson-Delmotte, P. Zhai, H. Pörtner, D. Roberts, J. Skea, P. Shukla, A. Pirani, W. Moufouma-Okia, C. Péan, R. Pidcock *et al.*, "Global warming of 1.5 c: Special report on the impacts of global warming of 1.5 c above pre-industrial levels and related global greenhouse gas emission pathways, in the context of strengthening the global," *Geneva, Switzerland*, 2018.

[13] International Renewable Energy Agency, "Global energy transformation: A roadmap to 2050 (2019 edition)," April 2019.

[14] S. A. Rackley, *Carbon capture and storage*. Butterworth-Heinemann, 2017.

[15] W.-H. Wang, X. Feng, and M. Bao, *Transformation of carbon dioxide to formic acid and methanol*. Springer, 2018.

[16] F. Dalena, A. Senatore, A. Marino, A. Gordano, M. Basile, and A. Basile, "Methanol production and applications: An overview," in *Methanol*. Elsevier, 2018, pp. 3–28.

[17] A. Irabien, M. Alvarez-Guerra, J. Albo, and A. Dominguez-Ramos, "Electrochemical conversion of co2 to value-added products," in *Electrochemical Water and Wastewater Treatment*. Elsevier, 2018, pp. 29–59.

[18] K. Shah, A. Pan, V. Gandhi, and P. Chiang, "Photo-electrochemical reduction of co2 to solar fuel: A review," in *Photocatalytic Nanomaterials for Environmental Applications*. Materials Research Foundations. Materials Research Forum LLC, 2018, vol. 27, pp. 211–235.

[19] G. A. Olah, "After oil and gas: methanol economy," *Catalysis Letters*, vol. 93, no. 1-2, pp. 1–2, 2004.

[20] G. Olah, "Towards oil independence through renewable methanol chemistry," *Angewandte Chemie International Edition*, vol. 52, no. 1, pp. 104–107, 2013.

[21] S. S. Araya, V. Liso, X. Cui, N. Li, J. Zhu, S. L. Sahlin, S. H. Jensen, M. P. Nielsen, and S. K. Kær, "A review of the methanol economy: the fuel cell route," *Energies*, vol. 13, no. 3, p. 596, 2020.

[22] M. Sinha, "Direct air capture: Characterization and design of a novel absorption process," Zero Emission Fuels, Delft University of Technology, 2019.

[23] P. Muchan, J. Narku-Tetteh, C. Saiwan, R. Idem, and T. Supap, "Effect of number of amine groups in aqueous polyamine solution on carbon dioxide (co2) capture activities," *Separation and Purification Technology*, vol. 184, pp. 128–134, 2017.

[24] E. I. Koytsoumpa, C. Bergins, and E. Kakaras, "The co2 economy: Review of co2 capture and reuse technologies," *The Journal of Supercritical Fluids*, vol. 132, pp. 3–16, 2018.

[25] C. Madeddu, M. Errico, and R. Baratti, *CO2 Capture by Reactive Absorption-Stripping: Modeling, Analysis and Design*. Springer, 2019.

[26] S.-i. Nakao, K. Yogo, K. Goto, T. Kai, and H. Yamada, *Advanced CO2 Capture Technologies: Absorption, Adsorption, and Membrane Separation Methods*. Springer, 2019.

[27] M. Broehm, J. Strefler, and N. Bauer, "Techno-economic review of direct air capture systems for large scale mitigation of atmospheric co2," *Available at SSRN 2665702*, 2015.

[28] A. Kumar, D. G. Madden, M. Lusi, K.-J. Chen, E. A. Daniels, T. Curtin, J. J. Perry IV, and M. J. Zaworotko, "Direct air capture of co2 by physisorbent materials," *Angewandte Chemie International Edition*, vol. 54, no. 48, pp. 14 372–14 377, 2015.

[29] E. S. Sanz-Perez, C. R. Murdock, S. A. Didas, and C. W. Jones, "Direct capture of co2 from ambient air," *Chemical reviews*, vol. 116, no. 19, pp. 11 840–11 876, 2016.

[30] M. Fasihi, O. Efimova, and C. Breyer, "Techno-economic assessment of co2 direct air capture plants," *Journal of cleaner production*, vol. 224, pp. 957–980, 2019.

[31] Climeworks, "Press release: Climeworks ag and antecy b.v. are joining forces," 2019, https://www.climeworks.com/wp-content/uploads/2019/09/Press-release_Climeworks-Antecy-join-forces.pdf Accessed on 14-05-2020.

[32] P. D. Vaidya and E. Y. Kenig, "Co2-alkanolamine reaction kinetics: a review of recent studies," *Chemical Engineering & Technology: Industrial Chemistry-Plant Equipment-Process Engineering-Biotechnology*, vol. 30, no. 11, pp. 1467–1474, 2007.

[33] N. El Hadri, D. V. Quang, E. L. Goetheer, and M. R. A. Zahra, "Aqueous amine solution characterization for post-combustion co2 capture process," *Applied Energy*, vol. 185, pp. 1433–1449, 2017.

[34] F. A. Chowdhury, H. Yamada, T. Higashii, K. Goto, and M. Onoda, "Co2 capture by tertiary amine absorbents: a performance comparison study," *Industrial & engineering chemistry research*, vol. 52, no. 24, pp. 8323–8331, 2013.

[35] I. Kim0F, K. A. Hoff, and T. Mejdell, "Heat of absorption of co2 with aqueous solutions of mea: new experimental data," *Energy Procedia*, vol. 63, pp. 1446–1455, 2014.

[36] J. Oexmann and A. Kather, "Minimising the regeneration heat duty of post-combustion co2 capture by wet chemical absorption: The misguided focus on low heat of absorption solvents," *International Journal of Greenhouse Gas Control*, vol. 4, no. 1, pp. 36–43, 2010.

[37] S. Kim, H. Shi, and J. Y. Lee, "Co2 absorption mechanism in amine solvents and enhancement of co2 capture capability in blended amine solvent," *International Journal of Greenhouse Gas Control*, vol. 45, pp. 181–188, 2016.

[38] B. Zhu, Q. Liu, Q. Zhou, J. Yang, J. Ding, and J. Wen, "Absorption of carbon dioxide from flue gas using blended amine solutions," *Chemical Engineering & Technology*, vol. 37, no. 4, pp. 635–642, 2014.

[39] F. Bougie and M. C. Iliuta, "Sterically hindered amine-based absorbents for the removal of co2 from gas streams," *Journal of Chemical & Engineering Data*, vol. 57, no. 3, pp. 635–669, 2012.

[40] G. Fytianos, A. M. Grimstvedt, H. Knuutila, and H. F. Svendsen, "Effect of mea's degradation products on corrosion at co_2 capture plants," 2014.

[41] J. Kim, J. Lee, Y. Lee, H. Kim, E. Kim, and K. S. Lee, "Evaluation of aqueous polyamines as co2 capture solvents," *Energy*, vol. 187, p. 115908, 2019.

[42] A. Hartono, E. F. da Silva, H. Grasdalen, and H. F. Svendsen, "Qualitative determination of species in deta- h2o- co2 system using 13c nmr spectra," *Industrial & engineering chemistry research*, vol. 46, no. 1, pp. 249–254, 2007.

[43] A. Hartono, K. A. Hoff, T. Mejdell, and H. F. Svendsen, "Solubility of carbon dioxide in aqueous 2.5 m of diethylenetriamine (deta) solution," *Energy Procedia*, vol. 4, pp. 179–186, 2011.

[44] R. C. Reid, J. M. Prausnitz, and B. E. Poling, "The properties of gases and liquids," 1988.

[45] J. Gmehling, B. Kolbe, M. Kleiber, and R. J., *Chemical Thermodynamics for Process Simulation*. Wiley-VCH Verlag & Co, 2012.

[46] T. Engel and P. Reid, *Physical Chemistry*, 3rd ed. Pearson Education, Inc., 2013.

[47] G. M. Kontogeorgis, B. Maribo-Mogensen, and K. Thomsen, "The debye-hückel theory and its importance in modeling electrolyte solutions," *Fluid Phase Equilibria*, vol. 462, pp. 130–152, 2018.

[48] G. M. Kontogeorgis and G. K. Folas, *Thermodynamic Models for Industrial Applications: from classical and advanced mixing rules to association theories*. John Wiley & Sons, 2010.

[49] K. Thomsen, “Electrolyte solutions: Thermodynamics, crystallization, separation methods,” 2009.

[50] G. Danckwerts and K. McNeil, “The absorption of carbon dioxide into aqueous amine solutions and the effects of catalysis,” *Transactions of the Institution of Chemical Engineers*, vol. 45, 1967.

[51] R. Kent and B. EIsenberg, “Better data for amine treating,” *Hydrocarbon Processing*, vol. 55, no. 2, pp. 87–90, 1976.

[52] J. Gabrielsen, “Co2 capture from coal fired power plants,” Ph.D. dissertation, 2 2007.

[53] J. Brønsted, “Studies on solubility. iv. the principle of the specific interaction of ions,” *Journal of the American Chemical Society*, vol. 44, no. 5, pp. 877–898, 1922.

[54] E. Guggenheim, “L. the specific thermodynamic properties of aqueous solutions of strong electrolytes,” *The London, Edinburgh, and Dublin Philosophical Magazine and Journal of Science*, vol. 19, no. 127, pp. 588–643, 1935.

[55] G. Scatchard, “Concentrated solutions of strong electrolytes.” *Chemical reviews*, vol. 19, no. 3, pp. 309–327, 1936.

[56] D. M. Austgen, G. T. Rochelle, X. Peng, and C. C. Chen, “Model of vapor-liquid equilibria for aqueous acid gas-alkanolamine systems using the electrolyte-nrtl equation,” *Industrial & engineering chemistry research*, vol. 28, no. 7, pp. 1060–1073, 1989.

[57] C.-C. Chen, H. I. Britt, J. Boston, and L. Evans, “Local composition model for excess gibbs energy of electrolyte systems. part i: Single solvent, single completely dissociated electrolyte systems,” *AIChE Journal*, vol. 28, no. 4, pp. 588–596, 1982.

[58] H. Renon and J. M. Prausnitz, “Local compositions in thermodynamic excess functions for liquid mixtures,” *AIChE journal*, vol. 14, no. 1, pp. 135–144, 1968.

[59] G. M. Wilson, “Vapor-liquid equilibrium. xi. a new expression for the excess free energy of mixing,” *Journal of the American Chemical Society*, vol. 86, no. 2, pp. 127–130, 1964.

[60] A. P. Manual, “Physical property systems, physical property methods and models 11.1,” *Aspen Technology Inc*, 2001.

[61] M. C. Iliuta, K. Thomsen, and P. Rasmussen, “Extended uniquac model for correlation and prediction of vapour–liquid–solid equilibria in aqueous salt systems containing non-electrolytes. part a. methanol–water–salt systems,” *Chemical Engineering Science*, vol. 55, no. 14, pp. 2673–2686, 2000.

[62] L. Faramarzi, G. M. Kontogeorgis, K. Thomsen, and E. H. Stenby, “Extended uniquac model for thermodynamic modeling of co2 absorption in aqueous alkanolamine solutions,” *Fluid phase equilibria*, vol. 282, no. 2, pp. 121–132, 2009.

[63] W. Fürst and H. Renon, “Representation of excess properties of electrolyte solutions using a new equation of state,” *AIChE Journal*, vol. 39, no. 2, pp. 335–343, 1993.

[64] G. Vallée, P. Mougin, S. Jullian, and W. Fürst, “Representation of co2 and h2s absorption by aqueous solutions of diethanolamine using an electrolyte equation of state,” *Industrial & engineering chemistry research*, vol. 38, no. 9, pp. 3473–3480, 1999.

[65] N. Mac Dowell, F. Llovell, C. Adjiman, G. Jackson, and A. Galindo, "Modeling the fluid phase behavior of carbon dioxide in aqueous solutions of monoethanolamine using transferable parameters with the saft-vr approach," *Industrial & engineering chemistry research*, vol. 49, no. 4, pp. 1883–1899, 2010.

[66] Dortmund Data Bank, "Saturated vapor pressure of water," http://ddbonline.ddbst.de/AntoineCalculation/AntoineCalculationCGI.exe?component=Water&tunit=\%C2\%B0C&punit=bar&TemperaturesEdit=&calculate=Calculate Accessed on 04-05-2020.

[67] National Institue of Standards and Technology, "Tetraethylenepentamine," https://webbook.nist.gov/cgi/cbook.cgi?ID=C112572&Mask=7FF. Accessed on 04-05-2020.

[68] R. Orye and J. Prausnitz, "Multicomponent equilibria—the wilson equation," *Industrial & Engineering Chemistry*, vol. 57, no. 5, pp. 18–26, 1965.

[69] T. J. Edwards, J. Newman, and J. M. Prausnitz, "Thermodynamics of aqueous solutions containing volatile weak electrolytes," *AIChE Journal*, vol. 21, no. 2, pp. 248–259, 1975.

[70] S. Ma'mun, R. Nilsen, H. F. Svendsen, and O. Juliussen, "Solubility of carbon dioxide in 30 mass% monoethanolamine and 50 mass% methyldiethanolamine solutions," *Journal of Chemical & Engineering Data*, vol. 50, no. 2, pp. 630–634, 2005.

[71] Y. E. Kim, S. J. Moon, Y. I. Yoon, S. K. Jeong, K. T. Park, S. T. Bae, and S. C. Nam, "Heat of absorption and absorption capacity of co2 in aqueous solutions of amine containing multiple amino groups," *Separation and Purification Technology*, vol. 122, pp. 112–118, 2014.

[72] N. McCann, M. Maeder, and H. Hasse, "Prediction of the overall enthalpy of co2 absorption in aqueous amine systems from experimentally determined reaction enthalpies," *Energy Procedia*, vol. 4, pp. 1542–1549, 2011.

[73] I. Kim and H. F. Svendsen, "Heat of absorption of carbon dioxide (co2) in monoethanolamine (mea) and 2-(aminoethyl) ethanolamine (aeea) solutions," *Industrial & engineering chemistry research*, vol. 46, no. 17, pp. 5803–5809, 2007.

[74] Engineering Toolbox, "Water - specific heat," 2004, https://www.engineeringtoolbox.com/specific-heat-capacity-water-d_660.html. Accessed on 10-06-2020.

[75] National Institute of Standards and Technology, "Tetraethylenepentamine," 2018, https://webbook.nist.gov/cgi/cbook.cgi?ID=C112572&Mask=200/. Accessed on 10-06-2020.

[76] Engineering Toolbox, "Water - heat of vaporization," 2010, https://www.engineeringtoolbox.com/water-properties-d_1573.html. Accessed on 10-06-2020.

[77] W. Zhang, H. Liu, Y. Sun, J. Cakstins, C. Sun, and C. E. Snape, "Parametric study on the regeneration heat requirement of an amine-based solid adsorbent process for post-combustion carbon capture," *Applied energy*, vol. 168, pp. 394–405, 2016.

Appendix A

Matlab code for Vapor curve experiment

Code structure and description:

1. Raw data from the experiment is imported. Specifically the pressure (P), temperature (T) and time data are required.
2. The T and P data is averaged from per second to per minute data.
3. The derivative of the averaged T and P data is calculated.
4. The points where the T was manually increased are located using the 'findpeaks' function on the derivative of the T. The average of T and P over 3 minutes before these points are calculated. These are the equilibrium T and P.
5. (Optional: If the 'findpeaks' function finds points that are not correct, these points are removed from the equilibrium T and P vectors.)
6. Two plots are created. The first plot shows the averaged T and P as a function of time. The second plot shows the equilibrium P versus the equilibrium T.

```
%% Vapor Curve code template
clc;clear all;close all

%% Import the data
% Sample information (manually)
conc=70; % wt% TEPA
% Load raw data
Raw=importdata('rawdata.txt');
P=Raw(:,12);          % pressure inside vessel, accurate sensor [mbar]
T=Raw(:,3);           % temperature inside the liquid [K]
time = Raw(:,1);      % time vector, skips some seconds..

%% Manipulate the data
% Smooth out the temperature data to find the equilibrium points
% take an average over
t_avg=60; %s
max=(int32(length(T))/t_avg)-1; %length of the T_avg vector
% select the first 180 data points of the temperature
for i=1:max
   T_selection=T(((i-1)*t_avg)+1:(i*t_avg));% Temperature selection
   T_avg(i)=mean(T_selection); %calculate the mean of the selection and store
   P_selection=P(((i-1)*t_avg)+1:(i*t_avg));
   P_avg(i)=mean(P_selection);
end

% Calculate the 1st derivative of the average T
dT_avg=zeros(1,length(T_avg)); ddT_avg=zeros(1,length(T_avg));
j=0;
for i=2:length(T_avg)
```

```
    dT_avg(i)=T_avg(i)-T_avg(i-1);
    %ddT_avg(i)=dT_avg(i)-dT_avg(i-1);
    dP_avg(i)=P_avg(i)-P_avg(i-1);
    %ddP_avg(i)=dP_avg(i)-dP_avg(i-1);
end

%% Find the equilibrium points
% Find peaks in the 1st derivative -> where T is increased sharply
minpeakheight=1; % set this by looking at the dT_avg data
minpeakdistance=60; % at least an hour between two steps
[pks, loc,width] = findpeaks(dT_avg,'MinPeakHeight', minpeakheight, ...
    'MinPeakDistance',minpeakdistance);

% Correct the point where equilibrium occurs by the peakwidth
index=int32(loc-width);
% The last equilibrium point is not found by the findpeaks function
% Add it manually:
last_index=length(P_avg);
index= [index last_index];

% Take the average of the T and P over 3 minutes before the next step
% This is the approximation of the equilibrium point
t_avg2=3; %minutes
for i=1:length(index)
    P_selection2=P_avg(index(i)-(t_avg2-1):index(i));
    T_selection2=T_avg(index(i)-(t_avg2-1):index(i));
    Peq(i)=mean(P_selection2); % mbar
    Teq(i)=mean(T_selection2); % K
end
% Delete points that are wrong, find manually..
wrong=6;
Teq(wrong)=[];
Peq(wrong)=[];
index(wrong)=[];

% Convert Kelvin to Celsius
T_avg_C=T_avg-273.15;
Teq_C=Teq-273.15;

%% Plotting
F1=figure(1);
hold on
yyaxis right
plot(T_avg_C)
scatter(index,T_avg_C(index))
ylabel('Temperature / C')
xlabel('Time / min')
yyaxis left
ylabel('Pressure / mbar')
plot(P_avg)
scatter(index,P_avg(index))
hold off
filename1 = sprintf('%d wt%% TEPA Vapor Curve Equilibrium Points.jpg',conc);
saveas(F1,filename1)

F2=figure(2);
scatter(Teq_C,Peq)
```

```
ylabel('Vapor pressure / mbar')
xlabel('Temperature / C')
xlim([0 125])
% title2=sprintf('Vapor curve %d wt%% TEPA', conc);
% title(title2)
filename2 = sprintf('%d wt%% TEPA Vapor Curve.jpg',conc);
saveas(F2,filename2)
```

Appendix B

Matlab code for CO_2 loading experiment

Code structure and description:

1. The raw data from the CO_2 loading experiment is imported, as well as the VLE data file that is generated by the software.
2. The sample information spreadsheet for the experiment is read and makes an array out of the information.
3. The timestamps of the CO_2 pulse are taken from the VLE file. An average of the temperature (T) and pressure (P) inside the vessel is calculated over a timescale of 500 seconds. These points are the equilibrium T and P.
4. The equilibrium P and T and the CO_2 volume of each pulse are concatenated horizontally and are pasted into the Excel spreadsheet template, see Appendix C. Additionally, the specific sample information is pasted into the same Excel sheet. Using this information, the absorption isotherm can be calculated for the experiment.
5. The calculated loading and partial pressure of CO_2 are taken from the spreadsheet and imported back into Matlab, to create plots.
6. Plots are made of the raw data and of the VLE curve.

```
clc;clear all;close all
tic
%% Script to convert experimental data to VLE curve plots and Excel spreadsheet

%% Load data

% import the raw datafile
Raw = importdata('rawdata.txt');
% import the VLE file
Vle = importdata('vledata.txt');
% import the sample information
Sample_info=readtable('Sample information.xlsx','Range','K1:K18');
Sample_info_array=table2array(Sample_info); % make an array for easy indexing

% Raw data
P=Raw(:,12);          % pressure inside vessel [mbar]
M=Raw(:,7);           % volume through massflow controller [nL/min]
Temp=Raw(:,3);        % temperature inside the liquid [K]
time = Raw(:,1);      % time vector, skips some seconds.. so not the same as linspace

% VLE data
Peq_sw=Vle(:,12);     % equilibrium pressure according to VLE software [mbar]
T=Vle(:,2);           % time at which the software takes VLE points [s]
T=int32(T);           % make sure it reads it as integers
stepvolume=Vle(:,8);  % Volume CO2 out of MFC for each step [nL]
timescale = 500;      % timescale of which to take the average [s]
```

```
for i=1:length(T)
    % find the index of the point in the array corresponding to the time reported in VLE file
    index(i)=find(time==T(i));
    % select al the P's of the period before the next step
    pressures=P(index(i)-(timescale-1):index(i));
    % select all the T's of the period before the next step
    temperatures=Temp(index(i)-(timescale-1):index(i));
    %calculate the mean of these pressures
    Peq(i)=mean(pressures);
    % calculate mean of temperatures
    Teq(i)=mean(temperatures);
end

% Create the [Peq   T   Step volume] matrix to put into spreadsheet
Peq=Peq';
Teq=Teq';
P_T_MFC=table(Peq,Teq,stepvolume);

%% Create the spreadsheet
date=Sample_info_array(1); conc=Sample_info_array(2);temp=Sample_info_array(3);
%title contains date, concentration & temperature
new_file=string(date)+" TEPA "+string(conc)+" wt% "+string(temp)+" C.xlsx";
copyfile('SuperMAC spreadsheet template.xlsx', char(new_file));

%insert the inputs from the Sample information
writetable(Sample_info,new_file,'Sheet',2,'Range','A1:A18');

%inert the inputs from the VLE data
range_end = int16(1 + length(Peq));
range = "A1:C" + range_end;
writetable(P_T_MFC,new_file,'Sheet',3,'Range',range);

% Extract from the spreadsheet the Loading vs pCO2
steps=length(Teq)-1;
PCO2=readtable(new_file,'Range',"F49:F"+(49+steps),'ReadVariableNames',false);
Loading_molmol=readtable(new_file,'Range',"L49:L"+(49+steps),'ReadVariableNames',false);
Loading_molkg=readtable(new_file,'Range',"K49:K"+(49+steps),'ReadVariableNames',false);
PCO2_kPa=PCO2.Var1/10;

%% Plotting
% Plot of raw data
F1=figure(1);
%title('Raw data')
xlabel('Time / s','fontweight','bold')
yyaxis left
plot(time,P)
ylabel('Pressure in the vessel / mbar','fontweight','bold')
yyaxis right
plot(time,M)
ylabel('CO_2 volume flow / nL/min ','fontweight','bold')
filename1 = sprintf('%d Raw data plot.jpg',date);
saveas(F1,filename1)

% Plot of the VLE curve, mol/kg
F2=figure(2);
plot(Loading_molkg.Var1,PCO2.Var1,'-o')
```

```
%title2=sprintf('VLE curve %d wt%% %d C mol/mol', conc, temp);
%title(title2)
xlabel('Loading / mol CO_2/kg TEPA','fontweight','bold')
ylabel('Partial pressure CO_2 / mbar','fontweight','bold')
filename2 = sprintf('%d VLE plot mol per kg.jpg',date);
saveas(F2,filename2)

F3=figure(3);
plot(Loading_molmol.Var1,PCO2.Var1,'-o')
%title3=sprintf('VLE curve %d wt%% %d C mol/mol', conc, temp);
%title(title3)
xlabel('Loading / mol CO_2/mol N','fontweight','bold')
ylabel('Partial pressure CO_2 / mbar','fontweight','bold')
filename3 = sprintf('%d VLE plot mol per mol.jpg',date);
saveas(F3,filename3)

% Logarithmic scale
F4=figure(4);
semilogy(Loading_molmol.Var1,PCO2_kPa,'-o')
grid on
%title4=sprintf('VLE curve %d wt%% %d C mol/mol', conc, temp);
%title(title4)
xlabel('Loading / mol CO_2/mol N','fontweight','bold')
ylabel('Partial pressure CO_2 / kPa','fontweight','bold')
filename4 = sprintf('%d VLE plot mol per mol semilogplot.jpg',date);
saveas(F4,filename4)

%% Data output
% Data file containing the pco2 & loading in mol/mol N and mol/kg
DATA=table(PCO2.Var1,Loading_molmol.Var1,Loading_molkg.Var1);
filename5 = sprintf('%d VLE data.txt',date);
writetable(DATA,filename5,'Delimiter','tab')
toc
```

Appendix C

Excel Spreadsheets for CO_2 loading measurements

The spreadsheet used to calculate the CO_2 absorption isotherms are shown below. As an example, the 30 wt% TEPA 393 K measurement is used. The specific sample information and experimental settings are logged in these sheets.

Table C.1: Example of sample information spreadsheet for 30 wt% TEPA 393 K measurement.

VLE Experiments Spreadsheet

Experiment info

Date	20200217	yyyy-mm-dd
C	30	wt%
T	120	C
Performed by	Wino&Rebecca	
Comments	30 wt% TEPA to compare to Bart's data	

Legend	
	Inputs
	Constants (for every experiment

Sample information

Constants	**Value**	**Unit**
MW TEPA	189.307	g/mol
MW H2O	18.01528	g/mol
rho TEPA	0.998	g/ml
rho H2O	0.997	g/ml
Vessel volume	1.05	L
N/molecule	5	-
van mol naar L	22.40	L/mol
R	8.314	J/molK
T	273	K
P	100000	Pa
100% output of mfc	1.233	L/min

Sample	**Theoretical**	**Actual**	**In vessel**	**Units**
Volume tot	248.590	250.001	248.590243	mL
Mass tot	247.919	249.326	247.919	g
Mass TEPA	74.376	74.801	74.379	g
Mass H2O	173.543	174.525	173.540	g
wt% TEPA	30.00%	30.00%	30.00%	-
wt% H2O	70.00%	70.00%	70.00%	-

Concentrations	**Value**	**Unit**
TEPA concentration	1.581	mol/L
theoretical CO2	2.5	mol/mol TEPA
theoretical CO2	3.951	mol/L

Experimental Settings

Inputs Software	**Value**	**Unit**
Volume of liquid	0.249	L
Theoretical molarity of liquid	3.951	mol CO2/L
Loading for this measurement	100%	-
Amount of CO2 per step	0.067	mol/step
Duration of step	120	s

Calculations	**Value**	**Unit**
Volume during step	0.3350	L/step
Flow during step	0.1675	L/min
Total liters of Co2	4.6900	L
Number of steps	14	steps
Output of the massflow controller	0.00%	-

Equilibrium criteria	**Value**	**Unit**
Stabilize pressure	7	mbar
Stabilize time	90	min

Liquid baths	**Value**	**Unit**
Liquid bath vessel	120.5	C (ext.contr)
Liquid bath lid	138	C (int.contr)

Stirrer	**Value**	**Unit**
Stirring speed	600	rpm

Table C.2: Example of CO_2 absorption isotherm calculation spreadsheet from raw data.

Results

Experimental data				Calculations						
Step	Pressure extra 1 [mBarG]	Temperature [K]	Step Volume [L]	pCO2 mBarA	Total CO2 mol	CO2 gasphase mol	CO2 absorbed mol	Loading mol CO2/mol TEPA	Loading mol/kg	Loading mol/mol N
0	1794.987406	393.005076	0	0	0	0	0	0	0	0
1	1815.376898	393.215534	1.507	20.389492	0.066396	0.000499828	0.065895969	0.167716532	0.88594998	0.03354331
2	1831.055684	393.243612	1.507	36.068278	0.132792	0.000884114	0.131907479	0.335727137	1.77345337	0.06714543
3	1859.95303	393.259224	1.506	64.965624	0.199143	0.001592389	0.197550942	0.502800999	2.65600849	0.1005602
4	1909.154758	393.296934	1.505	114.16735	0.265451	0.002798118	0.262652894	0.668496622	3.53128316	0.13369932
5	1987.328244	393.276024	1.505	192.34084	0.331759	0.004714315	0.327044376	0.832383978	4.39700581	0.1664768
6	2119.05993	393.286562	1.505	324.07252	0.398066	0.007942875	0.390123496	0.992931149	5.24508417	0.19858623
7	2345.522516	393.287914	1.505	550.53511	0.464374	0.013493326	0.450880725	1.147568707	6.06194545	0.22951374
8	2725.585302	393.332182	1.505	930.5979	0.530682	0.022805899	0.507875832	1.292631022	6.82822623	0.2585262
9	3337.280446	393.348598	1.513	1542.293	0.597342	0.037794961	0.559546916	1.424142786	7.52292723	0.28482856

Appendix D

Matlab code for binary TEPA-H_2O model using Wilson's equation.

The purpose of this code is to fit the Wilson activity coefficient model to the experimental binary VLE data presented in this work. The necessary functions are found below the main code. Code structure and description:

1. The experimental equilibrium pressure and temperature data are imported.
2. The required constants are listed together.
3. The mass percentages of TEPA and H_2O are converted to mole fractions.
4. The model is regressed by trying to minimise the objective function (ObjFun), which is the difference between the model predictions of the equilibrium pressure and the experimental data. The minimum is found by using the 'fminunc' function, combined with 'Multistart' with 1000 starting points to find the global minimum of the objective function. The computation speed is increased by using parallel computing.
5. The solution to the optimization are the two parameters of the Wilson model. Using this solution, the model is used to calculate the equilibrium pressure at the same conditions as the measured data. This way, the agreement between the model and the data can be quantified, in terms of AARD or SSQRE.
6. Two plots are constructed. The first graph contains the model P-T curves of the different TEPA concentrations combined with the experimental data points. The second graph shows the parity plot of the calculated and measured equilibrium pressure.

```
%% TEPA-H2O binary model: Wilson's activity model + modified Raoult's law
clc;clear all;close all

%% Inputs
% Import the P-T data
VC0 = importdata('VC0.txt');
VC30 = importdata('VC30_2.txt');
VC70 = importdata('VC70.txt');
VC80 = importdata('VC80.txt');
VC100 = importdata('VC100.txt');
% Allocate columns
wt_TEPA = [VC0(:,1);VC30(:,1);VC70(:,1);VC80(:,1);VC100(:,1)]/100;
T_exp = [VC0(:,2);VC30(:,2);VC70(:,2);VC80(:,2);VC100(:,2)];
P_exp = [VC0(:,3)*10;VC30(:,3);VC70(:,3);VC80(:,3);VC100(:,3)]/10; %kPa

%% Constants
DENSITY_H2O=0.997;                  % density water, [g/mL]
MW_H2O=18.015;                      % molar mass water [g/mol]
DENSITY_TEPA=0.998;                 % density TEPA, [g/mL]
MW_TEPA=189.314;                    % molar mass TEPA, [g/mol]
```

```
R = 8.3145;                          % Gasconstant, [J/molK]
T_boil = 613.5;                      % Boiling point of TEPA, [K]
Hvap = -71.3;                        % Heat of vaporisation of TEPA , [kJ/mol]
P_atm = 100;                         % Atmospheric pressure, [kPa]

% Antoine coefficients for pure water
% If T < 100 C
A.A1 = 8.196213;          % mbar, C
A.B1 = 1730.755;          % mbar, C
A.C1 = 233.5509;          % mbar, C
% If T > 100 C
A.A2 = 8.265093;          % mbar, C
A.B2 = 1811.065;          % mbar, C
A.C2 = 244.6099;          % mbar, C

%% Calculations
% mole fraction TEPA (2)
x2 = (wt_TEPA./MW_TEPA)./((wt_TEPA./MW_TEPA) + ((1-wt_TEPA)./MW_H2O));
% mole fraction H2O (1)
x1 = 1-x2;                           % mole fraction water

%% Regression of the Wilson model parameters
% Initial guess parameters
C0 = [100 -100];
% Objective function: difference between model and data must be minimised
fun=@(C)ObjFun(C,x1,x2,T_exp,P_exp,A,R,T_boil,P_atm,Hvap,MW_H2O,...
    DENSITY_H2O,MW_TEPA,DENSITY_TEPA);

% Set up the problem
problem = createOptimProblem('fminunc',...
    'objective',fun,...
    'x0',C0,'options',...
    optimoptions(@fminunc,'Algorithm','quasi-newton'));
% Set the Multistart options
ms = MultiStart('UseParallel',true,'Display','iter');
% Use parallel computing to speed up the process
parpool
% Use Multistart with 1000 startpoints, to find the global minimum of the
% problem
[sol,fval,eflag,output,manymins] = run(ms,problem,10000);
% Stop parallel computing
delete(gcp)

% Fitted parameters
%sol =[-156.028134964897 220.939936337709];

%% Recalculate the model using the fitted parameters
% For all datapoints, include all the 30 wt% data
VC30 = importdata('VC30.txt');
% Redefine the model inputs
wt_TEPA_exp = [VC0(:,1);VC30(:,1);VC70(:,1);VC80(:,1)]/100;
T_exp = [VC0(:,2);VC30(:,2);VC70(:,2);VC80(:,2)];
P_exp = [VC0(:,3).*10;VC30(:,3);VC70(:,3);VC80(:,3)]/10; % kPa

% mole fraction TEPA (2)
x2 = (wt_TEPA_exp./MW_TEPA)./((wt_TEPA_exp./MW_TEPA) + ...
    ((1-wt_TEPA_exp)./MW_H2O));
```

```
% mole fraction H2O (1)
x1 = 1-x2;                          % mole fraction water

% Total pressure predicted by the model
P_mod = wilson(sol,x1,x2,T_exp,A,R,T_boil,P_atm,...
    Hvap,MW_H2O,DENSITY_H2O,MW_TEPA,DENSITY_TEPA);

% Sum of squared relative error
SSQRE = sum(((P_mod - P_exp)./P_exp).^2);

% Absolute average relative deviation (%)
AARD = (1/length(T_exp))*(sum(abs(P_mod - P_exp)./P_exp))*100;

%% Plots
% Formatting the plots using the same markers and colors
marker = {'s','d','^','o','x'};
color = {[0 0.4470 0.7410],[0.8500 0.3250 0.0980],[0.9290 0.6940 0.1250]...
        ,[0.4940 0.1840 0.5560],[0.4660 0.6740 0.1880],...
        [0.6350 0.0780 0.1840],[0.3010 0.7450 0.9330],'b','g','c',''};
c = [wt_TEPA(1) .30 .70 .80];

% Figure 1: Plot of datapoints and the model prediction
hold on
fig=figure(1);
grid on
for i=1:length(c)
        % find the index of the datapoints corresponding to 1 isotherm
        index=(wt_TEPA_exp==c(i));
        plot(T_exp(index),P_mod(index),'Color',color{i})
        scatter(T_exp(index),P_exp(index),marker{i},...
            'MarkerFaceColor',color{i},'MarkerEdgeColor',color{i})
end
box on
xlabel('Temperature (K)','fontweight','bold')
ylabel('Pressure (kPa)','fontweight','bold')
title=sprintf('Vaporcurves.jpg');
legend('0wt% calculated','Pure water data (Lide, 2004)',...
    '30wt% calculated','30wt% measured','70 wt% calculated',...
    '70 wt% measured','80 wt% calculated','80 wt% measured',...
    'Location','northwest')
saveas(fig,title)
hold off

% Figure 2: Parity plot of the model vs data P
x=linspace(0,max(P_exp),100);
y = x;
fig=figure(2);
grid on
hold on
box on
plot(x,y,'-','Color',color{2})
scatter(P_exp,P_mod,'MarkerFaceColor',color{1},'MarkerEdgeColor',color{1})
xlabel('Pressure measured (kPa)','fontweight','bold')
ylabel('Pressure calculated (kPa)','fontweight','bold')
saveas(fig,'Parity plot binary.jpg')
hold off
```

```
function SSQ = ObjFun(C,x1,x2,T_exp,P_exp,A,R,T_boil,P_atm,Hvap,MW_H2O,...
    DENSITY_H2O,MW_TEPA,DENSITY_TEPA)

% Function Description:
% 'ObjFun' calculates the sum of squared relative error between the
% measured and the calculated pressure above the TEPA-H2O solution as a
% function of Wilson parameters (C(1) and C(2), temperature (T) and liquid
% composition (x) using Wilson's activity model and modified Raoult's law.
%
% Water = component 1
% TEPA = component 2
%
% Inputs:
% - C(1) and C(2) are lambda_12-lambda_11 and lambda_12 - lambda_22, which
% determine the value of the Wilson interaction parameters (A12 and A21) as
% a function of T.
% - x1 and x2 are the liquid mole fractions of water and TEPA respectively.
% - T_exp is measured temperature data, given in Kelvins.
% - P_exp is measured pressure data, given in mbars
% - A is a struct, containing two sets of Antoine coefficients. One for T <
% 100 C and one for T > 100 C.
%
% Output:
% - SSQ is the sum of the squared difference between the model and the
% data. It expresses the difference between the model prediction and the
% experimental data.


    % Calculate the Wilson parameters
    A12 = ((MW_TEPA/DENSITY_TEPA)/(MW_H2O/DENSITY_H2O))*exp(-C(1)./(R.*T_exp));
    A21 = ((MW_H2O/DENSITY_H2O)/(MW_TEPA/DENSITY_TEPA))*exp(-C(2)./(R.*T_exp));

    % Calculate the activity coefficients using Wilsons Equation
    lny1= -log(x1+A12.*x2)+x2.*((A12./(x1+(A12.*x2)))-(A21./(x2+(A21.*x1))));
    lny2= -log(x2+A21.*x1)-x1.*((A12./(x1+(A12.*x2)))-(A21./(x2+(A21.*x1))));
    y1 = exp(lny1);
    y2 = exp(lny2);

    % Calculate pure water vapor pressure (mbar) at T_exp using Antoine
    % coefficients
    T_exp_C = T_exp-273.15;
    index=T_exp_C<=100;
    P_H2O(index) = 10.^(A.A1-(A.B1./(A.C1+T_exp_C(index))));
    index=T_exp_C>100;
    P_H2O(index) = 10.^(A.A2-(A.B2./(A.C2+T_exp_C(index))));

    % Convert mbar to kPa
    P_H2O = P_H2O./10;

    % Calculate pure TEPA vapor pressure (kPa) at T_exp using the Clausius
    % Clapeyron Equation
    P_TEPA = P_atm*exp((Hvap*1000/R).*((1./T_exp)-(1/T_boil)));

    % Calculate model pressure (kPa)
    P_mod = y1.*x1.*P_H2O'+y2.*x2.*P_TEPA;

    % Sum of the squares
```

```
    SSQ = sum((P_mod - P_exp).^2);
end


function [P_mod,y1,y2,P_H2O,P_TEPA] = wilson(C,x1,x2,T_exp,A,R,T_boil,...
    P_atm,Hvap,MW_H2O,DENSITY_H2O,MW_TEPA,DENSITY_TEPA)

    % Calculate the Wilson parameters
    A12 = ((MW_TEPA/DENSITY_TEPA)/(MW_H2O/DENSITY_H2O))*exp(-C(1)./(R.*T_exp));
    A21 = ((MW_H2O/DENSITY_H2O)/(MW_TEPA/DENSITY_TEPA))*exp(-C(2)./(R.*T_exp));

    % Calculate the activity coefficients using Wilsons Equation
    lny1= -log(x1+A12.*x2)+x2.*((A12./(x1+(A12.*x2)))-(A21./(x2+(A21.*x1))));
    lny2= -log(x2+A21.*x1)-x1.*((A12./(x1+(A12.*x2)))-(A21./(x2+(A21.*x1))));
    y1 = exp(lny1);
    y2 = exp(lny2);

    % Calculate pure water vapor pressure at T_exp using Antoine
    % coefficients
    T_exp_C = T_exp-273.15;
    index=T_exp_C<=100;
    P_H2O(index) = 10.^(A.A1-(A.B1./(A.C1+T_exp_C(index))));
    index=T_exp_C>100;
    P_H2O(index) = 10.^(A.A2-(A.B2./(A.C2+T_exp_C(index))));

    % Convert mbar to kPa
    P_H2O = P_H2O./10;

    % Calculate pure TEPA vapor pressure at T_exp using Clausius Clapeyron
    P_TEPA = P_atm*exp((Hvap*1000/R).*((1./T_exp)-(1/T_boil)));

    % Calculate model pressure
    P_mod = y1.*x1.*P_H2O'+y2.*x2.*P_TEPA;

end
```

Appendix E

Matlab code for ternary MEA-H_2O-CO_2 chemical model using extended Debye Hückel equation.

This appendix contains two main scripts. The first code presented contains the parameter regression for the MEA model. The second shows how these parameters are implemented to calculate the partial pressure of CO_2 for a range of loadings, MEA concentrations and temperatures.

E.1 Regression of parameters of MEA-H_2O-CO_2 model

Structure and description of the regression code:

1. The MEA_DATA file is imported, which contains the experimental data (temperature, concentration, loading and partial pressure measured for every data point), as well as the total concentration of water, amine and CO_2 and the temperature dependent Debye Hückel constant and Henry constant for each data point.
2. An initial guess is defined for the speciation solver and an initial guess is defined for the parameter regression.
3. The parameters are regressed by finding the minimum of the objective function (ObjFun), which calculates sum of the squared relative error between the calculated and the model partial pressure of CO_2. For regression, the 'fmincon' function is used to ensure the regressed parameters are in the same range as published literature values (see [7]).

```
clc
clear all
tic

%% Specific ionic interaction model - Puxty & Maeder MEA
% Written by Rebecca Dowling
% 31-03-2020

%% Model inputs
% Import MEA_DATA.txt:
% [(1)     (2)        (3)     (4)        (5)        (6)         (7)     (8)   (9)]
% [T concentration loading pco2_exp c_h2o_tot c_am_tot c_co2_tot A_DH kH_m]
data =importdata('MEA_DATA.txt');

% Allocate columns
T=data(:,1);                    % Temperature [K]
pco2_exp=data(:,4);             % Partial pressure CO2 [kPa]
c_h2o_tot = data(:,5);          % Total water concentration [mol/dm3]
c_am_tot = data(:,6);           % Total MEA concentration [mol/dm3]
c_co2_tot = data(:,7);          % Total CO2 concentration [mol/dm3]
A_DH = data(:,8);               % Debye Huckel constant [dm(3/2) mol(-1/2)]
kH_m=data(:,9);                 % Henry constant [kPa/(mol/dm3)]
```

```
% Constants
DENSITY_H2O=0.997;              % density water, [g/mL]
R = 8.314;                      % Gas constant

% Initial speciation guess solver
x0=[0.00738322211927187;1.27016886926981e-10;0.0139437405423064;...
46.7218198964990;9.34935498306061e-07;0.0212300493482523;...
0.402927286450505;1.70359052000307;0.346426534025385;0.000220258175743386;1;1];

%% Regress the parameters
% inital guess parameters (equivalent to Table 2 to in Puxty, Maeder (2013))
% [ K04_ref    H_4   K05_ref    H_5    K06_ref   H_6]
%n0 = [10 -50 10 -50 10 -50];
n0 = [9.27 -53 1.44 -20 7 -23];
fun=@(n)ObjFun(n,T,R,x0,kH_m,pco2_exp,c_h2o_tot,c_am_tot,...
c_co2_tot,A_DH,DENSITY_H2O);

A = [];
b = [];
Aeq = [];
beq = [];
lb=[1 -60 1 -25 1 -30];
ub=[10 -50 10 -15 10 -20];
nonlcon=[];
sol = fmincon(fun,n0,A,b,Aeq,beq,lb,ub,nonlcon);

toc



function SSQRE = ObjFun(n,T,R,x0,kH_m,pco2_exp,c_h2o_tot,c_am_tot,...
    c_co2_tot,A_DH,DENSITY_H2O)

    % Calculate the value of equilibrium constants at that temperature
    % using the van 'T Hoff equation
    K0 = calc_K0(n,T,R);

    % Calculate the speciation for all values of T
    spec = calc_speciation_gamma(T,x0,K0,c_h2o_tot,c_am_tot,...
    c_co2_tot,A_DH,DENSITY_H2O);

    % Calculate the predicted CO2 partial pressure
    pco2_mod=kH_m.*spec(5,:)'; % kPa

    %% Compare model prediction to experimental data of pCO2
    % Sum of the squared relative error
    SSQRE = sum(((pco2_exp - pco2_mod)./pco2_exp).^2);

end
```

E.2 Main script of the MEA-H_2O-CO_2 model

Structure and description of the regression code:

1. The MEA_DATA file is imported.

2. The regressed parameters of the model are defined, as well as the initial speciation guess.
3. The equilibrium constants for the reactions are calculated as a function of temperature, using the 'calc_K0' function.
4. The speciation is solved using the 'calc_speciation_gamma'. Inside this function, using a for loop the speciation of the system at each data point is calculated by solving a set of nonlinear equations using the 'lsqnonlin' solver. These equation are defined inside the function 'speciation_gamma'. Because this is a badly scaled system, the concentrations are normalized. After the solution, the concentrations must be scaled back.
5. The set of non-linear equations in the function 'speciation_gamma' comprises of the equilibrium constants, mass balances, charge balance and activity coefficient correlations.
6. Once the speciation is calculated for every data point, the partial pressure is calculated using the henry constant.
7. The agreement between the model and the data is calculated using the SSQRE and AARD.
8. Three different types of plots can be created. The 'plotresults' function creates plots of multiple CO_2 absorption isotherms, and compares the model prediction to the experimental data. The 'plotparity' function creates a plot of the measured vs. the calculated partial pressure of CO_2. If desired, the speciation of the system can be plotted as well, using the 'plotspeciation' function.

```
clc
clear all
close all
tic

%% Specific ionic interaction model - Puxty & Maeder MEA
% Written by Rebecca Dowling
% 31-03-2020

%% Model inputs
% Import MEA_DATA.txt:
% [(1)     (2)       (3)    (4)       (5)       (6)        (7)    (8)   (9)]
% [T concentration loading pco2_exp c_h2o_tot c_am_tot c_co2_tot A_DH kH_m]
data =importdata('MEA_DATA.txt');

% Allocate columns
T=data(:,1);                    % Temperature [K]
conc = data(:,2);               % MEA concentration [wt%]
pco2_exp=data(:,4);             % Partial pressure CO2 [kPa]
c_h2o_tot = data(:,5);          % Total water concentration [mol/dm3]
c_am_tot = data(:,6);           % Total MEA concentration [mol/dm3]
c_co2_tot = data(:,7);          % Total CO2 concentration [mol/dm3]
A_DH = data(:,8);               % Debye Huckel constant [dm(3/2) mol(-1/2)]
kH_m=data(:,9);                 % Henry constant [kPa/(mol/dm3)]

% Constants
DENSITY_H2O=0.997;              % density water, [g/mL]
R = 8.314;                      % Gas constant

%% Insert the regressed parameters
% Regressed parameters (equivalent to Table 2 to in Puxty, Maeder (2013))
```

```
% [ K04_ref    H_4  K05_ref   H_5   K06_ref  H_6]
n =[9.2701 -46.0855 1.4979 -21.7160 4.1726 -23.0325];

% Calculate the value of equilibrium constants at that temperature
% using the van 'T Hoff equation
K0 = calc_K0(n,T,R);

%% Model prediction of pCO2
% Initial speciation guess solver
x0 = [0.003863899;
3.65413E-10;
0.002737458;
37.3824064;
2.03093E-06;
0.000855935;
0.222240555;
4.134169315;
0.212045539;
0.212045539;
0.5;
0.5];

% Calculate the speciation for all values of T
spec = calc_speciation_gamma(T,x0,K0,c_h2o_tot,c_am_tot,c_co2_tot,A_DH,DENSITY_H2O);

% Calculate the predicted CO2 partial pressure
pco2_mod=kH_m.*spec(5,:)'; % kPa

%% Compare model prediction to experimental data of pCO2
% Sum of the squared relative error
SSQRE = sum(((pco2_exp - pco2_mod)./pco2_exp).^2);

% Average absolute relative deviation
AARD = 100 * 1/length(data)*sum((abs(pco2_exp - pco2_mod)./pco2_exp));

toc

%% Plotting
t=[40 60 80 100 120]+273.15;
c=[15 30 45 60];
k=1;
% Plot the model results vs the data
[vle_fig,k] = plotresults(pco2_mod,data,c,t,k);

% Create the parity plot
[parity_fig,k] = plotparity(pco2_mod,pco2_exp,k);

%spec_fig = plotspeciation(conc,c,t,T,spec,loading);



function K0 = calc_K0(n,T,R)
    log10K0 = zeros(length(T),6);

    % Known equilibrium constants at infinite dilution
    log10K0(:,1) =-(-(12431.7./T)-(35.4819.*log(T))+220.067)./2.3026; % bicarbonate dissociation
    log10K0(:,2) =-(-(12092.1./T)-(36.7816.*log(T))+235.482)./2.3026; % CO2 dissociation
```

```
    log10K0(:,3) =-(-(13445.9./T)-(22.4773.*log(T))+140.932)./2.3026; % H2O dissociation

    % Regressed equilibrium constants at infinite dilution
    log10K0(:,4)=((n(1))-((n(2)*1000/2.3026/R).*((1./T)-(1/313.15))));
    log10K0(:,5)=((n(3))-((n(4)*1000/2.3026/R).*((1./T)-(1/313.15))));
    log10K0(:,6)=((n(5))-((n(6)*1000/2.3026/R).*((1./T)-(1/313.15))));

    K0=10.^(log10K0);
end


function spec = calc_speciation_gamma(T,x0,K0,c_h2o_tot,c_am_tot,...
c_co2_tot,A_DH,DENSITY_H2O)

    % Preallocation for speed
    spec = zeros(length(x0),length(T));

    for i=1:length(T)

        % Use the solution of previous datapoint as initial guess to
        % initiate solver
        if i > 1
            x0 = spec(:,i-1);
        end

        % Normalize the concentrations, this makes them all 1
        xScalingVec = x0;
        x0 = x0./xScalingVec;

        % Make paramvector for iteration
        paramVec=[K0(i,1);K0(i,2);K0(i,3);K0(i,4);K0(i,5);K0(i,6);c_co2_tot(i);...
        c_am_tot(i);c_h2o_tot(i);A_DH(i)];

        % Solve the speciation and activity coefficients for each data point
        % Described by the equations in the function:
        fun=@(x)speciation_gamma(x,paramVec,xScalingVec,DENSITY_H2O);
        options = optimoptions('lsqnonlin','MaxFunctionEvaluations',1000,...
        'StepTolerance',1e-25,'MaxIterations',1000,...
        'FunctionTolerance',1e-25,'Display','none');
        lb = zeros(length(x0),1); % All concentrations must be above 0
        x=lsqnonlin(fun,x0,lb,[],options);

        % Scale the solution back
        x = x.*xScalingVec;

        % Store the speciation at every data point in spec
        spec(:,i) = x;

    end

end


function F=speciation_gamma(x,paramVec,xScalingVec,DENSITY_H2O)
% x=[(1) (2)   (3)    (4)    (5)   (6)   (7)    (8)     (9)       (10)     (11)    (12)]
%   HCO3- H+  CO3--  H2O  CO2  OH-  MEAH+  MEA   MEACOO- MEACOOH  y(1)    y(2)]
```

```
    % The function must be evaluated at the 'real' x, thus we scale it back
    x = (x.*xScalingVec);

    % Ionic strength, as a function of charged species
    I = (0.5*(x(1)+x(2)+4*x(3)+x(6)+x(7)+x(9))); % [mol/dm3]

    % Equilibrium constants
    F(1)=log10(paramVec(1)/(1/x(12)))-log10(x(1)/(x(2)*x(3)));
    F(2)=log10(paramVec(2)/(1/(x(11)^2)))-log10(x(5)/(x(2)*x(1)));
    F(3)=log10(paramVec(3)/(1/(x(11)^2)))-log10(x(4)/(x(2)*x(6)));
    F(4)=log10(paramVec(4))-log10(x(7)/(x(2)*x(8)));
    F(5)=log10(paramVec(5))-log10(x(9)/(x(1)*x(8)));
    F(6)=log10(paramVec(6)/(1/(x(11)^2)))-log10(x(10)/(x(2)*x(9)));

    % Mass balances
    F(7) =(paramVec(7)) - (x(3)+x(1)+x(5)+x(9)+x(10));
    F(8) = (paramVec(8)) - (x(8)+x(7)+x(9)+x(10));
    F(9) = (paramVec(9)) - (x(6)+x(4));

    % Charge balance
    F(10)= (x(1)+2*x(3)+x(6)+x(9))-(x(7)+x(2));

    % Activity coefficient correlation: Specific Ionic Interaction Theory
    F(11)=log10(x(11))+(paramVec(10)*sqrt(I)/(1+1.5*DENSITY_H2O^(-1/2)*sqrt(I)));
    F(12)=log10(x(12))+(4*paramVec(10)*sqrt(I)/(1+1.5*DENSITY_H2O^(-1/2)*sqrt(I)));

end



function [fig,k] = plotresults(pco2_mod,data,c,t,k)

marker = {'s','d','^','o','x'};
color = {[0 0.4470 0.7410],[0.8500 0.3250 0.0980],...
[0.9290 0.6940 0.1250],[0.4940 0.1840 0.5560],...
[0.4660 0.6740 0.1880]};

for i = 1:length(c)
    fig(k)=figure(k)
    hold on
    for j=1:length(t)
    tindex=find(data(:,2)==c(i) & data(:,1)==t(j));
    plot(data(tindex,3),pco2_mod(tindex),'Color',color{j})
    scatter(data(tindex,3),data(tindex,4),...
    marker{j},'MarkerFaceColor',color{j},...
    'MarkerEdgeColor',color{j})
    end
    box on
    xlabel('Loading (mol CO2/mol MEA)','fontweight','bold')
    ylabel('Partial Pressure of CO2 (kPa)','fontweight','bold')
    title=sprintf('%d wt MEA model vs experiment.jpg',c(i));
    legend('40 C calculated','40 C measured','60 C calculated','60 C measured',...
    '80 C calculated','80 C measured','100 C calculated','100 C measured',...
    '120 C calculated','120 C measured','Location','northeastoutside')
    set(gcf,'position',[10,10,700,400]);
    set(gca,'YScale','log');
    saveas(fig(k),title)
```

```
    hold off
    k=k+1;
end

end


function fig = plotparity(pco2_mod,pco2_exp)

    x = linspace(0.0001,10000,100);
    y=x;
    fig=figure
    hold on
    box on
    set(gca, 'YScale', 'log', 'XScale', 'log')
    plot(pco2_exp,pco2_mod,'o')
    plot(x,y,'--')
    ylim([0.0001 10000])
    xlim([0.0001 10000])
    ylabel('Calculated CO_2 Partial Pressure (kPa)','fontweight','bold')
    xlabel('Measured CO_2 Partial Pressure (kPa)','fontweight','bold')
    saveas(fig,'Parity plot.jpg')
    hold off

end


function fig = plotspeciation(conc,k,c,t,T,spec,loading)
X_molefrac_nowater = zeros(10,length(conc));
X_molefrac = zeros(10,length(conc));

% calculate the molefractions of all species
%
for col=1:length(conc)
    for row=1:10
    X_molefrac_nowater(row,col)=spec(row,col)/sum(spec([1,2,3,5,6,7,8,9,10],col));
    X_molefrac(row,col)=spec(row,col)/sum(spec(:,col));
    end
end

% Speciation when molefraction defined without water
for i = 1:length(c)
    for j=1:length(t)
        fig(k)=figure(k);
        tindex=find(conc==c(i) & T==t(j));
        plot(loading(tindex),X_molefrac_nowater([1,3,5,7,8,9],tindex))
        box on
        xlabel('Loading (mol CO2/mol MEA)','fontweight','bold')
        ylabel('Species molefraction (mol/total moles(no water)))',...
        'fontweight','bold')
        legend('HCO3-','CO3--','CO2','MEAH+','MEA','MEACOO-')
        title = sprintf('Speciation X_nowater %d wt %d C.jpg',c(i),t(j)-273.15);
        saveas(fig(k),title)
        k=k+1;
    end
end
```

```
% Speciation when molefraction defined with water

for i = 1:length(c)
    for j=1:length(t)
        fig(k)=figure(k);
        tindex=find(conc==c(i) & T==t(j));
        plot(loading(tindex),X_molefrac([1,3,5,7,8,9],tindex))
        box on
        xlabel('Loading (mol CO2/mol MEA)','fontweight','bold')
        ylabel('True mole fraction','fontweight','bold')
        title = sprintf('Speciation X_withwater %d wt %d C.jpg',c(i),t(j)-273.15);
        saveas(fig(k),title)
        legend('HCO3-','CO3--','CO2','MEAH+','MEA','MEACOO-')
        k=k+1;
    end
end
close all
end
```

Appendix F

Matlab code for ternary TEPA-H_2O-CO_2 chemical model using extended Debye Hückel equation.

This appendix contains the Matlab code developed to describe the vapor liquid equilibrium of the ternary TEPA-H_2O-CO_2 mixture.

F.1 Regression of parameters of TEPA-H_2O-CO_2 model

Structure and description of the code:

1. The VLE data for 30 wt% and 70wt% TEPA is imported and converted to the required model inputs. These are the temperature, TEPA concentration, CO_2 loading and partial pressure of CO_2 measured, as well as the total concentration of water, amine and CO_2 and the temperature dependent Debye Hückel constant and Henry constant for each data point.
2. Inside the 'convertdata' function, the TEPA concentration is scaled using the scaling factor of 2.5.
3. The initial guess is defined for the parameter regression, which is taken from the piperazine parameters from [7].
4. The temperature dependent equilibrium constants are calculated using the function 'calc_K0' and the initial guess of the parameters.
5. An initial speciation guess is made for the point of highest loading of each isotherm (for this reason the data was flipped upside down, to go from high loading to low loading) using the 'initialguess' function.
6. The initial guess is generated using a genetic algorithm. It tries to minimise the sum of of the absolute values of the nonlinear equations that govern the system ('minsum'). The genetic algorithm is repeated until the value of minsum reaches a threshold of 2.5 to ensure that the initial guess is good.
7. The parameters are regressed by finding the minimum of the objective function (ObjFun), which calculates sum of the squared relative error between the calculated and the model partial pressure of CO_2. For regression, the 'fmincon' function is used, together with 'MultiStart' to find a global minimum. Parallel computing speeds up the computations.

```
%% TEPA-H2O-CO2 VLE model using extended Debye Huckel law
clc;close all;tic

%% Inputs
% Constants
DENSITY_H2O=0.997;          % density water, [g/mL]
MW_H2O=18.015;              % molar mass water [g/mol]
R=8.314;                    % gas constant [J/mol/K]
```

```
ER=80.2;                    % rel. perimittivity of water at 20C [-]
T_C=647.126;                % critical temperature water, [K]
% Amine specific
DENSITY_AMINE=0.998;        % density TEPA, [g/mL]
MW_AMINE=189.314;           % molar mass TEPA, [g/mol]
nAminegroups=5;             % number of amine groups per molecule [mol/mol]

% VLE data
% [ (1)       (2)            (3)           (4)  ]
% [  T   concentration     loading         pCO2 ]
% [  C        wt%         mol/mol N        mbar ]
tepa30= importdata('tepa_30.txt'); % VLE data of 30 wt% TEPA
tepa30 = flipud(tepa30);
tepa70= importdata('tepa_70.txt'); % VLE data of 30 wt% TEPA
tepa70 = flipud(tepa70);
VLE_DATA =[tepa30;tepa70];

%% Calculations
% Convert the VLE data to the required inputs of the model: AMINE_DATA.
% The array contains the following information:
% [(1)       (2)          (3)         (4)      (5)          (6)          (7)
% [ T   concentration   loading      pCO2   c_h2o_total c_amine_total c_co2_total
% [ K         wt%      mol/mol N      kPa      mol/dm3      mol/dm3     mol/dm3
%
%          (8)                        (9)          ]
% Debye Huckel constant        Henry's constant   ]
%  dm(3/2) mol(-1/2)            kPa/(mol/dm3)     ]
AMINE_DATA = convertdata(VLE_DATA,DENSITY_H2O,MW_H2O,DENSITY_AMINE,...
MW_AMINE,ER,T_C,nAminegroups);

% Allocate columns
T=AMINE_DATA(:,1);                    % Temperature [K]
pco2_exp=AMINE_DATA(:,4);             % Partial pressure CO2 [kPa]
c_h2o_tot = AMINE_DATA(:,5);          % Total water concentration [mol/dm3]
c_am_tot = AMINE_DATA(:,6);           % Total TEPA concentration [mol/dm3]
c_co2_tot = AMINE_DATA(:,7);          % Total CO2 concentration [mol/dm3]
A_DH = AMINE_DATA(:,8);               % Debye Huckel constant [dm(3/2) mol(-1/2)]
kH_m=AMINE_DATA(:,9);                 % Henry constant [kPa/(mol/dm3)]

%% Initial guess for regression
% Regressed parameters for piperazine from Puxty&Maeder (2013), Table 4
% [logK04 H4 logK05 H5 logK06 H6 logK07 H7 logK08 H8]
n0 = [9.3 -38 1.2 -32 8.9 -18 0.8 -24 8.9 -24];

% Calculate the value of equilibrium constants at that temperature
% using the van 'T Hoff equation
K0 = calc_K0(n0,T,R);

% Find the places where T changes
index=find(diff(T)~=0)+1;
% index contains the index of every first point of each isotherm
index=[1;index];

% Generate an initial speciation guess for every first point of an isotherm
[x0,fval] = initialguess(index,K0,c_co2_tot,c_am_tot,c_h2o_tot,A_DH,DENSITY_H2O);
x0=x0';
```

```
%% Regression

fun=@(n)ObjFun(n,T,R,x0,kH_m,pco2_exp,c_h2o_tot,c_am_tot...
    ,c_co2_tot,A_DH,DENSITY_H2O);
A = [];
b = [];
Aeq = [];
beq = [];
f1 = [0.5 1.5 0.5 1.5 0.5 1.5 0.5 1.5 0.5 1.5];
f2 = [1.5 0.5 1.5 0.5 1.5 0.5 1.5 0.5 1.5 0.5];
lb = f1.*n0;
ub = f2.*n0;
nonlcon=[];
%n = fmincon(fun,n0,A,b,Aeq,beq,lb,ub);

problem = createOptimProblem('fmincon','objective',fun,'x0',n0,...
    'lb',lb,'ub',ub,'options',[]);
ms = MultiStart('UseParallel',true,'Display','iter');
% Use parallel computing to speed up the process
parpool
% Use Multistart with 1000 startpoints, to find the global minimum of the
% problem
[sol,fval,eflag,output,manymins] = run(ms,problem,100);
% Stop parallel computing
delete(gcp)



function AMINE_DATA = convertdata(VLE_DATA,DENSITY_H2O,MW_H2O,DENSITY_AMINE,MW_AMINE,ER,T_C,nAmi

% Function Description:
% This function converts the incoming VLE_DATA array to an array containing
% all the required inputs of the model, called AMINE_DATA.
%
% Inputs:
% - VLE_DATA: [T concentration loading pco2_exp]
% - DENSITY_H2O,DENSITY_AMINE: density of water and amine, [kg/dm3].
% - MW_H2O, MW_AMINE: molar mass of water and amine, [g/mol].
% - ER: relative permittivity of water, [-]
% - T_C: critical temperature of water, [K].
% - nAminegroups: number of NH-groups per molecule of amine.
%
% Output
% - AMINE_DATA: array containing the following information:
% [T concentration loading pco2_exp c_h2o_tot c_am_tot c_co2_tot A_DH kH_m]

    % Assign the columns
    T=VLE_DATA(:,1)+273.15;           % Temperature [K]
    concentration=VLE_DATA(:,2);      % concentration amine [wt%]
    loading=VLE_DATA(:,3)*5;          % CO2 loading [mol CO2/mol TEPA]
    pco2_exp=VLE_DATA(:,4).*0.1;      % pCO2 converted from [mbar] to [kPa]

    %% Convert data to total concentrations of H2O, AMINE and CO2
    % Total water concentration [mol/L]
    c_h2o_tot=((100-concentration)./MW_H2O)./(0.001*((concentration./...
        DENSITY_AMINE)+((100-concentration)./DENSITY_H2O)));
    % Total amine concentration [mol/L]
    c_am_tot=(concentration./MW_AMINE)./(0.001*((concentration./...
```

```
        DENSITY_AMINE)+((100-concentration)./DENSITY_H2O)));
    % Total co2 concentration [mol/L]
    c_co2_tot=loading.*c_am_tot;
    % Debye Huckel constant [dm(3/2) mol(-1/2)]
    A_DH=(1.8248*10^6)./((ER.*T).^(3/2));

    % Scale the total amine concentration by the factor nAminegroups/2
    % This is the concentration the solution would have if the amine was a
    % diamine, while the concentration of NH-groups remains the same.
    ScalingFactor = nAminegroups/2;
    c_am_tot = c_am_tot.*ScalingFactor;

    %% Calculate the Henry constant, kH, as function of T
    ln_kH=zeros(length(T),1);

    % When T < 353.15, kH follows the formula:
    index=find(T<=353.15);
    ln_kH(index)=9.4052+(3934.4./T(index))-(941290.2./T(index).^2);

    % When T > 353.15, kH follows the folmula:
    index2=find(T>353.15);
    ln_kH(index2)=((1713.53.*(1-(T(index2)./T_C)).^(1/3))./T(index2))...
        +8.4802+(3680.09./T(index2))-(1198506.1./T(index2).^2);
    kH=exp(ln_kH);      % Henry constant, [kPa]

    % Convert to molarity units by dividing by the molarity of pure water
    kH_m=kH./(1000*DENSITY_H2O/MW_H2O); % Henry constant, [kPa/(mol/dm3)]

    %% Create the DATA matrix
    % by horizontally concatenating the calculated vectors
    AMINE_DATA = [T concentration loading pco2_exp c_h2o_tot c_am_tot...
        c_co2_tot A_DH kH_m];

end



function K0 = calc_K0(n,T,R)

% Function Description:
% This function calculates the infinite dilution equilibrium constants as a
% function of temperature (T) and model parameters (n) using the Van 'T
% Hoff equation for the following liquid phase reactions:
% (1)    H+    + CO3--      <-->   HCO3-
% (2)    H+    + HCO3-      <-->   CO2        + H2O
% (3)    H+    + OH-        <-->   H2O
% (4)    H+    + Am         <-->   AmH+
% (5)    HCO3- + Am         <-->   AmCOO-     + H2O
% (6)    H+    + AmCOO-     <-->   HAmCOO
% (7)    HCO3- + AmCOO-     <-->   Am(COO)2-- + H2O
% (8)    H+    + Am(COO)2-- <-->   HOOCAmCOO-

    log10K0 = zeros(length(T),8);

    % Known equilibrium constants at infinite dilution
    log10K0(:,1) =-(-(12431.7./T)-(35.4819.*log(T))+220.067)./2.3026; % bicarbonate dissociation
    log10K0(:,2) =-(-(12092.1./T)-(36.7816.*log(T))+235.482)./2.3026; % CO2 dissociation
    log10K0(:,3) =-(-(13445.9./T)-(22.4773.*log(T))+140.932)./2.3026; % H2O dissociation
```

```
    % Regressed equilibrium constants at infinite dilution
    log10K0(:,4)=((n(1))-((n(2)*1000/2.3026/R).*((1./T)-(1/313.15))));
    log10K0(:,5)=((n(3))-((n(4)*1000/2.3026/R).*((1./T)-(1/313.15))));
    log10K0(:,6)=((n(5))-((n(6)*1000/2.3026/R).*((1./T)-(1/313.15))));
    log10K0(:,7)=((n(7))-((n(8)*1000/2.3026/R).*((1./T)-(1/313.15))));
    log10K0(:,8)=((n(9))-((n(10)*1000/2.3026/R).*((1./T)-(1/313.15))));

    K0=10.^(log10K0);
end


function   [x0,fval] = initialguess(index,K0,c_co2_tot,c_am_tot,c_h2o_tot,A_DH,DENSITY_H2O)

    x0=zeros(length(index),14);
    fval=zeros(length(index),1);

    for i=1:length(index)
        % Make paramvector for iteration
        paramVec=[K0(index(i),1);K0(index(i),2);K0(index(i),3);K0(index(i),4);K0(index(i),5);K0(
        % Solve the speciation and activity coefficients for each data point
        % Described by the equations in the function:
        fun=@(x)minsum(x,paramVec,DENSITY_H2O);
        nvars=14;
        A = [];
        b=[];
        Aeq=[];
        beq=[];
        nonlcon=[];
        lb = zeros(1,nvars); % All concentrations must be above 0
        lb(4) = 0.9*paramVec(11); %
        ub = [paramVec(9) 1E-06 paramVec(9) paramVec(11) paramVec(9) paramVec(11) paramVec(10) p
        Pop = 300;
        options = optimoptions('ga','PopulationSize',Pop);
        [x0(i,:),fval(i)] = ga(fun,nvars,A,b,Aeq,beq,lb,ub,nonlcon,options);
        if fval(i)>=2.5
                while fval(i) > 2.5
                fprintf('Initial guess not good enough :(. Fval = %.3f. \n',fval(i));
                Pop = Pop+300;
                options = optimoptions('ga','PopulationSize',Pop,'Display','none');
                [x0(i,:),fval(i)] = ga(fun,nvars,A,b,Aeq,beq,lb,ub,nonlcon,options);
                end
                fprintf('A good initial guess was found :) ! Fval = %.3f \n',fval(i));

            else
                fprintf('A good initial guess was found :) ! Fval = %.3f. \n',fval(i));

            end
   end

end



function Z=minsum(x,paramVec,DENSITY_H2O)

% Function description:
```

```
% This function is used as the objective function that is minimised by
% a genetic algorithm to make a good initial speciation guess.
% Essentially, it is a modified version of speciation_gamma.m, where the
% function output is the sum of the absolute values of F. This modification
% is necessary because the genetic algorithm needs an objective function
% that returns a scalar value.
%
% Inputs:
% - x: unknowns vector, containing speciation and activity coefficients
%   x=[(1) (2)  (3)   (4)   (5)  (6)  (7)   (8)    (9)      (10)
%     HCO3- H+  CO3--  H2O  CO2  OH-  AmH+  Am    AmCOO-   AmCOOH
%      (11)        (12)        (13)   (14)]
%    Am(COO)2--  HAm(COO)2-    y(1)   y(2)]
% - paramVec: vector containing the parameters required to solve the set of
%   nonlinear equations.
%   paramVec = [(1)  (2)  (3)  (4)  (5)  (6)  (7)  (8)
%               [K01  K02  K03  K04  K05  K06  K07  K08
%                   (9)       (10)      (11)     (12) ]
%                c_co2_tot  c_am_tot  c_h2o_tot  A_DH ]
% - DENSITY_H2O: density of water, [kg/dm3]
%
% Output:
% - Z: sum of the absolute values of F. These should be near 0.

    % Ionic strength, as a function of charged species
    I = (0.5*(x(1)+x(2)+4*x(3)+x(6)+x(7)+x(9)+4*x(11)+x(12))); % [mol/dm3]

    % Equilibrium constants
    F(1)=log10(paramVec(1)*x(14))-log10(x(1)/(x(2)*x(3)));
    F(2)=log10(paramVec(2)*(x(13)^2))-log10(x(5)/(x(2)*x(1)));
    F(3)=log10(paramVec(3)*(x(13)^2))-log10(x(4)/(x(2)*x(6)));
    F(4)=log10(paramVec(4))-log10(x(7)/(x(2)*x(8)));
    F(5)=log10(paramVec(5))-log10(x(9)/(x(1)*x(8)));
    F(6)=log10(paramVec(6)*(x(13)^2))-log10(x(10)/(x(2)*x(9)));
    F(7)=log10(paramVec(7)*(x(13)^2)/x(14))-log10(x(11)/(x(1)*x(9)));
    F(8)=log10(paramVec(8)*x(14))-log10(x(12)/(x(2)*x(11)));

    % Mass balances
    F(9) =  (paramVec(9)) - (x(3)+x(1)+x(5)+x(9)+x(10)+2*x(11)+2*x(12));
    F(10) = (paramVec(10)) - (x(8)+x(7)+x(9)+x(10)+x(11)+x(12));
    F(11) = (paramVec(11)) - (x(6)+x(4));

    % Charge balance
    F(12)= (x(1)+2*x(3)+x(6)+x(9)+2*x(11)+x(12))-(x(7)+x(2));

    % Activity coefficient correlation: Specific Ionic Interaction Theory
    F(13)=log10(x(13))+(paramVec(12)*sqrt(I)/(1+1.5*DENSITY_H2O^(-1/2)*sqrt(I)));
    F(14)=log10(x(14))+(4*paramVec(12)*sqrt(I)/(1+1.5*DENSITY_H2O^(-1/2)*sqrt(I)));

    Z=sum(abs(F));

end



function AARD = ObjFun(n,T,R,x0,kH_m,pco2_exp,c_h2o_tot,c_am_tot,c_co2_tot,A_DH,DENSITY_H2O)
```

```
    % Calculate the value of equilibrium constants at that temperature
    % using the van 'T Hoff equation
    K0 = calc_K0(n,T,R);

    % Find the places where T changes
    index=find(diff(T)~=0)+1;
    index=[1;index];

    % Calculate the speciation for all values of T
    spec = calc_speciation_gamma(T,x0,K0,c_h2o_tot,c_am_tot,c_co2_tot,A_DH,DENSITY_H2O,index);

    % Calculate the predicted CO2 partial pressure
    pco2_mod=kH_m.*spec(5,:)'; % kPa

    %% Compare model prediction to experimental data of pCO2
    % Sum of the squared relative error
    SSQRE = sum(((pco2_exp - pco2_mod)./pco2_exp).^2);

    % Absolute average relative deviation
    AARD = 100 * 1/length(T)*sum((abs(pco2_exp - pco2_mod)./pco2_exp))

end
```

F.2 Main code for TEPA-H_2O-CO_2 model

Structure and description of the code:

1. The VLE data for 30 wt% and 70wt% TEPA is imported and converted to the required model inputs.
2. The regressed parameters of the model are defined.
3. The equilibrium constants for the reactions are calculated as a function of temperature, using the 'calc_K0' function.
4. An initial guess can be made using the 'initialguess' function or by importing a previously made initial guess ('x0.mat').
5. The speciation is solved using the 'calc_speciation_gamma'. Inside this function, using a for loop, the speciation of the system at each data point is calculated by solving a set of nonlinear equations using the 'fsolve' solver. These equation are defined inside the function 'speciation_gamma'. Because this is a badly scaled system, the concentrations are normalized. After the solution, the concentrations must be scaled back.
6. The set of non-linear equations in the function 'speciation_gamma' comprises of the equilibrium constants, mass balances, charge balance and activity coefficient correlations.
7. Once the speciation is calculated for every data point, the partial pressure is calculated using the henry constant.
8. The agreement between the model and the data is calculated using the SSQRE and AARD.
9. The 'plotresults' function creates plots of multiple CO_2 absorption isotherms, and compares the model prediction to the experimental data. The 'plotparity' function creates a plot of the

measured vs. the calculated partial pressure of CO_2.

```
%% TEPA-H2O-CO2 VLE model using extended Debye Huckel law

clc;close all;clear all
tic
%% Inputs
% Constants
DENSITY_H2O=0.997;          % density water, [g/mL]
MW_H2O=18.015;              % molar mass water [g/mol]
R=8.314;                    % gas constant [J/mol/K]
ER=80.2;                    % rel. perimittivity of water at 20C [-]
T_C=647.126;                % critical temperature water, [K]
% Amine specific
DENSITY_AMINE=0.998;        % density TEPA, [g/mL]
MW_AMINE=189.314;           % molar mass TEPA, [g/mol]
nAminegroups=5;             % number of amine groups per molecule [mol/mol]

% VLE data
% [ (1)       (2)            (3)           (4)  ]
% [  T   concentration     loading         pCO2 ]
% [  C        wt%         mol/mol N        mbar ]
tepa30= importdata('tepa_30.txt'); % VLE data of 30 wt% TEPA
tepa30 = flipud(tepa30);
tepa70= importdata('tepa_70_cor.txt'); % VLE data of 30 wt% TEPA
tepa70 = flipud(tepa70);
VLE_DATA =[tepa30;tepa70];

%% Calculations
% Convert the VLE data to the required inputs of the model: AMINE_DATA.
% The array contains the following information:
% [(1)       (2)          (3)         (4)      (5)          (6)          (7)
% [ T   concentration   loading      pCO2   c_h2o_total c_amine_total c_co2_total
% [ K         wt%      mol/mol TEPA   kPa      mol/dm3      mol/dm3     mol/dm3
%
%          (8)                        (9)          ]
% Debye Huckel constant        Henry's constant   ]
%  dm(3/2) mol(-1/2)            kPa/(mol/dm3)     ]
AMINE_DATA = convertdata(VLE_DATA,DENSITY_H2O,MW_H2O,DENSITY_AMINE,...
    MW_AMINE,ER,T_C,nAminegroups);

% Allocate columns
T=AMINE_DATA(:,1);              % Temperature [K]
pco2_exp=AMINE_DATA(:,4);       % Partial pressure CO2 [kPa]
c_h2o_tot = AMINE_DATA(:,5);    % Total water concentration [mol/dm3]
c_am_tot = AMINE_DATA(:,6);     % Total TEPA concentration [mol/dm3]
c_co2_tot = AMINE_DATA(:,7);    % Total CO2 concentration [mol/dm3]
A_DH = AMINE_DATA(:,8);         % Debye Huckel constant [dm(3/2) mol(-1/2)]
kH_m=AMINE_DATA(:,9);           % Henry constant [kPa/(mol/dm3)]

%% Model prediction of pCO2
% Regressed parameters for TEPA
% [logK04 H4 logK05 H5 logK06 H6 logK07 H7 logK08 H8]
n = [8.05 -19.45 1.05 -26.37 8.9 -26.51 2.368 -21.28 6.74 -24.53];

% Calculate the value of equilibrium constants at that temperature
% using the van 'T Hoff equation
```

```
K0 = calc_K0(n,T,R);

% Find the places where T changes
index=find(diff(T)~=0)+1;
% index contains the index of every first point of each isotherm
index=[1;index];

% Generate an initial speciation guess for every first point of an isotherm
% [x0,fval] = initialguess(index,K0,c_co2_tot,c_am_tot,c_h2o_tot,A_DH,DENSITY_H2O);
% x0=x0';
x0=importdata('x0.mat');

% Calculate the speciation for all values of T
spec = calc_speciation_gamma(T,x0,K0,c_h2o_tot,c_am_tot,c_co2_tot,A_DH,...
    DENSITY_H2O,index);
% Check for imaginary numbers
imag_spec = imag(spec);

% Calculate the predicted CO2 partial pressure
pco2_mod=kH_m.*spec(5,:)'; % kPa

%% Compare model prediction to experimental data of pCO2
% Sum of the squared relative error
SSQRE = sum(((pco2_exp - pco2_mod)./pco2_exp).^2);

% Average absolute relative deviation
AARD = 100 * 1/length(T)*sum((abs(pco2_exp - pco2_mod)./pco2_exp));

toc

%% Plotting
% Plot the model results vs the data
vle_fig = plotresults(pco2_mod,AMINE_DATA);

% Create the parity plot
parity_fig = plotparity(pco2_mod,pco2_exp);



function spec = calc_speciation_gamma(T,x0,K0,c_h2o_tot,c_am_tot,...
    c_co2_tot,A_DH,DENSITY_H2O,index)

% Function Description:
% This function calculates the liquid phase speciation for every datapoint,
% by solving a set of nonlinear equations (defined in 'speciation_gamma.m')
% comprised of equilibrium conditions, mass balances, a charge balance and
% activity coefficient equations.
% Because the species concentrations vary over orders of magnitude, they
% are normalised to help the solver along and increase computation speed.
%
% Required files
% - speciation_gamma.m
%
% Inputs:
% - T: temperature (K)
% - x0: initial speciation guesses array for the end of each isotherm.
% - K0: infinite dilution equilibrium constants for each T
% - c_h2o_tot, c_am_tot, c_co2_tot: total concentrations of water, amine
```

```
%   and CO2, respectively.
% - A_DH: Debye Huckel parameters for each T.
% - DENSITY_H2O: density of water (kg/dm3)
% - index: row number of the datapoints corresponding to the end of each
%   isotherm.
%
% Output:
% - spec: array containing the species concentration at each datapoint.
%   The column number corresponds to the datapoint.
%   The row numbers correspond to the different unknowns as follows:
%   (1)    (2)   (3)    (4)   (5)   (6)   (7)    (8)     (9)       (10)
%   HCO3-  H+  CO3-- H2O  CO2  OH-  AmH+   Am    AmCOO-   AmCOOH
%     (11)         (12)         (13)    (14)
%   Am(COO)2--  HAm(COO)2-     y(1)    y(2)

    % Preallocation for speed
    spec = zeros(length(x0),length(T));

    for i=1:length(T)

        % Evaluate if i equals one of the values of index
        [Lia(i),Locb(i)] = ismember(i,index);

        if Lia(i) == 1 % i equals one of the values of index
            x0i = x0(:,Locb(i)); % use a new initial guess
        else
            x0i = spec(:,i-1);
        end

        % Normalize the concentrations, this makes them all 1
        % This helps the solver solve this otherwise badly scaled system.
        xScalingVec = x0i;
        x0i = x0i./xScalingVec;

        % Make a vector out of all the required parameters to calculate
        % speciation for this datapoint.
        paramVec=[K0(i,1);K0(i,2);K0(i,3);K0(i,4);K0(i,5);K0(i,6);K0(i,7)...
            ;K0(i,8);c_co2_tot(i);c_am_tot(i);c_h2o_tot(i);A_DH(i)];

        % Solve the speciation and activity coefficients for each datapoint
        % Described by the equations in the function:
        fun=@(x)speciation_gamma(x,paramVec,xScalingVec,DENSITY_H2O);
        options = optimoptions('fsolve','Display','none',...
            'MaxFunctionEvaluations',1000,'StepTolerance',1e-15,...
            'MaxIterations',10000,'FunctionTolerance',1e-30);
        x=fsolve(fun,x0i,options);

        % Scale the solution back
        x = x.*xScalingVec;

        % Store the speciation at every data point in spec
        spec(:,i) = x;

    end

end
```

```
function F=speciation_gamma(x,paramVec,xScalingVec,DENSITY_H2O)
% Function description
% This function contains the set of nonlinear equations that need to be
% solved to find the species concentrations and activity coefficients for
% each datapoint.
%
% Inputs:
% - x: unknowns to be solved, containing all species concentrations and
%   activity coefficients.
%   x = [ (1)   (2)   (3)    (4)    (5)   (6)    (7)    (8)     (9)       (10)
%       [HCO3- H+  CO3--  H2O   CO2   OH-  AmH+   Am   AmCOO-   AmCOOH
%        (11)         (12)         (13)    (14) ]
%      Am(COO)2--  HAm(COO)2-    y(1)    y(2) ]
% - paramVec: vector containing the parameters required to solve the set of
%   nonlinear equations.
%   paramVec = [(1)   (2)   (3)   (4)   (5)   (6)   (7)   (8)
%               [K01  K02  K03  K04  K05  K06  K07  K08
%                   (9)       (10)       (11)      (12) ]
%                c_co2_tot  c_am_tot  c_h2o_tot  A_DH ]
% - xScalingVec: vector used to normalise the unknowns.
% - DENSITY_H2O: density of water, required for the Debye-Huckel equation.
%
% Output:
% - F: All values of F should be as close to zero as possible.


    % The function must be evaluated at the 'real' x, thus we scale it back
    x = (x.*xScalingVec);

    % Ionic strength, as a function of charged species
    I = (0.5*(x(1)+x(2)+4*x(3)+x(6)+x(7)+x(9)+4*x(11)+x(12))); % [mol/dm3]

    % Equilibrium constants
    F(1)=log10(paramVec(1)*x(14))-log10(x(1)/(x(2)*x(3)));
    F(2)=log10(paramVec(2)*(x(13)^2))-log10(x(5)/(x(2)*x(1)));
    F(3)=log10(paramVec(3)*(x(13)^2))-log10(x(4)/(x(2)*x(6)));
    F(4)=log10(paramVec(4))-log10(x(7)/(x(2)*x(8)));
    F(5)=log10(paramVec(5))-log10(x(9)/(x(1)*x(8)));
    F(6)=log10(paramVec(6)*(x(13)^2))-log10(x(10)/(x(2)*x(9)));
    F(7)=log10(paramVec(7)*(x(13)^2)/x(14))-log10(x(11)/(x(1)*x(9)));
    F(8)=log10(paramVec(8)*x(14))-log10(x(12)/(x(2)*x(11)));

    % Mass balances
    F(9) =  (paramVec(9)) - (x(3)+x(1)+x(5)+x(9)+x(10)+2*x(11)+2*x(12));
    F(10) = (paramVec(10)) - (x(8)+x(7)+x(9)+x(10)+x(11)+x(12));
    F(11) = (paramVec(11)) - (x(6)+x(4));
    F(12)= (x(1)+2*x(3)+x(6)+x(9)+2*x(11)+x(12))-(x(7)+x(2));

    % Activity coefficient correlation: Specific Ionic Interaction Theory
    F(13)=log10(x(13))+(paramVec(12)*sqrt(I)/(1+1.5*DENSITY_H2O^(-1/2)*sqrt(I)));
    F(14)=log10(x(14))+(4*paramVec(12)*sqrt(I)/(1+1.5*DENSITY_H2O^(-1/2)*sqrt(I)));

end



function fig = plotresults(pco2_mod,data)
```

```
% This function creates plots of the partial pressure of CO2 versus the
% loading. Both the VLE dat and the prediction of the model are combined in
% the graph. One graph is created for each concentration, containing the
% isotherms at the different temperatures measured.

t=[40 80 120]+273.15;
c=[30 70];
marker = {'s','d','^','o','x'};
color = {[0 0.4470 0.7410],[0.8500 0.3250 0.0980],...
    [0.9290 0.6940 0.1250],[0.4940 0.1840 0.5560],...
    [0.4660 0.6740 0.1880]};
k=1;
iter = 1;
for i = 1:length(c)
    fig(k)=figure(k);
    hold on
    grid on
    Legend = {};
    for j=1:length(t)
        % find the index of the datapoints corresponding to 1 isotherm
        tindex=find(data(:,2)==c(i) & data(:,1)==t(j));
        if isempty(tindex) == 0
            A = (data(tindex,3));    % loading for that isotherm [mol/mol]
            C = data(tindex,4);      % pCO2 measured [kPa]
            B = (pco2_mod(tindex));  % pCO2 calculated [kPa]
            %ensure that the loading is sorted from low to high
            [A,idx]=sort(A);
            %sort the pCO2 in the same way as the loading
            B=B(idx);
            C=C(idx);
            plot(A,B,'Color',color{j}) % plot the model
            scatter(A,C,marker{j},'MarkerFaceColor',color{j},...
                'MarkerEdgeColor',color{j})    %scatter the data
            Legend1{iter}=sprintf('%.2f K calculated',t(j));
            Legend2{iter}=sprintf('%.2f K measured',t(j));
            Legend = [Legend, Legend1{iter},Legend2{iter}];
        end
        iter = iter + 1;
    end
    box on
    grid on
    xlabel('Loading (mol CO_2/mol TEPA)','fontweight','bold')
    ylabel('Partial Pressure of CO_2 (kPa)','fontweight','bold')
    title=sprintf('%d wt TEPA model vs experiment.jpg',c(i));
    legend(Legend,'Location','northeastoutside')
    set(gcf,'position',[10,10,700,400]);
    set(gca,'YScale','log');
    saveas(fig(k),title)
    hold off
    k=k+1;
end

end



function fig = plotparity(pco2_mod,pco2_exp)
```

```
% This function creates a parity plot of the experimental and calculated
% partial pressure of CO2.
color = {[0 0.4470 0.7410],[0.8500 0.3250 0.0980]};

    x = linspace(0.0001,10000,100);
    y=x;
    fig=figure;
    hold on
    box on
    grid on
    set(gca, 'YScale', 'log', 'XScale', 'log')
    plot(x,y,'Color',color{2})
    scatter(pco2_exp,pco2_mod,12,'o','MarkerFaceColor',color{1},...
        'MarkerEdgeColor',color{1})
    ylim([0.0001 10000])
    xlim([0.0001 10000])
    ylabel('Calculated CO_2 Partial Pressure (kPa)','fontweight','bold')
    xlabel('Measured CO_2 Partial Pressure (kPa)','fontweight','bold')
    saveas(fig,'Parity plot.jpg')
    hold off

end
```